Freezing in Kinetic Ferromagnets

A thesis presented in candidature for the degree Doctor of Philosophy.
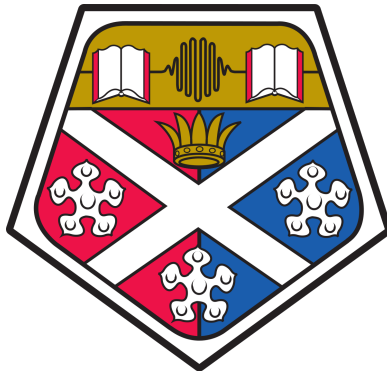
Written By

JAMES DENHOLM

The University of Strathclyde

Department of Physics

Glasgow, Scotland

2020

PUBLICATIONS, AWARDS & TALKS

PUBLICATIONS

— J. Denholm and B. Hourahine. "Anomalous Ising freezing times". In submission, arXiv:2001.11774v2.

— J. Denholm and S. Redner. "Topology-controlled Potts coarsening". In: Physical Review E 99 (6 2019). doi: 10.1103/PhysRevE.99.062142, arXiv:1812.05655.

AWARDS

— Mac Robertson travelling scholarship, May 2018. Full award used to fund a research visit to the Santa Fe Institute, Santa Fe, New Mexico, USA.

— Best research presentation (jointly awarded), August 2017. University of Strathclyde, Department of Physics, end of year post-graduate research conference. Ross Priory, Scotland.

TALKS

— Nordita: Statistical Physics of complex systems, Stockholm, Sweeden, May 2019.

— Open Statistical Physics, Milton Keynes, England, United Kingdom, Mar 2018.

DECLARATION OF AUTHORS RIGHTS

This thesis is the result of the author's original research. It has been composed by the author and has not been previously submitted for examination which has led to the award of a degree.

The copyright of this thesis belongs to the author under the terms of the United Kingdom Copyright Acts as qualified by University of Strathclyde Regulation 3.50. Due acknowledgement must always be made of the use of any material contained in, or derived from, this thesis.

Signed:

Dated: July 28, 2020

ABSTRACT

In this thesis I present studies of the non-equilibrium dynamics of Ising and Potts ferromagnets in two spatial dimensions. While the conception of these models was originally motivated by a desire to understand the phenomena surrounding equilibrium phase transitions, they have found considerable use in non-equilibrium Statistical Physics.

Despite being well studied, even from a non-equilibrium viewpoint, a number of surprisingly basic and fundamental gaps in our understanding of Ising and Potts models have come to light in recent decades. For example, the tacit assumption that Ising ferromagnets should always reach their ground state at zero-temperature has been found incorrect, and unexpected features of the associated relaxation process have come to light. With the Potts model the situation is stranger still: the late time final states that persist in two dimensions are considerably richer than those of the Ising model, and the relaxation times are complex and not yet well understood.

In this thesis I examine basic aspects of zero-temperature coarsening in two-dimensional Ising and Potts ferromagnets. I explore the timescales associated with zero-temperature freezing in the Ising model, and uncover the existence of an over-looked relaxation timescale. I then investigate the final states of the zero-temperature Potts model on the triangular lattice, which prior to this work had not been examined. I continue my studies of the Potts model to situations of increased ground state degeneracy and extended local interaction rules.

ACKNOWLEDGEMENTS

CONTENTS

INTRODUCTION

There exist no natural phenomena that are described perfectly by any set of physical laws, yet through the construction of mathematical models and well reasoned arguments, physicists may approximate and understand nature to a powerful extent. Often there is great beauty in the depth of insight that one may gain through the study of emergent behaviours in surprisingly simple models. In fact, one may argue that the goal of all theoretical physics is to capture the dominant mechanisms behind natural phenomena with the simplest possible models, and to settle for less is lazy and insufficient. This idea is captured well in the following quote, which is often—though perhaps dubiously—attributed to Albert Einstein.

"Everything should be made as simple as possible, but not simpler"

This is particularly true in the field of Statistical Physics, which is concerned with the study of collective behaviour in systems with many components through use of probability theory and statistics. In systems with many interacting bodies, constituents, or particulates, it is important to seek the underlying simplicity by looking for emergent collective behaviour. Perhaps the archetypal example of an elementary model that yields surprisingly rich behaviour is the simple Ising ferromagnet, which was proposed as a toy model to explain ferromagnetism. Before we discuss the Ising model in more detail,

let us briefly remind ourselves about ferromagnets.

Ferromagnets are "everyday" magnets; the kind we see stuck to our refrigerators, in simple bar magnets, and even in our computer's hard drives. Molecular constituents within these materials can be viewed as magnetic "spins" which "point" in certain directions. Ferromagnetic interactions promote alignment in the spins, and thermal agitation attempts to randomise them. At low temperatures—beneath a critical point—the ferromagnetic interactions prevail; the system magnetises and we have a "good" magnet. At high temperatures—above a critical point—thermal noise dominates, and the magnetisation is lost. When one varies temperature slowly across the critical point, the system spontaneously transitions between these two "phases". This puzzling behaviour was first understood by studying the eponymously named Ising model.

1.1   THE ISING MODEL

1.1—A   ORIGIN

In the field of Statistical Physics, the Ising model is steeped in a rich and fruitful history—a history that begins with its conception in 1920. Originally conceived by Willhelm Lenz as a problem for his PhD student, Ernst Ising, the Ising model was intended to explain the onset of ferromagnetism—i.e. the abrupt change in magnetisation observed when one *slowly* varies temperature across a critical point [1]. Tasked with investigating the temperature-dependant *equilibrium* behaviour of a chain of magnetic spins that could point either up or down, Ising concluded that the spins could not spontaneously magnetise and break their symmetry.

Unfortunately, Ising famously blundered by assuming his conclusions also applied in two- and three-dimensions [2]. However, Ising's incorrect extension of his one-dimensional findings only added to the unexpected fame surrounding the model. The Ising model, and the wider class of spin models it belongs to, was used to unveil powerful concepts such as universality, symmetry-breaking and the renormalization

group [2]. We shall explore some of this vibrant history in the following.

1.1—B HISTORY AND SIGNIFICANCE

The Ising model has proven hugely fruitful; even today it still underpins our theory of ferromagnetic phase transitions and second-order phase transitions in general. It was recently referred to in the literature, somewhat whimsically, as the "hobbyhorse" of magnetic systems [3]. Around a decade after its conception, Rudoplh Peirles showed to the Philosophical Society of Cambridge that the Ising model must undergo a order–disorder phase transition in two-dimensions, thus suggesting Ising's claims were erroneous outside of one-dimension [4].

In an impressive feat, Lars Onsager provided analytically the solution to Ising's two-dimensional model of ferromagnetism in the absence of an external magnetic field, showing that a second-order critical point does exist, and thus explaining the sudden change in magnetisation when temperature crosses the critical point [5]. The model was used by Leo Kadanoff to study scaling laws near the critical point [6, 7], which expanded on previous study of thermodynamic observables near critical points—namely the work of Ben Widom [8–10]. Then, more formally, Kenneth Wilson proposed that second-order phase transitions should be understood through a scheme known as the Renormalization group [11, 12]. Wilson was awarded the 1982 Nobel prize in Physics "for his theory for critical phenomena in connection with phase transitions" [1]. The Ising model has also been used to as a tool for teaching the renormalization group [13].

Even in recent years, the universality of the of the Ising model has seen it used in understanding both magnetic systems and other seemingly disparate systems. Some examples include the evolution of alloys under radiation [14], critical behaviour of ferromagnets [15], socio-economic models of opinions, urban segregation and language change [16], image processing [17], ecological populations [18], integrated circuit performance in computation [19] and even—perhaps most bizarrely—the dynamics of

---

[1]See https://www.nobelprize.org/prizes/physics/1982/wilson/facts/ for more information.

traffic lights in the grid-like city of Kyoto, Japan [20]. An Ising spin network has even been realised using optical parametric oscillator systems [21].

Another active area of research involves machine learning studies aiming to identify critical points and phases in systems that undergo phase transitions [22–26]. Here the Ising model is a useful tool in the training and testing of such models.

1.1—C SOME BASICS

Despite the impressive reach of the Ising model into seemingly disconnected areas, its Hamiltonian in incredibly simple. Generally speaking, one considers a system of N spins on sites of a regular lattice—for example the square lattice—which are uniformly immersed in a thermal bath of temperature T (see Figure 1.1). Each spin interacts with its four nearest-neighbours in a fashion described by the Hamiltonian

$$H = -J \sum_{i,j} S_i S_j, \tag{1.1}$$

where $J > 0$ is a ferromagnetic coupling constant that sets the energy of the nearest-neighbour interactions, i indexes each spin in the system and j the nearest neighbours of each S_i. The spins may take integer values of $S_i = \pm 1$, thus, when all the spins are

Ordered	Disordered

Thermal bath: $T \ll T_c$ Thermal bath: $T_c \ll T$
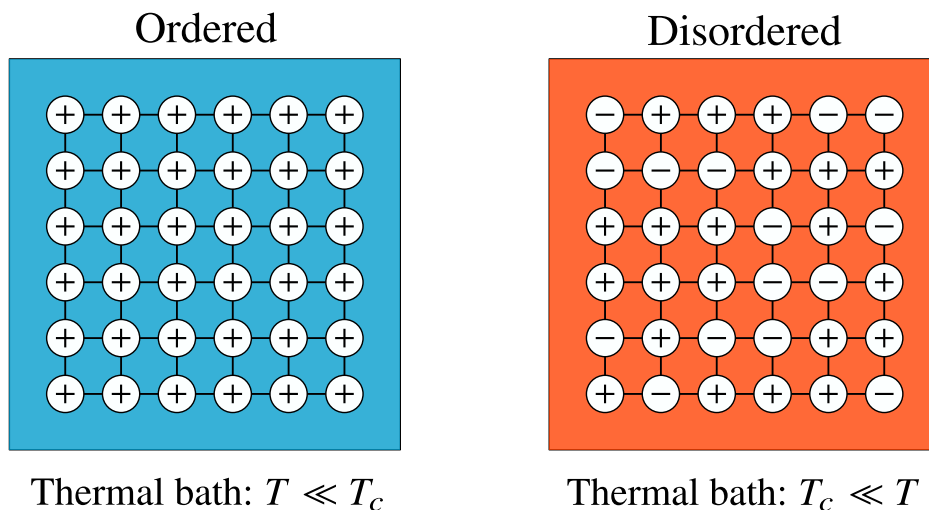
FIGURE 1.1 – 6×6 square-lattice Ising ferromagnets below and above the critical temperature, T_c.

aligned the system is in its ground state.

As always, the partition function is

$$Z_N = \sum_i^N e^{-\beta E_i}, \tag{1.2}$$

where E_i is the energy of each of the N system constituents. If one successfully computes the partition function, they can subsequently obtain expectation values of all thermodynamic observables. The probability of finding the system in a given state is given by the Boltzmann distribution, which is

$$P_B = \frac{1}{Z_N} e^{-\beta E_i}, \tag{1.3}$$

where E_i is the energy of the state, and as usual the partition function normalises the Boltzmann distribution. On the square lattice, Lars Onsager derived an analytical expression for the free energy which, to cut a long story short, becomes singular at a critical temperature

$$T_c = \frac{2J}{k_B \ln\left(1 + \sqrt{2}\right)} = 2.269 \text{ Jk}_B^{-1}. \tag{1.4}$$

It is a good point to note here that we deal in these reduced temperature units when working with the Ising model; Boltzmann's constant has the units of energy per temperature, so J/k_B still gives units of temperature. At the critical point, first order thermodynamic properties exhibit step functions between ordered and disordered phases, and second order properties diverge at the critical point. For example, the magnetisation and the magnetic susceptibility are

$$M = \frac{1}{\beta} \frac{dZ_N}{dh}, \tag{1.5} \qquad\qquad \chi = \beta \frac{dM}{dh}, \tag{1.6}$$

where h is an external magnetic field which, in this case, is zero [3, 27]. If at T_c, the slope of $M(T)$ diverges, then $\chi(T)$ must be singular. Another example is the internal

energy and specific heat capacity, which are (see Ref [3, 13])

$$U = k_B T^2 \frac{d}{dT} \ln(Z_N), \qquad (1.7) \qquad\qquad C = \frac{dU}{dT}. \qquad (1.8)$$

1.2 THE POTTS MODEL

1.2—A ORIGIN

The Potts model, which is as an extension of the Ising model, was also suggested as a problem for a PhD student—this time: Renfrey Potts—by supervisor Cyril Domb, and is in keeping with the eponymous naming convention of spin models [28]. An equivalent model, with four degenerate ground states, was studied by Ashkin and Teller in 1943, so it is sometimes referred to as "the Ashkin-Teller-Potts model" or "the Ashkin-Teller model" [29]. Furthermore, the model was also considered two years later in an independent study by Kihara *et al.* presented in Ref. [30]. For simplicity, we shall refer to this system as the Potts model in the thesis.

1.2—B SOME BASICS

The Potts model is a generalisation of the Ising model; in the Ising model spins had only two states available to them, up or down, whereas spins in the Potts model can be in q integer states. Or, in other words, spins may point in q distinct directions. In the Ising model diagram in Figure 1.1, the spins are denoted by ± 1, but in the Potts model the spin orientations are denoted simply the integers $S_i \in \{1, 2, \ldots, q\}$. Because of this change in the denomination of the spin types, the Potts Hamiltonian is normally written as a delta function. One way is

$$H = -2J \sum_{i,j} \left[\delta(S_i, S_j) - 1 \right], \qquad (1.9)$$

where $J > 0$ is again the nearest-neighbour coupling strength and δ is the delta function, i indexes each spin in the system and j the nearest neighbours of each S_i. Thus, misaligned neighbouring spins yield an energy contribution of $+2J$. The Potts model undergoes a phase transition at a critical temperature (see Refs. [31, 32])

$$T_c(q) = \frac{2J}{k_B \ln\left(1 + \sqrt{q}\right)}.$$ (1.10)

The phase transition of the Potts model comes with additional oddities which make it richer than the simple Ising model. For example: when $2 \leq q \leq 4$ the transition is second-order, and when $q > 4$ it is first-order.

1.3 THESIS OVERVIEW

Our brief discussion of spin models has so far focused only on *equilibrium* phenomena, where one varies the temperature of the system slowly—i.e. quasi-statically—meaning the system is always in thermal equilibrium. However, the behaviour of Ising and Potts systems in response to a *sudden* temperature change is markedly richer.

When cooled *suddenly*—i.e. quenched—the spins no longer have enough thermal energy to "escape" locally magnetised regions, which makes their time evolution more diverse, and allows them to "freeze" into a myriad of partially magnetised states. It is in these unexpected behaviours that my research focus lies: I examine the time evolution of two-dimensional Ising and Potts systems that undergo an extreme temperature change—from *infinite-* to *zero*-temperature. Here we delve into the realm of coarsening, or phase ordering kinetics, which occurs in Ising and Potts systems when they are quenched. We study this process using Monte Carlo computer simulations, which are methods that harness randomness.

Before we examine my work, we will first acquaint ourselves with coarsening in Chapter 2, and why people consider zero-temperature quenches, before reviewing the simulation methods one uses in order to study these systems in Chapter 3. We then

examine my studies of the relaxation time scaling of Ising ferromagnets in finite square-lattice geometries in Chapter 4, where I unveil a previously overlooked coarsening timescale. In Chapter 5, we will explore the late-time final states that persist when a triangular-lattice Potts model with only three spin states undergoes a deep quench to zero-temperature. Then, we shall continue our study of Potts coarsening in Chapter 6 by considering triangular-lattice Potts models with $q > 3$ spin states. In Chapter 7, we examine three-state Potts models on the square lattice with extended local interaction rules. Finally, we will conclude by summarising my findings in Chapter 8, and discussing potential lines of enquiry for future work.

COARSENING OF ISING AND POTTS MODELS

Coarsening in Ising and Potts models has been readily studied. In this chapter I review studies of zero-temperature coarsening in both the kinetic Ising and Potts ferromagnets. I give a brief introduction to coarsening in Section 2.1, and then discuss coarsening in the zero-temperature Ising model in Section 2.2. Finally, I discuss coarsening of Potts models in Section 2.3.

2.1 COARSENING

Coarsening occurs when an open system undergoes a local ordering process in response to a sudden environmental change; the system tends towards its equilibrium states until it achieves the maximum order allowed by conservation laws, thermal fluctuations, boundary conditions, and—to a lesser extent—local interaction rules [33]. It generally occurs when a system is driven *abruptly* across a phase transition. That is, when some external control parameter such as temperature is varied *suddenly*—and not quasi-statically [34].

The approach to equilibrium is not instantaneous, and there are generally associated features including domain formation, growing lengths, and scaling behaviours such as power law growths and decays. Early studies of coarsening focused on how the

evolution of interfaces was curvature driven and the motion of domain walls, both in continuum systems and in Monte Carlo simulations [35–37].

As a system coarsens, it tends towards its equilibrium states in a fashion that is not spatially uniform: different regions may tend towards different degenerate ground states, and these patch-like regions are known as domains. The universality of a coarsening systems is expressed in the growth of the domains. The domain length is intrinsically connected to all other statistical properties of the system, and the exponent governing the domain growth tells one information about the quenched system which is universal to other systems that exhibit the same exponents. The general idea of universality in a quenched system is that the statistical properties of systems with the same dynamical exponents are universal.

In order to study coarsening in kinetic spin systems, one generally prepares their system of choice in a physically appropriate initial condition, and then *suddenly* places it in contact with a thermal bath of significantly lower temperature. Local interactions cooperatively promote consensus in the orientation of the spins, while thermal noise attempts to randomise them. The idea of instantaneously cooling the system allows one to purely study the coarsening process, without interference from artefacts of the quenching procedure [38].

In the study kinetic ferromagnets people often consider zero-temperature quenches because the characteristics are universal, the results more crisp, the numerics less cumbersome, and, perhaps, the zero-temperature limit will allow analytical simplifications [38].

2.2 ISING SPIN SYSTEMS

Here I review previous work on the zero-temperature Ising model, of which our understanding begins with Roy. J. Glauber in one spatial dimension.

2.2—A   ONE-DIMENSION

In his seminal 1963 paper, Roy. J. Glauber presented analytically a time dependant means of studying the Ising Model that is commonly known as Glauber dynamics [39]. Glauber assigned kinetic transition rates to spin-flip events on the basis of their associated energy change, thus allowing study of the non–equilibrium time evolution of the system. Glauber solved this model in one dimension, showing that, at zero-temperature, the ground state is *always* reached and the number of interfaces—or meeting points between domains of opposite spin—decays in time as $t^{-1/2}$ [39].

In one dimension, the domain length distributions of Ising and Potts models have also been studied analytically, and the time to reach the ground state grows as $\sim L^2$, where L is the length of the system [40, 41]. Other studies of the zero-temperature Ising model in one dimension have examined slow coarsening due to ferromagnetic nearest-neighbour and competing antiferromagnetic n_{th}-neighbour interactions [42], where there is a slow temporal approach to the ground state of $1/t^n$ [42], as well as the driven dynamics of spin-exchange Ising chains [43]. A ferromagnetic-antiferromagnetic phase diagram that considers the density of active bonds and local update rules in the one-dimensional Ising chain is presented in Ref. [44].

2.2—B   TWO DIMENSIONS

Here I focus on two-dimensional Ising coarsening, which is most relevant to the research presented in this thesis.

2.2—B.i   *Dynamical scaling*

Perhaps the most significant contribution to understanding the evolution of the Ising model in two-dimensions at zero-temperature came from Alan Bray [45, 46]. The evolution is generally understood within the framework of the so-called *dynamical scaling hypothesis* [46]. Alan Bray's work on dynamical scaling in Ising models was

built upon previous numerical and experimental work examining scaling and coarsening phenomena in binary alloys, binary fluid mixtures and spin systems [47–52].

The beauty of this theory comes from its simplicity; the dynamical scaling hypothesis states that the entire coarsening evolution of the system is governed by a *single* relevant process: the growth of a characteristic length $R(t)$, which is the average domain size [45, 46]. When the Ising model is quenched from an initial temperature $T_i \gg T_c$ to a temperature $T_f \ll T_c$, it progresses from a symmetric unmagnetised initial state to an ordered final state. Throughout this ordering process, magnetic domains nucleate and grow in area as the square root of time, before ultimately spanning the linear dimension of the system. More generally, the domain growth is said to be governed by a so-called dynamical exponent z, ergo $R(t)$ scales as

$$R(t) \propto t^{1/z}.\tag{2.1}$$

The study of the dynamical properties of quenched systems is generally circumscribed to the time evolution of two-point same-time correlation functions, which may be written as

$$C(r,t) = \langle S_0 S_r \rangle.\tag{2.2}$$

The correlation function is essentially the expectation value of the product of spin variables that are separated by distances r, and provides a measure of the probability that they are aligned. Thus, it also gives a measure of $R(t)$, and is actually related to $R(t)$ through

$$C(r,t) = G\left(\frac{r}{R(t)}\right) \equiv G\left(\frac{r}{t^{1/z}}\right),\tag{2.3}$$

where G is some unknown function. The reason the correlation functions give a measure of $R(t)$ is that spin products taken *within*—that is, $r < R(t)$—the typical domain size are essentially always positive because the spins are aligned, whereas products with spins outside—i.e. $r > R(t)$—average to zero, and are therefore uncorrelated. In order to show that this dependence is true, one may simply measure the average correlation

over many realisations at fixed points in time, and plot it against a rescaled horizontal variable $r/t^{1/z}$. In doing this, they should notice that the correlation functions collapse onto a universal curve, thus showing Equation 2.3 to be true. Alan Bray, in an extension of previous studies of dynamical scaling phenomena, demonstrated this as a way in which to understand domain growth in the Ising model: by obtaining a data collapse in the correlation functions against a rescaled horizontal variable of $r/\sqrt{t}$, Bray showed that the typical domain size grows as $\sqrt{t}$—i.e. $z = 2$ [45, 46].

This also tells us something about the energy of the system; since the residual energy in a zero-temperature quench comes from interactions between the domain walls, the total length of which is $\sim R(t)$, it is natural to expect the energy to decay as $R(t)$ grows [45]. In Ref. [45], one can see that the energy, $E(t)$, is linear with $1/t^{1/z}$.

In the regime where the typical domain size $R(t)$ is comparable with the linear dimension of the system, we say the system has left the dynamical scaling regime and at such times the domain growth saturates.

When the quench is from $T_i = \infty$ to $T = T_c$, the exponent is roughly $z = 2.15$, and when $T_i = T_c$ and $T_f = 0$, $z = 2$. It is also worth mentioning that when the quench is from an initial temperature $T_i = \infty$ to a final temperature $T_f = T_c$, the correlation functions take the form

$$C(r, t) = r^{-(d-2+\eta)} G_c \left(\frac{r}{\epsilon(t)} \right), \tag{2.4}$$

where d is the spatial dimensionality of the system, $\eta = 1/4$ for the two-dimensional Ising model and $\epsilon(t)$ is the non-equilibrium correlation length [45, 46].

In general, people seem to have tacitly assumed that the ultimate fate of the zero-temperature Ising model in two-dimensions is to *always* reach the ground state after leaving the dynamical scaling regime. We shall discuss the validity of this assumption in the following.

2.2—B.ii *Late time surprises*

After the work of Alan Bray, the zero-temperature coarsening of the kinetic Ising model was thought fully understood. From a symmetric and unmagnetised initial state, magnetic domains nucleate and grow in length as the square root of time, before ultimately engulfing the system—however, the dynamics is richer still.

Around twenty years ago, a Boston University graduate student named Victor Spirin was studying the zero-temperature Ising model under his thesis advisor, Sid Redner [53–55]. Spirin noticed some anomalous relaxation features in the zero-temperature Ising evolution which were initially treated with suspicion. It then transpired that these features were in fact genuine, and Spirin *et al.* had stumbled across a remarkable and deep connection between the dynamics of the Ising ferromagnet and critical continuum percolation [53, 54]—though this realisation was made in work that came years later [56–58].

The first surprise—"frozen" two-stripe states,which span only a single lattice dimension and are forever trapped at constant energy—occurred with a probability of roughly 34%. Furthermore, the ground state was only reached on a timescale of $O(L^2)$ around 62% of the time, with L the linear dimension of the system [53, 54]. Perhaps most interestingly, "diagonal winding" configurations occurred with a probability of $\approx 4\%$, and ultimately decayed to homogeneity on an estimated timescale of $O(L^{3.5})$.

The reason, perhaps, that Spirin noticed these behaviours when few others did is that studies of phase ordering kinetics in the Ising model typically focused on the regime where $R(t) \ll L$, so they could study unrestricted coarsening—that is, coarsening in the regime were the boundary conditions or size of the system could not influence the domain growth. Other people were aware of the stripe states, but never rigorously investigated them [1].

Example realisations from my own simulations of the various behaviours discovered

---

[1]Leticia Cugliandolo informed me in a private communication that she knew of others who were aware of the stripe features prior to the work of *Spirin et al.*

$$t = 10^{-3}L^2 \quad t = 10^{-2}L^2 \quad t = 10^{-1}L^2 \quad t = T_F$$
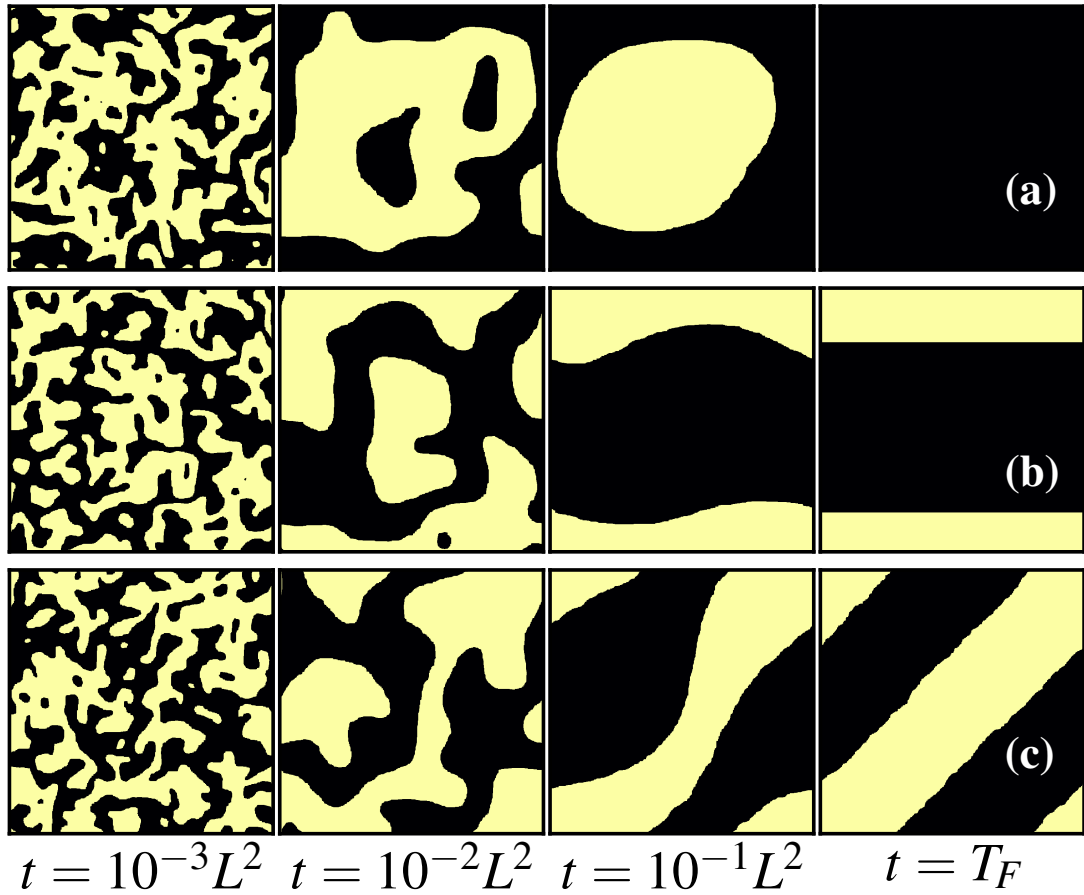
FIGURE 2.1 – Snapshots of zero-temperature coarsening on periodically bounded square lattices of 1024^2 spins for realisations reaching (a) a ground state, (b) a frozen two-stripe state and (c) a long-lived diagonal winding configuration. The latter snapshots in (a) and (b) are the final states, reached at $T_F \approx 0.33L^2$ and $T_F \approx 0.48L^2$ respectively, while the latter snapshot in (c) was terminated early at $T_F \approx 10.01L^2$.

by Victor Spirin are shown in Figure 2.1 (a)–(c). In Figure 2.1 (a), the realisation coarsens directly to the ground state. In Figure 2.1 (b), the system reaches a "frozen" on-axis two-stripe state. By "frozen", I mean the system is forever trapped in this metastable configuration—i.e. there are no flippable spins and the energy remains at a constant value greater than the ground state energy. In Figure 2.1 (c) the system falls into a long-lived off-axis winding configuration, which, although halted early in this example, ultimately undergoes a slow decay to homogeneity.

It is import for the reader to note the topology of each of the realisations shown in Figure 2.1. Recall that the system has *periodic* boundary conditions—i.e. the right hand neighbour of the rightmost spin in a given row is the leftmost spin in the same row, and

the same is true for spins on the "top" and "bottom" of the system. In other words, the system has the topology of a torus.

By inspecting the right-hand panels only, we see that in (a) the surviving domain winds around the lattice in *both* lattice directions, and in (b) *both* domains wind in a *single* direction only. In (c), *both* domains wind the lattice in *both* lattice directions. These realisations are therefore topologically distinct.

2.2—B.iii   *Continuum description*

An alternative description of zero-temperature Ising coarsening exists in the form of Ginzburg-Landau theory [46, 57]. Consider a coarse-grained order parameter field, which is the magnetisation density ϕ. The Ginzburg-Landau free energy surface

$$F[\phi] = \int d\phi \left\{ (\nabla \phi)^2 + V(\phi) \right\} \tag{2.5}$$

suitably describes the ordered phase of the Ising system. In the case of a non-conserved order parameter, the magnetisation density evolves as the time-dependent Ginzburg-Landau (TDGL) equation

$$\frac{\partial \phi}{\partial t} = \nabla^2 \phi - V'(\phi), \tag{2.6}$$

where $V(\phi) = \frac{1}{2} \left(1 - \phi^2 \right)^2$ is the classic double-well potential (see Figure 2.2).
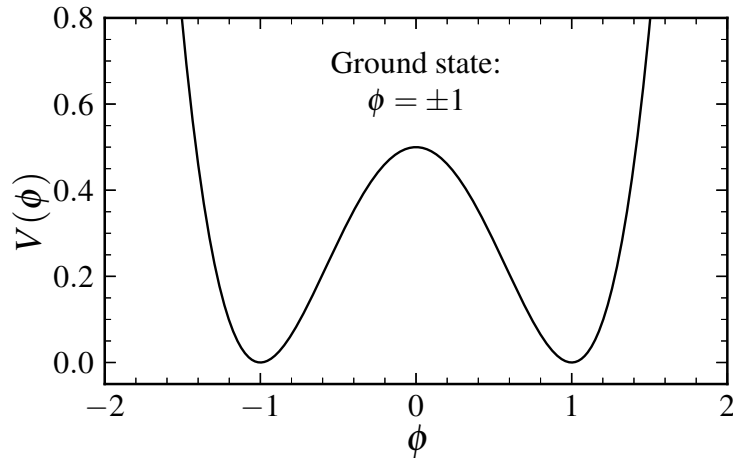
FIGURE 2.2 – Typical form of the double-well potential $V(\phi) = \frac{1}{2} \left(1 - \phi^2 \right)^2$.

The time evolution of Equation 2.6 provides an alternative description of the zero-temperature Ising coarsening process. It is exactly this equation that was used in Ref. [57] to confirm the authors belief in the connection between continuum percolation and the Ising model, and also to show that this phenomenon is general to curvature driven coarsening and not just a feature of the zero-temperature Ising model.

While similar in nature, the coarsening domain mosaics that arise in the evolution of the TDGL equation are even more beautiful than those in the Ising model. I show examples from my simulations of the TDGL equation, specifically realisations that reach the three most common topologies of critical percolation, in Figure 2.3 (a)–(c).

The reader should now compare the realisations in both Figure 2.1 and Figure 2.3

$$t = 1.49 \qquad t = 2.48 \qquad t = 19.80 \qquad t = 301.27$$
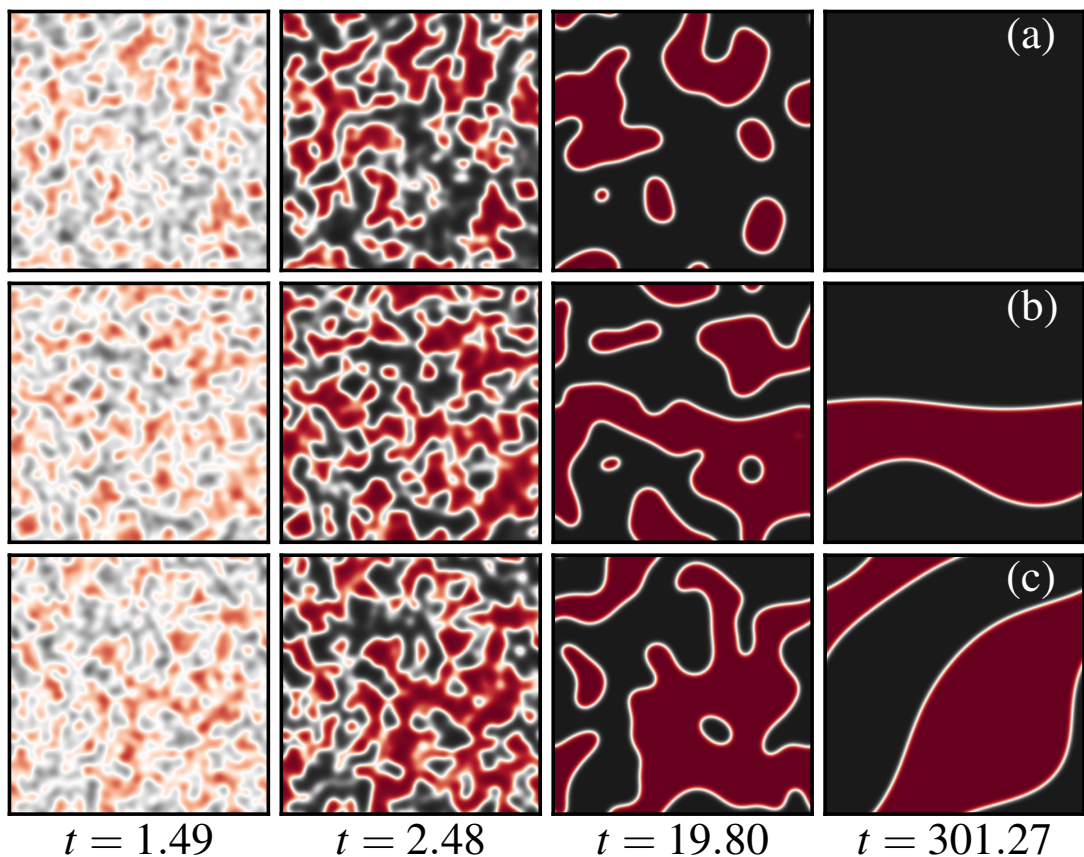
FIGURE 2.3 – Snapshots of coarsening in the time-dependant Ginzburg-Landau evolution (Equation 2.6) for realisations reaching (a) the ground state, (b) stripes that wind in a single dimension only and (c) stripes that wind in both dimensions. The initial conditions are randomly ordered configurations of zero magnetisation and the times are in arbitrary units.

as it is helpful to observe the similarity in these systems, particularly the topological nature of the examples shown.

2.2—B.iv   *Percolation in Ising coarsening*

There exists a deep connection between the zero-temperature dynamics of the Ising ferromagnet and continuum percolation, which explains the emergence of various topologically distinct behaviours and is the subject of this subsection. This connection between the *equilibrium* phenomenon of site percolation and the *non-equilibrium* dynamics of the zero-temperature Ising ferromagnet allows the precise conjecture of the probability of reaching the various topologies that arise. However, before we explore this connection, we first must familiarise ourselves with the problem of percolation.

2.2—B.v   *Percolation*

Percolation is concerned with connectivity within systems—do connected paths within systems exist, and do they span the system [59–63]? Site percolation on the square lattice with open boundary conditions is a classic example. The problem of percolation is simple to describe: consider our openly bounded square lattice of $L \times L$ "empty" sites. In order to study percolation, we "populate" each site with probability p, and otherwise leave sites empty with probability $(1 - p)$ [59, 64]. Each site is connected to its four adjacent sites, i.e. the North, South, East and West neighbours, and occupied neighbouring sites form clusters.

In the continuum limit, or infinite lattice case, the probability of finding a giant spanning cluster is unity when the fraction of occupied sites is above a critical value p_c, and zero when the occupation probability is less than p_c [59]. That is, when $p < p_c$ there is *never* a giant spanning cluster, and when $p > p_c$, there is *always* a giant spanning cluster. Examples of percolation below, roughly at, and above critical percolation are shown in Figure 2.4 (a)–(c); the top snapshots show the actual binary microstates and the bottom show the images labelled used the Hoshen-Kopelman algorithm, which is an

$$p/p_c = 0.950 \qquad p/p_c = 1.003 \qquad p/p_c = 1.050$$
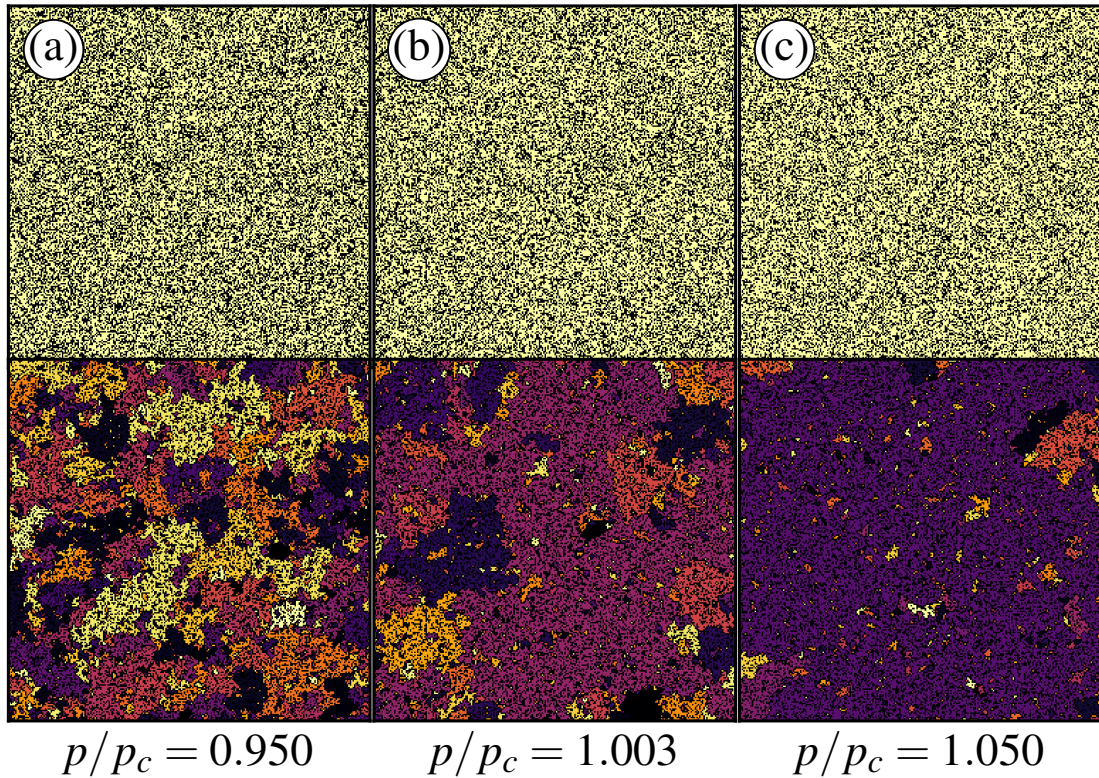
FIGURE 2.4 – Top: percolation snapshots (a) below, (b) roughly at and (c) above criticality. Bottom: cluster labelling of top—occupied neighbouring sites form clusters which, when labelled by colour, reveal the presence of spanning clusters (or not in the case of (a)). The lattices contain 2^{16} sites that are randomly populated with probability p.

efficient cluster labelling scheme, applied to the configurations [65]. If a cluster touches both of two opposite edges of the system, it is said to span in that direction [II].

As is the case with the equilibrium transition of the Ising model in two-dimensions, the transition between zero and non-zero in the spanning probability is spontaneous at the critical point in the limit of $L \to \infty$, where L is the length of system. In finite systems the probability of finding a giant spanning cluster P_∞ exhibits a sigmoidal-like behaviour as a function of the occupation probability. (see Figure 2.5 (a)).

Critical percolation occurs when the occupation probability is *exactly* equal to p_c [59, 64, 67], which, on the square lattice, is $p_c = 0.59274$ [67]. At p_c, in the continuum limit, the situation is even richer—in the case of open or free boundary

---

[II]An alternative scheme for identifying percolating clusters is the "burning algorithm" proposed by Hans Herrmann, which involves setting occupied edge sites *ablaze* and allowing the fire to spread through nearest-neighbour contact [66]. Should the fire span the system, a spanning cluster exists.
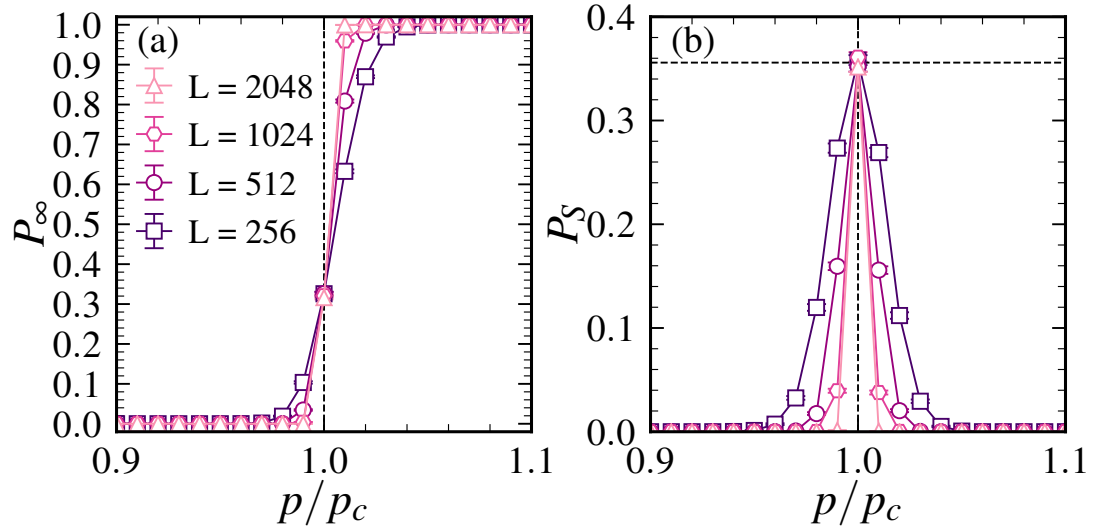
FIGURE 2.5 – Probability of a cluster spanning in (a) *both* and (b) a *single* lattice dimension versus the fraction of occupied sites p; as the system size (L) increases, the transition of P_∞ approaches a step function and P_S—which is the probability of spanning in a single dimension only—approaches a delta function. The probability estimates are based on 10^4 trials.

conditions, clusters may span in two ways: across a single lattice dimension, or both lattice dimensions [56, 57]. The probability of finding a cluster spanning only a single lattice dimension, with open boundaries, is $P_S = 0.3558$ [56, 57]. The probability of finding a cluster spanning in only one dimension is plotted as a function of the occupation probability in Figure 2.5 (b). As L increases, P_S approaches a delta function.

However, in the study of percolation—and kinetic ferromagnets—people also consider *periodic* boundary conditions, which further complicates the situation. A square lattice with periodic boundary conditions is equivalent to wrapping the square lattice around a torus. On the torus, the *winding* nature of clusters is considered, rather than whether or not they span the system. At criticality, clusters can wind in a host of topologically distinct ways [60–62]. The four most common examples are shown in Figure 2.6 (a)–(d).

The spanning nature of the clusters shown in Figure 2.6 (a)–(d) are distinguished by so-called winding numbers: (a, b). A cluster of winding number (a, b) winds a times horizontally (toroidally) and b times vertically (poloidally). Clusters of winding numbers (a, b) and $(-a, -b)$ are equivalent so we set $a \geq 0$ (see annotations in Figure 2.6).
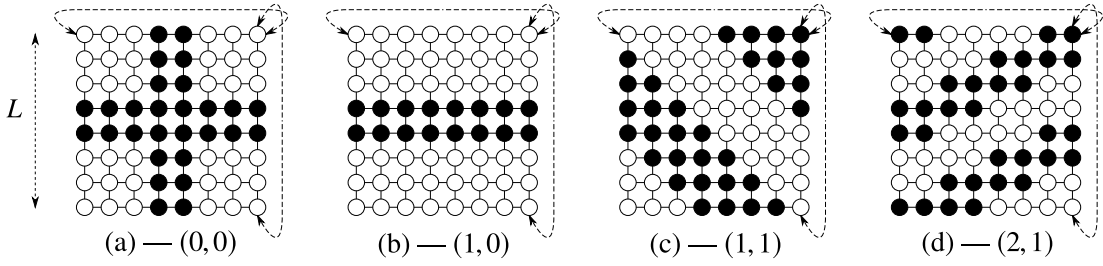
FIGURE 2.6 – Common spanning topologies of percolation on the torus. (a) A single cluster winds the torus in both lattice directions. (b) Two clusters wind the torus in a single lattice dimension only. (c) Both clusters wind the torus in both lattice directions. (d) Both clusters wind twice horizontally and once vertically.

A further simplification I employ is as follows: winding configurations $(1, 0)$ and $(0, 1)$, as well as $(1, -1)$ and $(1, 1)$, are equivalent in probability, so I restrict the notation to only $(1, 1)$ and $(1, 0)$ only etc.

The crossing probabilities of critical continuum percolation on the torus, or periodically bounded square lattice, are exactly known (see Refs. [57, 61]), and are:

$$P_{(0, 0)} = 0.6180, \tag{2.7}$$

$$P_{(1, 0)} + P_{(0, 1)} = 0.3388, \tag{2.8}$$

$$P_{(1, \pm 1)} = 0.04196, \tag{2.9}$$

$$P_{(2, \pm 1)} = 0.0001567. \tag{2.10}$$

These probabilities will become relevant in the following. Higher order winding configurations are also possible, but they occur a probability so small that they will essentially never be observed; for example: $P_{(3, \pm 1)} = 4.438 \times 10^{-9}$ [57]. An interesting point of note in the diagonal stripe configurations is that the winding numbers need to be relatively prime—that is coprime—in order to actually fit the system. Demonstrating this graphically should prove an interesting exercise for the reader.

2.2—B.vi   *Ising connection to percolation*

Around seven years after the work of Victor Spirin, the presence of critical percolation in the Ising model was first realised [58]. Later still, Barros *et al.* [56] proposed an elegant and simple explanation for both *how* the final state of the Ising model is decided and *why* each unique behaviour occurs with its respective probability. This work built upon the key observation made in Ref. [58], where the authors showed that continuum percolation occurs in curvature driven coarsening. First, we must notice that the topologies of the final states in Figure 2.1 are the same as the three most common topologies of critical continuum percolation on the torus.

It transpires that there is a direct one-to-one mapping between the probability of finding each of the topologically distinct behaviours in the Ising model and critical continuum percolation. This connection was presented in a beautiful letter by Barros, Krapivsky and Redner. [56]. The argument they present is summarised in the following.

Within a short time, the microstates in zero-temperature coarsening seemingly become realizations of critical percolation [56–58, 68–72]. As functions of the aspect ratio of the system, the forms of the crossing probabilities are known [61, 62, 73, 74]. Thus, by realizing the dynamics of zero-temperature Ising ferromagnets with various aspect ratios for both open and periodic boundary conditions, and measuring the resulting crossing probabilities, the authors were able to show the one-to-one mapping between the crossing probabilities in the Ising model and critical continuum percolation [56].

Around three years later, Olejarz, Krapivsky and Redner confirmed the connection between the curvature driven coarsening of the Ising ferromagnet and critical continuum percolation [57]. They observed (2, 1) winding configurations, which had previously remained unseen in the Ising model, and also demonstrated the connection to critical percolation in a TDGL equation that described zero-temperature Ising coarsening—thus showing the phenomena to transcend specific models. Additional information, along

with some examples from my own simulations of the TDGL equation are shown in Section 2.2—B.iii.

2.2—B.vii   *Further studies*

Since the discovery of critical continuum percolation in bi-dimensional kinetic spin systems that exhibit curvature driven coarsening (Refs. [38, 56, 57]), the role of percolation has been studied quite extensively—excellent reviews of which have been given by Leticia Cugliandolo in Refs. [33, 75, 76].

Percolation influences the scaling regime; people have shown that after a very short time span, coarsening configurations resemble ones at critical percolation; the morphology and statistical properties of domain structures that are are larger than average are those of critical percolation [58, 77]. This connection has also been confirmed on the triangular lattice geometry [70]. The existence of a percolating growing length has been shown to extend the dynamical scaling hypothesis, meaning the statistical properties of the system should be rescaled by the percolating domain length [69].

Other studies have focused on the so-called "fate sealing" time by examining how the formation time of the dominant late-time topology scales with system size [69, 78]. Studies that examine critical percolation in spin exchange models have shown that temperature has essentially no influence on the timescale associated with the growth of the percolating domain t_p [72]. The time evolution of so-called hull areas and perimeters have also been studied [58, 77, 78].

The role of percolation in the coarsening of a disordered Ising ferromagnet, with random fields and random bonds, has also been investigated, thus showing the percolation phenomenon extends into the realm of disordered systems, and not just the clean zero-temperature case [79]. The influence the choice of dynamics has on the approach to percolation has also been studied [80]. Critical percolation and dynamical scaling have been examined in the slow cooling of the Ising ferromagnet [81].

Critical percolation has also been observed in the square-lattice Voter model, where the dynamics do not satisfy detailed balance, and the approach to percolation grows as $\sim L^{1.66}$ [71, 82]. Freezing in Ising ferromagnets with asymmetric energetic interactions has also been studied, showing richer final states [83].

There is also numerical evidence in favour of a so-called *hyper-universality* hypothesis, which states that the scaling functions of the correlation functions are independent of weak disorder [33]. That is, the length-scales influenced by weak disorder should be considerably shorter than the growing length $R(t)$ [33]. Favourable numerical evidence has been presented from work on Ising models [84–86], and other dynamical models [87]

2.2—B.viii   *Examples in other systems*

Universal coarsening features found in the Ising model occur in a diverse range of systems. Dynamical scaling has been observed in the growth of magnetic domains during quenches of binary Bose gasses [88–92], in optical parametric oscillator systems [93] and binary liquids [94]. Domain percolation has also been studied in Bose gasses [95].

The evolution of two bacteria species competing for survival has also been shown to exhibit universal characteristics found in the zero-temperature Ising model [96], and dynamical scaling has been demonstrated in natural swarms of insects [97]. There are a huge number of related systems given as examples in an editorial in *Comptes Rendus Physique* [34]—some of which include (see Ref. [34] and references therein): motion in bird flocks, bacterial systems, social science applications such as finance and opinion making and sustained reactions in chemistry, etc. . . .

2.2—C   HIGHER DIMENSIONS

The late-time final states that emerge in the zero-temperature coarsening of the three-dimensional Ising ferromagnet are bizarre. They are topologically complex configurations with perpetually blinking spins and have been referred to in the literature as
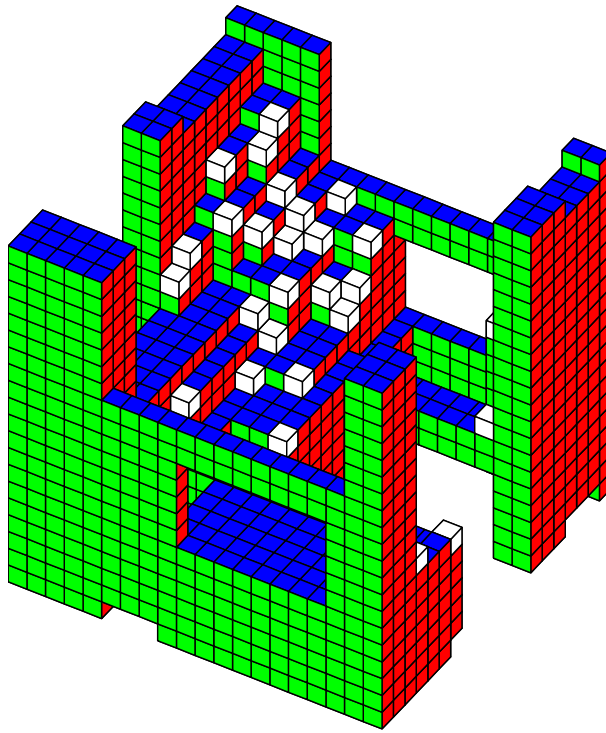
FIGURE 2.7 – A snapshot of a late time blinker domain in a zero-temperature cubic-lattice Ising model of linear dimension $L = 20$. The white spins have 3/6 aligned neighbours and are thus freely flippable. This Figure is from Ref. [99] and was provided in high resolution by Sid Redner.

"gyroid" and "plumbers nightmare" states [57]. An example of such a configuration is plotted in Figure 2.7, where the blinker spins are highlighted in white.

The probability of reaching the ground state is zero in all but the smallest system sizes [54, 98, 99], and it decays rapidly as the linear dimension of the system is increased. Other evidence suggests this trend of finding only complex, non-static, non-ground final states extends beyond three spatial dimensions [100, 101].

2.3   POTTS SPIN SYSTEMS

Studies of coarsening in Potts models from the 1980's onwards are seemingly more abundant than those of Ising systems, which is probably because of the increased number of readily available applications. Here I will review some of these studies and the reasons for studying coarsening in Potts models.

2.3—A GENERAL COARSENING STUDIES

One common application of zero-temperature Potts models involves understanding coarsening in two-dimensional soap froths; the ordering dynamics of a square lattice Potts model with second-nearest-neighbour interactions at zero-temperature has been compared experimentally with coarsening in a soap froth, thus showing the domain/bubble growth to exhibit the same universal features with small deviations due to the effects of thermal equilibration and anisotropy [102, 103].

Potts models have also been used to understand soap froths in thee spatial dimensions, where it was shown with the Potts model and soap froth analogues, the correlation functions, number of "bubbles" and domain size become constant at late time [104].

Coarsening in the Potts model has also been used as an analogue for understanding grain growth and magnetic domains [105–110], cellular tissue growth in biological systems [111, 112] and other natural tilings [113]. The time scaling exponents for the average domain radius have been studied in both two and three dimensions, and found to scale as roughly $t^{1/2}$, though it does matter what time regime of the simulation one examines these data [114].

Slow relaxation in the kinetic Potts model has been studied [115], as well as other coarsening features such as the domain growth and "pinning effects" that occur with $q \geq 3$ [116]. In Ref. [116] the authors actually noted that the pinning structures leading to slow relaxation were much more prevalent on the square lattice than on the triangular lattice. These structures will become very relevant in Section 2.3—B.

Other more recent studies have examined geometrical properties of the domains in the early time evolution after a zero temperature quench [117, 118], as well as domain nucleation during a shallow quench from a subcritical initial configuration [32].

An important point to note is that at very low subcritical temperatures, people realised that the model often becomes stuck in extremely long-lived metastable arrangements [119], and in the case of zero-temperature quenches, the ground state is rarely

reached and metastable stripe configurations arise [120, 121].

2.3—B FINAL STATES

After discovering the rich myriad of unexpected behaviours in the coarsening of the zero-temperature Ising model, the topologies of which govern the final state, it seems natural to explore what happens when one increases the degeneracy—i.e. the number of spin types / ground states—of the system. Though—as we have just seen—coarsening in Potts models had been studied much more extensively than in Ising models, there is still an apparent lack of studies that rigorously examine and quantify the final states at zero temperature.

When a q-state Potts model undergoes a supercritical quench to zero-temperature, each of the distinct spin states compete to survive the ensuing ordering process. The domain mosaics that arise are visually much richer than those of the Ising model, and even in only two-dimensions the emergent late-time final states are considerably more complex [122, 123].

Before the work I present in Chapter 5, the only dedicated study of the final states of the zero-temperature Potts model focused on the square lattice [122]. The first surprise is probably the rarity with which the ground state is reached, which, for $L \geq 192$ was roughly 10%. The majority of the time the system becomes trapped in frozen metastable tessellations, with both spanning and non-spanning domains, that have no flippable spins (we will examine these probabilities in more detail in Chapter 7).

The most curious findings on the square lattice however were so-called blinkers and pseudo-blinkers. Blinkers are configurations that forever wander at constant energy due to spins that may perpetually flip with no energy cost. Pseudo-blinkers are configurations that strongly resemble blinkers for orders of magnitude in time, before a sudden energy lowering flip triggers an "energy avalanche", where the system globally reorders and undergoes a macroscopic decline in energy. The authors of Ref. [122] suggested that the time taken for pseudo-blinkers to relax grows exponentially with the linear dimension

of the system, and determining if such evolutions could relax further was an extreme source of numerical expense.

The authors also considered a TDGL equation designed to describe zero-temperature Potts coarsening using a q-well potential [122]. In doing so, they found late-time hexagon configurations with varying numbers of clusters, along with octagonal and two-square configurations, none of which occurred in the square lattice Potts model.

In their conclusions, the authors noted that the effects of the lattice geometry are less strongly imposed on the dynamics if one considers the triangular lattice. This led them to speculatively pose two questions:

i. What is the extent of the universality between the square and triangular lattices if one considers a three-state Potts model?

ii. Is there some underlying simplicity that will emerge when the lattice coordination is an integer multiple of the number of spin states?

It is at this point that my work in Chapter 5 enters the picture; I investigate the final states of the zero-temperature Potts model on the triangular lattice, and address some of the questions posed in Ref. [122].

METHODS

The kinetics of the spin systems studied in this thesis are analytically intractable, meaning their kinetic evolution can only be studied numerically. In this chapter I cover the information underpinning the numerical methods I use in my simulations.

I first review the lattice geometries I use—including their numerical representations, boundary conditions and relevant initial conditions—in Section 3.1. I then briefly discuss the principle of detailed balance, and how any methods used *must* obey it, in Section 3.2. I then review some common algorithms that are often used in the simulation of spin systems at thermal equilibrium in Section 3.3.

I introduce the common choices of dynamical evolution rules used in the simulation of non-equilibrium dynamics in Section 3.4. I then explain the algorithms used to implement these dynamical evolution rules in Section 3.5. I first show how the "conventional method" is inefficient at low temperatures, and then introduce the so-called "*n*-fold" scheme that was developed to circumvent this issue. Finally, I summarise the chapter in Section 3.6.

3.1   LATTICE GEOMETRY AND INITIAL CONDITIONS

Throughout the work I present in this thesis I refer to two main lattice geometries, their boundary conditions and certain initial conditions; each of which the reader must be familiar with and are detailed in the following.

3.1—A   LATTICE GEOMETRIES

First, let us examine the two main geometries I use: the square and triangular lattices. The square lattice is as straightforward as is possible, and shown in Figure 3.1. Each site is "connected" to its four nearest-neighbours; thus we say the coordination number is four.
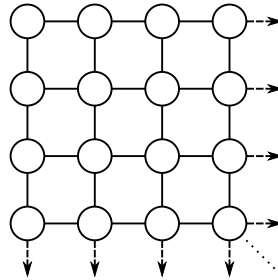
FIGURE 3.1 – Simple square-lattice geometry; each site is connected to its four nearest neighbours.

If one then takes a square lattice geometry and adds diagonal bonds to the North-West and South-East (or alternatively to the North-East and South-West) and treats every bond as equivalent, then they have a triangular lattice in disguise (see Figure 3.2 (a)–(b)).

At first this might seem a little peculiar, but it is done as a matter convenience numerically. So long as each of the nearest-neighbour bonds are treated equally, it makes no difference, however, the representation in Figure 3.2 (a) is the one used in showing snapshots of configurations later in this thesis, so it is important for the reader to be aware of this representation.
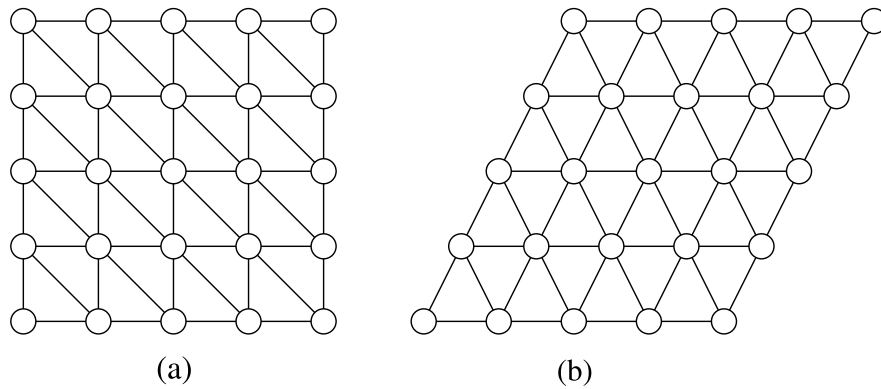
FIGURE 3.2 – Alternative representations of the triangular-lattice geometry. (a) Shows a scheme that is numerically convenient to employ and (b) a more visually realistic representation of the triangular lattice. Note in each case, the solid lines represent equivalent nearest-neighbour bonds.

3.1—B   BOUNDARY CONDITIONS

So far I have assumed that each site in the square and triangular lattice has the same number of neighbours, but if we look at the "edge sites" this is clearly not the case. To circumvent this issue, one normally considers periodic boundary conditions.

This means that the left-hand neighbour of the leftmost spin in a given row is the rightmost spin in the row, and vice versa. The same applies to edge sites in the "top" and "bottom" rows (see Figure 3.3). This is equivalent to wrapping the two-dimensional lattice around the surface of a torus.
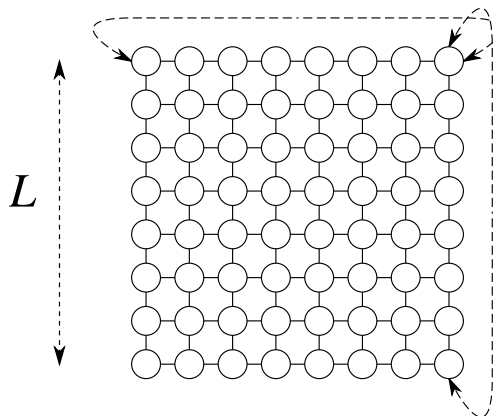
FIGURE 3.3 – Square lattice geometry with periodic boundary conditions. The nearest neighbours of spins on "edge sites" are spins on the other side of the lattice.

3.1—C INITIAL CONDITIONS

In almost all of my investigations I consider infinite–zero temperature quenches. Typically one approximates an infinite-temperature initial condition in two ways: by using a randomly ordered configuration or a so called antiferromagnetic configuration. Both of these are equally suitable in the sense that they are each symmetrically uniform and have no significant regions that are magnetised.

3.1—C.i   Random

To generate a "random" initial condition, I first populate a microstate with an equal number of each of the spin states and then randomly order the configuration. I ensure each spin state is initially equal in concentration to avoid the significant influence small biases in the populations can have on the final states one finds in small system sizes, thus making it, in a sense, a cleaner alternative to simply pointing each spin in a random direction.

3.1—C.ii   Antiferromagnetic

The antiferromagnetic initial condition is exactly as the name suggests: a perfect antiferromagnetic ordering, where no spin has any aligned neighbours and the system is as unmagnetised as is possible. Or, in other words, the initial condition is an antiferromagnetic ground state. In the context of the Ising model, this means the initial condition looks like a chess board (see Figure 3.4 (a)). Interestingly, it is not possible to have an antiferromagnetic configuration with two spin-states on the triangular lattice, as shown in Figure 3.4 (b).

However, when we go on to study the Potts model—where the number of spin states is an integer number q—we see that it is possible to produce an antiferromagnetic ordering on both the square and triangular lattices (see Figure 3.4 (c)–(d)). If one seeks an antiferromagnetic initial condition using more than three spin states, the solution is
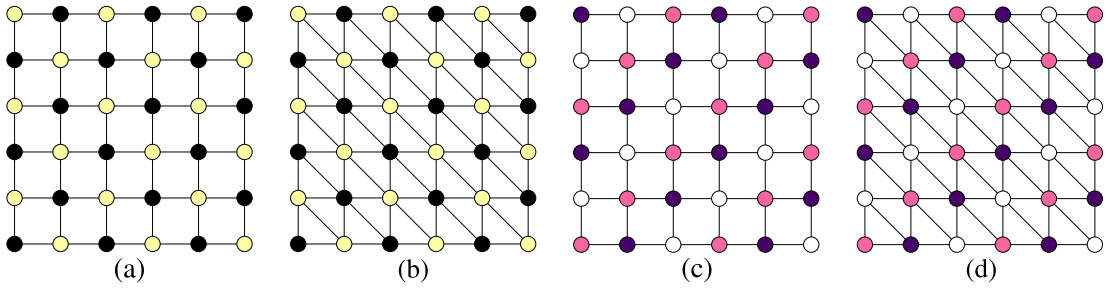
FIGURE 3.4 – (a) Two spin-state antiferromagnetic ordering on the square lattice. (b) Failure to to achieve an antiferromagnetic configuration with only two spin-states on triangular lattice. (c) Three-state antiferromagnetic tiling on the square lattice. (b) Three-state antiferromagnetic tiling on the triangular lattice.

simple; notice that in Figure 3.4 (a), the antiferromagnetic initial condition is simply an arrangement of diagonal stripes of alternating colour that run from the South-West to the North-East. In Figure 3.4 (c) this pattern of diagonal stripes is extended to use three colours. One can simply extend this further to use q colours.

3.2   DETAILED BALANCE

Before discussing simulation methods or dynamical evolution rules, we must be acquainted with the principle of detailed balance. Any transition rules assigned to spin flip events must satisfy this condition if thermal equilibrium is to be reached. In order words, at equilibrium, any thermodynamic process can be equilibrated by its reverse.

In order illustrate the principle of detailed balance, let us play the simple Monte Carlo "pebble game" [124], shown in Fig 3.5. Although conceptually trivial, the pebble game allows us to form a Monte Carlo algorithm that satisfies the detailed balance condition. In order to play the game, we require an algorithm that moves the pebble one step at a time, such that after a large number of iterations, it appears in each square with equal probability.

Naively, one may seek to realise this simple goal by throwing the pebble around randomly, however this would not yield the desired result. The pebble may move in any four directions, up, down, left or right. Consider the corner configuration (a).

(a)   (b)   (c)   (d)
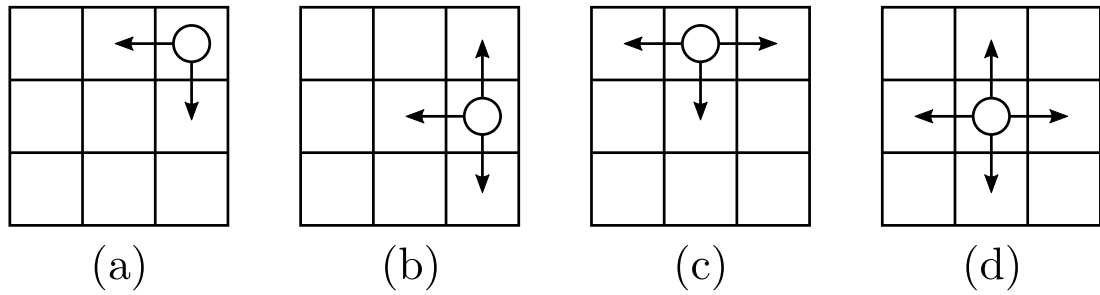
FIGURE 3.5 – The pebble game: the pebble may move in any direction, or not at all, so long as it stays on the grid.

(a) is connected to configurations (c) and (b), in that they are both one move away. Any algorithm we choose must generate configurations (a), (c) and (b) with equal probabilities $\pi(a) = \pi(b) = \pi(c)$.

The Monte Carlo algorithm is simply a list of transition probabilities denoted $p(a \rightarrow b)$ for moving from one configuration to another. There must also be a normalisation condition that says once at (a), the system may remain in configuration (a) or transition to either (b) or (c), i.e.

$$p(a \rightarrow a) + p(a \rightarrow b) + p(a \rightarrow c) = 1. \tag{3.1}$$

The two kinds of probabilities can be related by realising that configuration (a) can only be reached from (b), (c) or itself. Therefore

$$\pi(a) = \pi(b)p(b \rightarrow a) + \pi(c)p(c \rightarrow a) + \pi(a)p(a \rightarrow a), \tag{3.2}$$

which upon rearranging gives

$$\pi(a)\left[1 - p(a \rightarrow a)\right] = \pi(b)p(b \rightarrow a) + \pi(c)p(c \rightarrow a). \tag{3.3}$$

Solving Eqn. 3.1 for $\pi(a) - 1$ allows the former to be written as

$$\pi(a)p(a \rightarrow b) + \pi(a)p(a \rightarrow c) = \pi(c)p(c \rightarrow a) + \pi(b)p(b \rightarrow a) \tag{3.4}$$

This equation can be satisfied by

$$\pi(a)p(a \rightarrow b) \;=\; \pi(b)p(b \rightarrow a) \tag{3.5}$$

$$\pi(a)p(a \rightarrow c) \;=\; \pi(c)p(c \rightarrow a) \tag{3.6}$$

$$\vdots$$

thus we obey the detailed balance condition. This is because the probabilities for transitions between neighbouring sites are equal, and the probability of reversing the transition equals the transition probability itself.

If the pebble is thrown from the central site, it reaches another site with unit probability, as it can go in each of the four directions with probability 1/4. However, in the case of corner sites, there are only two available directions in which the pebble can be thrown and remain on the grid. Thus, in the configuration in Figure 3.5 (a): $\pi(a \rightarrow b) = \pi(a \rightarrow c) = 0.25$, and $\pi(a \rightarrow a = 0.50)$; in other words, the pebble moves to left with probability 25%, down with probability 25%, and stays put with probability 50%. The same is true of edge sites, however there are three possible directions the pebble may be thrown, so it only remains on the site 25% of the time.

If one invokes a simple Monte Carlo algorithm in order to demonstrate this, they indeed find that on average each site is occupied with probability 1/9. This would not be the case if the pebble was only thrown in allowed directions.

3.3 EQUILIBRIUM METHODS

Sampling spin systems computationally at thermal equilibrium is conceptually simple. Generally one begins from a given initial configuration, typically a randomly ordered microstate, and then visits each site of the lattice in regular or random order. Upon visiting each site, some update rule is applied to the spin that depends upon the bath temperature and the local environment of the spin—typically its nearest neighbour

configuration.

The rules for the acceptance and rejection of each move can vary depending on the particular algorithm of choice, however the equilibrium Physics should not. This is because any probabilities assigned to spin flip events must obey the principle of detailed balance [124]. In order to sample thermodynamic observables at equilibrium, it is desirable to take measurements from uncorrelated microstates only, therefore samples are typically taken at a frequency of once per grid sweep or less.

Common algorithmic choices include the Metropolis algorithm, the Heat Bath algorithm and the Wolff Cluster algorithm, which I now briefly review in context of the Ising model only [124, 125].

3.3—A   THE METROPOLIS ALGORITHM

The Metropolis algorithm was originally developed at Los Alamos National Laboratory, New Mexico, by Nicholas Metropolis *et al* in the 1950's [125]. It is perhaps the simplest algorithm used in the simulation of the equilibrium Physics of Ising spin systems [124, 126].

The implementation of the Metropolis Algorithm for the Ising model is as follows. Each lattice site is visited in random order in a single lattice sweep. Upon visiting each site, a spin flip is proposed and either accepted or rejected on the basis of the associated energy change. Therefore a site flips with probability

$$P(\Delta E) = \begin{cases} 1 \text{ if } \Delta E \leq 0, \\ \exp(-\beta \Delta E) \text{ if } \Delta E > 0 \end{cases} \tag{3.7}$$

where P is the probability that the site may flip, β is the Boltzmann factor and ΔE is the energy change associated with the flip. In order to determine if a site should flip or not numerically one employs random numbers. When a site is visited a uniform random number $r \in (0, 1)$ is generated and the spin is allowed to flip if $r < P$.

3.3—B   THE HEAT BATH ALGORITHM

The Heat Bath algorithm is an alternative to the Metropolis algorithm. Rather than accepting or rejecting proposed flips when sites are visited, spins are instead thermalised with their local environments [124]. In the presence of a nearest-neighbour field h, spins point up or down with probabilities

$$\pi_h^+ = \frac{\exp(-\beta E^+)}{\exp(-\beta E^+) + \exp(-\beta E^-)} = \frac{1}{1 + \exp(-2\beta h)}, \tag{3.8}$$

$$\pi_h^- = \frac{\exp(-\beta E^-)}{\exp(-\beta E^+) + \exp(-\beta E^-)} = \frac{1}{1 + \exp(+2\beta h)}. \tag{3.9}$$

Here E^+ and E^- are the energies corresponding to the spin pointing up or down respectively. The probabilities of orienting the spin up or down are normalised ($\pi_h^+ + \pi_h^- = 1$). Numerically this means the spin points upwards if $r < \pi_h^+$, and down otherwise, where $r \in (0, 1)$ is again a uniform random number. The implementation of the Heat Bath algorithm is then similar to that of the Metropolis. Lattice sites are visited in random order and the resident spin is oriented up or down based on the probabilities π_h^+ & π_h^-.

3.3—C   THE WOLFF CLUSTER ALGORITHM

The Wolff cluster algorithm is conceptually the most different of the three algorithms described. One first selects a spin at random at the seed of a cluster. One then allows the nearest neighbours of the seed site to join the cluster with probability P [127–129].

$$P = 1 - \exp(\beta J(1 + S_i S_j)), \tag{3.10}$$

where $\beta = (k_B T)^{-1}$, J is the coupling strength, S_i is the seed site and S_j one of its neighbours. The newly added members of the cluster are then used as seeds for further growth, until no new spins may join the cluster. The entire cluster is then flipped in a single Monte Carlo time step.

Away from the critical temperature, this algorithm is not efficient. At low temperatures almost every spin in the system is in the cluster, and a high temperatures the number of spins in the cluster is tiny. However, the Wolff cluster algorithm is powerful for sampling near to T_c, as it circumvents the phenomenon of critical slowing down [127–129].

3.4 CHOICE OF DYNAMICS

The choice of the dynamics is relatively straightforward and begins with the principle of detailed balance. So long as we obey detailed balance, equilibrium can be reached.

3.4—A   GLAUBER DYNAMICS

The principal of detailed balance states that from an equilibrium configuration, a kinetic process can be equilibrated by its reverse. This can be written mathematically as

$$P_i \omega_{i \to j} = P_j \omega_{j \to i} \qquad (3.11)$$

where P_{ij} is the Boltzmann weight, or the equilibrium probability of finding the system in configuration i or j, and ω denotes the kinetic transition rate between the two configurations. If a physical system is to reach thermal equilibrium, any kinetic transition rates assigned to events must satisfy this condition.

The detailed balance principle, Eqn. 3.11, can be written for the Ising model as

$$\frac{P(S')}{P(S)} = \frac{\omega_S}{\omega_{S'}} \qquad (3.12)$$

where S' and S represent the two possible spin states ± 1. Using the nearest neighbour Ising Hamiltonian allows one to write the Boltzmann weights as

$$\frac{P(S')}{P(S)} = \frac{e^{-\beta J S_i \sum S_j}}{e^{\beta J S_i \sum S_j}}. \qquad (3.13)$$

Using the identity

$$e^{ab} = \cosh(a) + b\sinh(a) = \cosh(a)\left(1 + b\tanh(a)\right) \tag{3.14}$$

allows one to write Eqn. 3.13 as

$$\frac{P(S')}{P(S)} = \frac{1 - S_i \tanh\left(\beta J \sum S_j\right)}{1 + S_i \tanh\left(\beta J \sum S_j\right)}. \tag{3.15}$$

One set of rates that satisfy this condition are those chosen by Glauber,

$$\omega_i(S) = \frac{1}{2}\left[1 - S_i \tanh\left(\beta J \sum S_j\right)\right]. \tag{3.16}$$

If takes the zero temperature limit of this form, where $\beta \to \infty$, the obtain the following transition probabilities:

$$\omega(S) = \begin{cases} 1 \text{ if } \Delta E < 0, \\ 0.5 \text{ if } \Delta E = 0, \\ 0 \text{ if } \Delta E > 0. \end{cases} \tag{3.17}$$

3.4—B   METROPOLIS DYNAMICS

While Glauber dynamics is one choice for non-equilibrium simulation, it is is possible to use simple Metropolis dynamics, which are presented in Section 3.3—A. Naturally, the zero temperature limit of these probabilities are

$$P(\Delta E) = \begin{cases} 1 \text{ if } \Delta E \leq 0, \\ 0 \ \Delta E > 0. \end{cases} \tag{3.18}$$

3.5   KINETIC METHODS

Here I briefly outline two numerical schemes for simulating non-equilibrium dynamics of kinetic ferromagnets; specifically, the Ising and Potts models. The general idea behind these methods is to simulate what happens when a kinetic ferromagnetic that is in thermal equilibrium with a bath of some temperature $T \gg T_c$ is suddenly placed in contact with a new bath of temperature $T \ll T_c$, and essentially watch what happens. I first introduce the conventional method, discuss why it is inefficient at low temperatures and then introduce an alternative method.

3.5—A   CONVENTIONAL METHOD

The conventional method typically invoked in the simulation of spin systems is simple and a little naive depending on the details of the simulation. For example, if one wishes to simulate the Ising model at high temperature—that is, temperatures well above the critical point—this algorithm makes sense. However, if one wishes to simulate a low-temperature quench then it is incredibly ineffective. I shall discuss why after introducing the algorithm. The description of the algorithm I give here—for both the Ising and Potts models—is that of Ref. [130].

Algorithm 1: Conventional Ising Monte Carlo method.

---

for $T_{\text{count}} = 0 \rightarrow T_{\text{max}}$ **do**

    for count $= 0 \rightarrow (N - 1)$ **do**

        choose integer site index $i \in [0, N)$

        get current energy E_c

        get energy if flipped E_f

        get $\Delta E = E_f - E_c$

        Accept or reject flip based on $P(\Delta E)$

    end

end

3.5—A.i   Ising model implementation

The general dogma of this algorithm is that each spin should be allowed to flip once in a single timestep in order to mimic a cooling system that is uniformly connected to a thermal reservoir. In practise—and in the context of the Ising model with N spins—N lattice sites are visited in random order. Upon visiting each site, one proposes to flip the resident spin, computes the energetic consequence and then probabilistically decides whether to accept or reject the move. The decision to reverse the spin or not depends on the dynamical rules one has elected to use. The algorithm is presented in Algorithm. 1.

Now that we have explored this simple algorithm, let's look at why it is so inefficient at low temperatures. Consider the following cartoon of a zero-temperature relaxation in the Ising model (Figure 3.6).
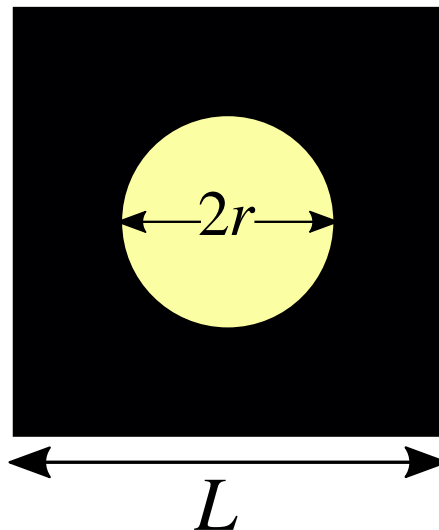
FIGURE 3.6 – A cartoon of a late-time snapshot of zero temperature coarsening in the two-dimensional kinetic Ising model. The minority domain (yellow) is eroded by the spanning majority domain (black).

The minority circle domain is doomed, and will be eroded to extinction by the surrounding domain. In a single timestep of the conventional algorithm, one attempts L^2 spin flips, but there are only roughly $2\pi r$ active sites. Thus, in a single timestep the number of successful flip attempts is $2\pi r/L^2$. If the radius r is some fraction of L, then the number of effective flips is $\sim 1/L$, which is terribly inefficient.

Algorithm 2: Conventional Potts model Monte Carlo method.

---

for $T_{\text{count}} = 0 \rightarrow T_{\text{max}}$ **do**
    for count $= 0 \rightarrow (N - 1)$ **do**
        choose integer site index $i \in [0, N)$
        propose a flip value $q_f \in \{1, \, 2 \ldots q\}$
        get energy if flipped E_f
        get $\Delta E = E_f - E_c$
        Accept or reject flip based on $P(\Delta E)$
    end
end

3.5—A.ii   *Potts model implementation*

The Potts model version of this algorithm is the same as the Ising case in spirit, but we have to account for the fact that each active site may have multiple transitions available to it. The Potts algorithm is shown in Algorithm. 2. Note here that the only significantly different step in the algorithm is that an additional random number is needed at each step in order to select a spin value the site can flip to.

3.5—B   *n*–FOLD METHOD

The numerical method typically invoked in the simulation of the dynamics of the Ising ferromagnet is generally known as the *n*-fold method, which is a rejection free—and therefore efficient—scheme for implementing the dynamics. This method is also known as continuous-time kinetic Monte Carlo, and the Gillespie algorithm (see following discussion). In the context of the Ising model, particularly at zero-temperature, this algorithm is much simpler than in generalised cases.

Citing the original work detailing this algorithm is challenging because there are a number of seemingly independent implementations of it. Apparently it has been theorised, discovered or implemented by a number of people and it is not immediately clear who should be awarded the credit; it rather seems that the subject matter determines which version one should cite. In the context of this thesis, the most important description or implementation of the algorithm is the version in Ref. [131], as it is

the most native to my work, so I shall draw upon this source for the most part of my description. However, I have included the following in the hope that it serves as a sufficient account of the history of the algorithm—even if it lacks *total* completeness.

The oldest description of the algorithm is seemingly in the form of a theoretical description in the 1940's [132, 133]. In an excellent overview of Kinetic Monte Carlo methods given by Arthur Voter, one finds a summary of the main implementations of this method in a variety of physical systems [134]. The earliest application of the method given in Voter's review is an atomistic study of cubic metals [135] published in 1966, but there is another article, Ref. [136], not mentioned in the review, that uses the same algorithm to study vacancy migration in binary alloys and was submitted for publication one month prior to Ref. [135]. Hopefully this serves to illustrate the difficulty in attributing the earliest implementation of this algorithm to someone.

Furthermore, the so-called "Residence time algorithm", which is again equivalent, was published in a book by Cox and Miller in 1965 (see Ref. [137]). Daniel Gillespie developed an equivalent algorithm, apparently independently, for simulating chemical kinetics that is known as the Gillespie Algorithm [138]. Gillespie developed this algorithm in 1976, and then famously used it in his 1977 paper to simulate biochemical systems of reactions with limited CPU power [139]. Furthermore, Bortz, Kalos and Lebowitz developed the so called "n-fold" method, specifically for the simulation of low-temperature Ising spin systems, in 1975, which is again equivalent [126, 131].

There have been a number of other developments using the algorithm in this area [140–142]. This algorithm has also readily been used in the area of surface adsorption, diffusion and growth [143–152]. The description of the algorithm from Bortz *et al.* is *by far* the most important version for the work I present in this thesis, but when I go on to discuss Potts models I will refer to adaptations to the n-fold method developed specifically for such studies.

Spin Class	Spin	Nearest-neighbour configuration
1	+	+ + + +
2	+	+ + + −
3	+	+ + − −
4	+	+ − − −
5	+	− − − −
6	−	+ + + +
7	−	+ + + −
8	−	+ + − −
9	−	+ − − −
10	−	− − − −

TABLE 3.1 – The ten possible spin configurations of the nearest-neighbour Ising model on the square lattice. The spin orientation is denoted by ± for up or down spins respectively.

3.5—B.i   Ising model implementation

The general idea of this algorithm is to avoid simulating null processes, or in language more appropriate to the Ising model, it's only worth trying to flip *active* spins. The description of the algorithm I give here in the context of the Ising model relies heavily on Refs. [126, 131]. At finite temperature, Bortz, Kalos and Lebowitz made the realisation that magnetic spins in the nearest-neighbour Ising model, at least on the square lattice, can only be in one of ten classes. These classes are defined by the spins and their nearest-neighbour configurations, as shown in Table. 3.1. The individual ordering of the nearest neighbour configuration itself does not matter, only the net field—i.e. the nearest-neighbour sum.

Now, consider a square lattice of L^2 interacting spins; each of which is in one of the ten configurations enumerated in Table. 3.1. Ferromagnetic interactions promote consensus in the orientation of the spins, while thermal noise attempts to randomise the ordering. At low temperatures—which are well below the critical point—the ferromagnetic interactions prevail, and at high temperatures—which are well above the critical point—thermal noise dominates.

Thus, there are three main factors in deciding if the spins are flippable or not:

the dynamical evolution rules, the interaction between the spins and their nearest-neighbours, and the influence of thermal noise. The choice of dynamics with which one endows the Hamiltonian determines the probability of flipping each spin. Let us define the activity of a given site, r_i, to be the total probability of it flipping.

In the conventional method, we visited every site roughly once in a single time step. This is inefficient—*especially* at low temperatures—as one often visits sites that are not flippable, proposes to flip them, rejects the flip, and then moves on. However, with the *n*-fold method, one visits a site with a probability that is proportional to its total activity and flips the resident spin with unit probability, thus eliminating the simulation of null processes—i.e. the algorithm becomes rejection free. This means a successful spin flip occurs at each step of the algorithm, and one must then calculate how much time should have passed if they had used the conventional algorithm [126, 131].

Let the probability that a given site S_i should flip—i.e. the activity of site S_i—be r_i, and the total system activity—the sum over each of the r_i in the system—be R. The *n*-fold algorithm says each site should be visited with a probability proportional to its activity, r_i/R, and the resident spin flipped with unit probability. After a spin is flipped, time advances as a stochastic variable Δt which has an expectation value proportional to $1/R$, making the total time t proportional to the number of attempts per site. The
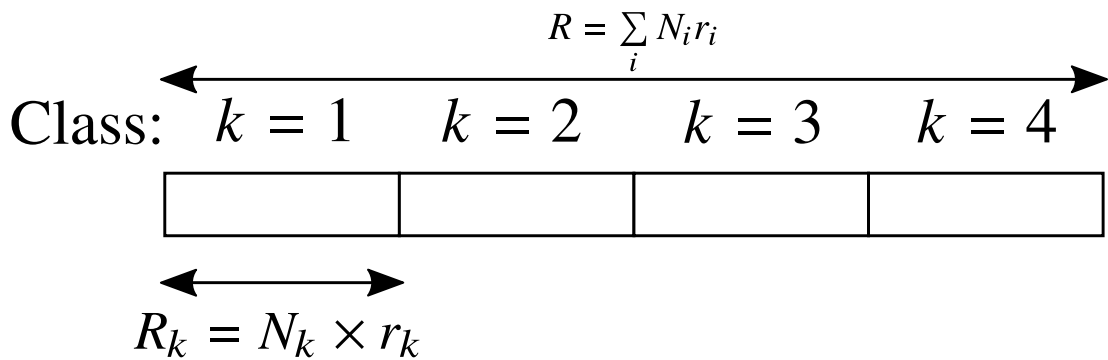
FIGURE 3.7 – Event selection scheme: to select a spin to flip one chooses a class with probability R_k/R, and then draws a spin at random from the class. R_k is the total activity of the class and R is the total system activity. The length of each block in the bar is therefore the total activity of the class.

time advance is

$$\Delta t = -\frac{1}{R} \ln(r), \tag{3.19}$$

where r is a random fraction uniformly distributed on $(0, 1)$.

Let us now explore the algorithm in a step-by-step basis. First, the system needs to be initialised; one must generate a physically appropriate initial condition and place each spin in a class depending on its local field. In doing this, one creates a count of the number of spins in each class and the total system activity R. Let the spins be divided into k classes, each containing N_k spins of activity r_k (Figure 3.7).

The the total activity of each class is therefore $R_k = N_k r_k$ (Figure 3.7). To flip a spin, one first selects a class with probability R_k/R, draws a member spin at random and flips it. The flipped spin and its nearest neighbours are then reclassified based on the new configuration after the flip. A summary of the algorithm is shown in Algorithm. 3.

Algorithm 3: Nearest-neighbour (NN) Ising model n-fold spin flip scheme

Initialise: Assign each spin S_i to a class k based on r_i.
while $R \neq 0$ **do**
  Throw Monte Carlo dart at position $x \in [0, R)$
  Use x to select a spin class k
  Draw a spin at random from class k
  Flip the spin
  Increment time by $\Delta t = -\ln(\mathrm{rand}\,[0, 1])/R$
  Remove flipped spin and NN from respective classes.
  Update R
  Reassign flipped spin and NN to classes based on new configuration.
  Update R
end

This algorithm is incredibly effective in the sense that it eliminates rejection, especially at low temperatures when most of the spins are not flippable. However, it does increase the cost of flipping an individual spin due to the associated bookkeeping and is also trickier to implement.

In this thesis I focus only on zero-temperature quenches, which allows considerable simplification with respect to the algorithm. In the zero-temperature Ising model, there are only two "kinds" of spin flips that matter: energy lowering and energy conserving

flips—energy raising flips are forbidden at zero-temperature. Now consider the two main choices of dynamics in the zero-temperature Ising model: Glauber and Metropolis.

In the Glauber case, there are only two distinct probabilities flippable spins may have: 1 for energy lowering flips and 0.5 for energy conserving flips, so there are only two classes of spins one need worry about algorithmically. In the Metropolis case, at zero-temperature, there is only one probability an active site may have: unity. Energy lowering and conserving flips occur with equal probability, and energy raising flips are again forbidden. In this case there is only a single class of spins to draw from—i.e. the list of active sites—in the algorithm.

3.5—B.ii *Potts model extension*

The Potts model version of this algorithm is trickier to implement compared to the Ising case. In the Ising model, active sites only ever have one possible transition: a spin flip event can only involve the reversal of the spin's orientation. However, in the Potts model, active sites often have more than one transition available to them. Consider a spin of state $S_i = 1$ on the square lattice Potts model with a nearest-neighbour configuration of $S_j = \{2, 2, 3, 3\}$. S_i is certainly flippable, but now the algorithm must decide whether it flips from $S_i = 1 \rightarrow 2$ or $S_i = 1 \rightarrow 3$.

Fortunately, extensions of the *n*-fold algorithm for the Potts model have been readily studied and used. Here I will describe the schemes used in Refs. [130, 153], and exactly what rules I have used. For numerical simplicity, I use only the Metropolis algorithm for the simulation of the Potts model at zero-temperature; this simplification will become clear momentarily.

In order to classify a Potts spin—in the context of the *n*-fold algorithm—one must determine the *total* probability of it flipping: i.e. the sum over each of the possible transitions. We begin our description of this algorithm by assuming zero-temperature dynamics only. Say we have a Potts spin of state $S_i = 1$ with a nearest-neighbour configuration of $S_j = \{1, 2, 3, 3\}$ and are using Glauber dynamics. Once we have

selected the spin to flip, we then need to decide if it should undergo the energy lowering transition $S_i = 1 \rightarrow 3$, or the energy conserving transition $S_i = 1 \rightarrow 2$. This requires another random dart throw selection and makes the simulation even more cumbersome.

So instead we use Metropolis dynamics. If energy lowering and energy conserving flips occur with unit probability, we need only select the spin to flip, and then draw randomly from a list of allowed transitions. Metropolis dynamics is further convenient numerically because the total activity of a site is an integer value, which is handy for indexing in simulations.

There is one additional note of ambiguity worth discussing in the Potts model algorithm. An explicit Potts implementation was presented by Sahni *et al* in Ref. [153] but they only described the algorithm rather briefly. However, Hassold and Holm describe the algorithm of Sahni *et al.* in Ref. [130]. To my mind, there is a slight disparity in the rules they implement.

Suppose in a three state Potts model we have a spin $S_i = 1$, with a nearest-neighbour configuration of $S_j = \{2,\ 2,\ 2,\ 2\}$. The scheme of Ref. [130] says the site may only flip from $S_i = 1 \rightarrow 2$, but zero-temperature dynamics also allows it to undergo an energy conserving flip from $S_i = 1 \rightarrow 3$. The consequence of this flip should not have a material effect on the relaxation timescale because the number of possible transitions is accounted for in the timestep. In order to avoid any artefacts of this simplification influencing the final states, I use the latter scheme. The Potts model algorithm is shown in Algorithm. 4.

Note, there is key difference in the Potts model algorithm: the factor of $(q - 1)$ in Δt. This factor is in place to enforce the rule that each site should flip once, on average, in a single timestep. For example, say in the Ising model we have a a single active site of $S_i = -1$ with neighbours $S_j = \{1,\ 1,\ 1,\ 1\}$. When this site is visited, the spin flips and time advances as one—the expectation value of Δt is unity.

Now say we have a ten-state Potts model with only a single active site of $S_i = 1$ with a nearest neighbour configuration of $S_j = \{2,\ 2,\ 2,\ 2\}$. The mean number of flips

taken for the site to align with its neighbours is $(q - 1) = 9$—remember that on average it takes six throws of a die to roll a six. If the average timestep for each flip is $1/9$—i.e. the inverse of the total probability—then the mean time to reach consensus is unity. However, we know that nine attempted flips should correspond to nine Monte Carlo timesteps, so the factor of $(q - 1)$ in Δt rectifies this, and in a sense stops the timestep depending on the number of spin states. It is also important to note that this factor does not effect the time scaling exponents.

3.6 SUMMARY

In this chapter I have given an overview of the information that underpins the simulations presented in this thesis. I have detailed the necessary lattice geometries, boundary conditions and initial conditions in Section 3.1. I discussed briefly the principle of detailed balance, and how any simulation rules must obey it if a physical system is to reach thermal equilibrium in Section 3.2. I then introduced some of the standard methods that used in simulating magnetic spin systems at thermal equilibrium in Section 3.3.

I detailed the two most common schemes invoked in the simulations of kinetic spins systems that out of equilibrium—Glauber dynamics and metropolis dynamics—in

---

Algorithm 4: Nearest-neighbour (NN) Potts model n-fold spin flip scheme

Initialise: Assign each spin S_i to a class k based on r_i.
while $R \neq 0$ **do**
    Throw Monte Carlo dart at position $x \in [0, R)$
    Use x to select a spin class k
    Draw a spin at random from class k
    Flip the spin
    Increment time by $\Delta t = -(q - 1) \times \ln(\text{rand}\,[0, 1])/R$
    Remove flipped spin and NN from respective classes.
    Update R
    Reassign flipped spin and NN to classes based on new configuration.
    Update R
end

Section 3.4. I then introduced the numerical methods for simulating the kinetic evolution of spin systems in Section 3.5. I first detailed the so-called "conventional method", and explain why it is inefficient at low temperatures, before introducing the "n-fold" scheme, which circumvents this issue. I explain each of these algorithms in the context of both Ising and Potts models.

CHAPTER

FOUR

ANOMALOUS ISING FREEZING TIMES

One surprising feature of zero-temperature coarsening in the two-dimensional Ising model that has come to light in the past two decades is the presence of multiple relaxation timescales. These timescales are the main focus of this chapter, but before we examine them in greater detail I will first recap the studies relating to their discovery.

Around two decades ago, Boston University graduate student Victor Spirin noticed that roughly four in every hundred of his zero-temperature Ising model simulations continued to run for excessively long times even though the remaining cases had all terminated. Spirin and his advisors initially viewed these findings with scepticism, and accordingly investigated further [I].

Spirin investigated further and produced snapshots of these anomalous relaxations, and in doing so took the first step towards showcasing the rich features of the Ising dynamics that had otherwise been completely overlooked. The anomalous simulation times originated from realisations reaching so-called diagonal winding configurations, which ultimately reached the ground state on a timescale of roughly $\sim L^{3.5}$ [53–55]—with L the linear dimension of the system. Spirin *et al.* presented their findings as surprising and anomalous features of Ising coarsening [53–55].

[I]This information was given to me in a private communication with Sid Redner during our collaboration in October–November 2018.

However, these studies were by no means the final words on the matter, and around eight years later, another Boston University Graduate student—Kipton Barros—conjectured that the probability of finding each topologically distinct behaviour has a one-to-one mapping with the equivalent crossing probability in continuum percolation [56]. These findings agreed with the predictions from percolation theory both on the torus (i.e. a square lattice with periodic boundary conditions) and the square lattice with open boundary conditions (a simple finite square lattice geometry).

Later still, Jason Olejarz confirmed the deep connection between the dynamics of the Ising ferromagnet and continuum percolation theory [57]. Not only did Olejarz observe another distinct topology from percolation theory in the Ising model, but he showed this phenomenon is general to curvature driven coarsening by demonstrating it in a time-dependant Ginzburg-Landau equation appropriate to zero-temperature Ising coarsening [57].

Due to work I present later in this thesis (in Chapter 5) which is concerned with zero-temperature coarsening in the triangular lattice Potts model, and some small hints in the literature I have reviewed, there is reason to believe in the existence of an additional coarsening timescale in the Ising model that remains unexplored.

In this chapter I detail my own time scaling studies of the Ising model—when quenched from both random and biased initial conditions—showing there is indeed *another* coarsening timescale overlooked in the literature. I present provisional evidence of this new timescale in Section 4.1. In Section 4.2—A, I attribute this timescale to the formation of on-axis two-stripe states—which were among the discoveries made by Victor Spirin—and confirm the mechanism behind it using a biased initial condition in Section 4.2—B. I then explain its origin in Section 4.2—C. My main result is that this anomalous timescale appears to grow as $\sim L^2 \log(L)$. I also explore the remaining relevant timescales in the zero-temperature Ising evolution using biased initial conditions in Section 4.3. Finally, I summarise my findings in Section 4.4.

The choice of the dynamics should not influence these timescales, If we consider

the two common choices of Glauber and Metropolis dynamics, there should be no fundamental different in the scaling—only a renormalisation of the timescales. Before proceeding any further, the reader should be familiar with the winding numbers presented in Section 2.2—B.v.

4.1   EXTINCTION AND SURVIVAL

The extinction and survival probabilities are useful diagnostics for identifying multiple relaxation timescales. Let the extinction time E_t be the time taken for a given realisation to reach its final state. By realising the dynamics N times one may construct the distribution of E_t—the extinction probability, $P_E(t)$—which, upon integration, gives the probability of reaching a final state within some time interval Δt. The survival probability is then simply the likelihood that the system is still active at time t. Trivially, the survival probability is related to $P_E(t)$ through

$$S_P(t) = 1 - \int_0^t P_E(t) dt. \tag{4.1}$$

The cumulative of $P_E(t)$ gives the fraction of realisations that have reached their final state by time t, and the remaining fraction, or the survival probability, is simply one minus the cumulative. Note, Eqn. 4.1 assumes $P_E(t)$ is a normalised probability density function.

For each timescale in the coarsening dynamics, there is an associated coarsening time $\tau(L)$ that depends on linear dimension of the system L [57, 123]. Realisations reaching their final state around this time cause the survival probability to undergo an exponential decay of the form $\sim \exp(-t/\tau(L))$ [57, 123]. Consequently, each coarsening timescale is expressed as a distinct exponential decay regime in the survival probability.

Consider now the extinction and survival probabilities given by Figure 4.1. Based on the literature [53, 57], we expect to observe two distinct decay regimes in $S_P(t)$, but,
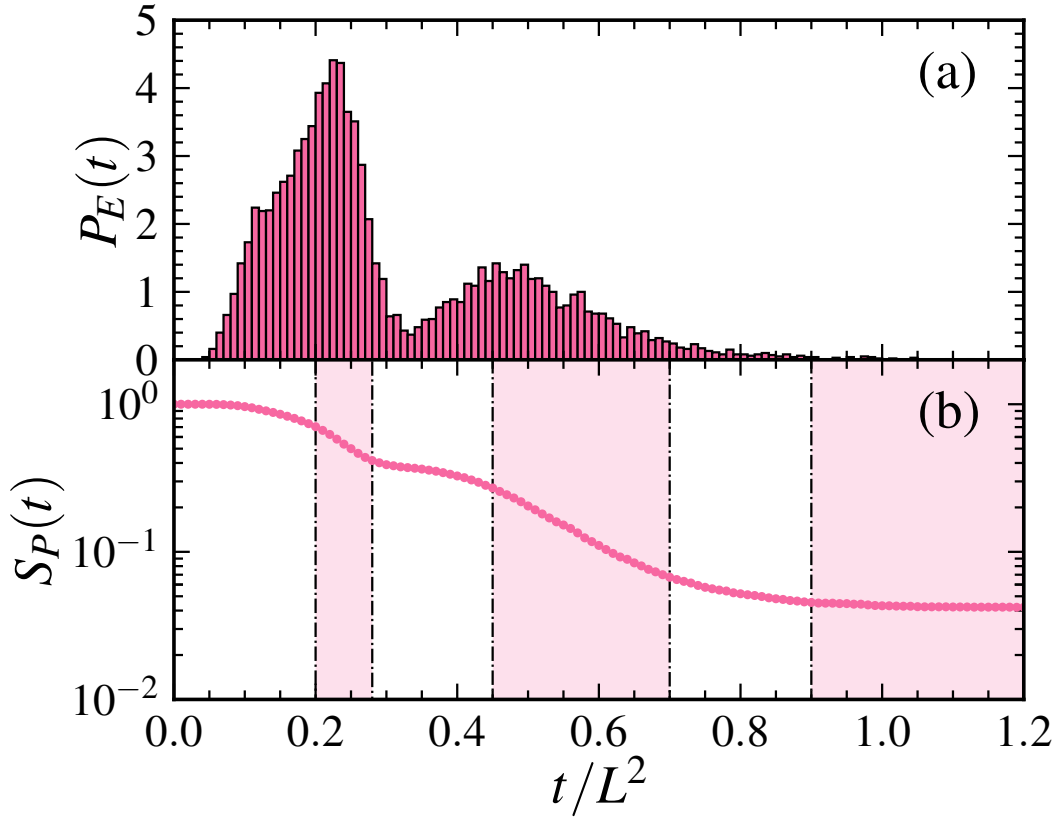
FIGURE 4.1 – (a) Extinction and (b) survival probabilities versus time for a square lattice of length $L = 512$. The data are based on 10^4 realisations with a bin width of $0.01L^2$. The tail of the survival probability exhibits a slow linear (note semi-log scale) decay before reaching zero at $t \approx 500.525L^2$.

strikingly, there are actually three. Recall: on a semi-logarithmic scale exponential decays appear as linear decays. This is an immediate indication that there could be yet *another* overlooked timescale in the zero-temperature coarsening of the Ising model. If one examines the survival probabilities presented in Refs. [53, 57], there are actually subtle hints of an intermediate timescale, but its influence on $S_P(t)$ is almost visually imperceptible in the small system sizes used. Perhaps this subtlety is why it has been overlooked.

The three timescales are roughly marked by the shaded regions in Figure 4.1 (b). The first is standard $O(L^2)$ coarsening, the second is a new timescale that is seemingly overlooked and the final timescale comes from the long-lived off-axis winding configurations. The cumulative over the range shown in Figure 4.1 (a) is ≈ 0.96—which is highlighted by $S_P(t = 1.2L^2) \approx 0.04$ in Figure 4.1 (b)—and the remaining $\approx 4\%$ corre-
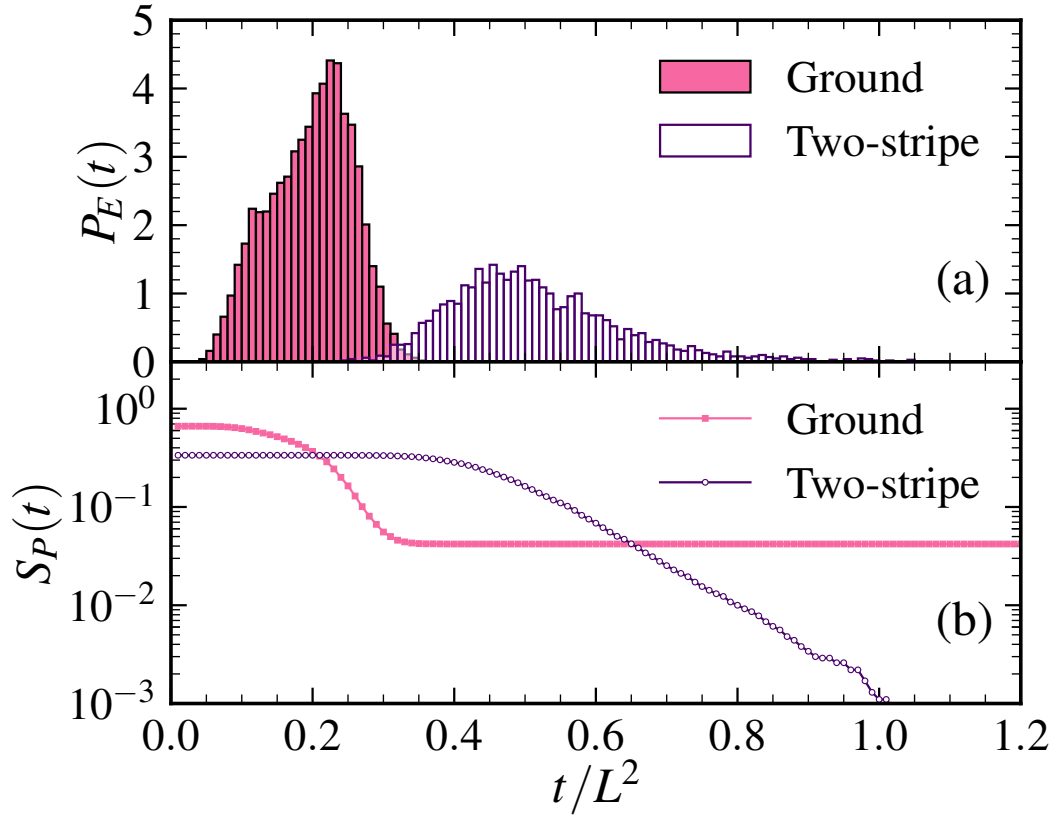
FIGURE 4.2 – (a) Extinction and (b) survival probabilities for realizations reaching ground and two-stripe states. The data are the ground and "frozen" two-stripe cases taken from the distribution in Figure 4.1, with the same bin width.

sponds to realisations still evolving through diagonal stripe states. The final timescale appears to have plateaued, but on the semi-logarithmic scale shown in Figure 4.1 it is actually a slow linear decay.

To explain the two peaks in the extinction probability, and the three decay regimes in the survival probability, we consider $P_E(t)$ and $S_P(t)$ for two categories of evolution: cases reaching ground states and cases reaching "frozen" two-stripe states (see Figure 4.2). While the ground state is typically reached directly, it is also reached by realisations that first evolve through off-axis winding configurations, whereas the "frozen" two-stripes are always reached directly.

In Figure 4.2 (a) we see the left and right hand peaks are associated with relaxations to ground and two-stripe states respectively. In Figure 4.2 (b), the survival probability for ground state cases decays exponentially roughly over $0.2L^2 \lesssim t \lesssim 0.3L^2$, after-

wards entering a regime of even slower exponential decay associated with off-axis winding configurations. The survival probability for the on-axis two-stripe state cases in Figure 4.2 (b) exhibits an exponential decay from $0.4L^2 \lesssim t$, before reaching zero at $t \approx 1.133L^2$.

4.2 ANOMALOUS TWO-STRIPE TIME SCALING

Here we explore the relaxation time associated with "freezing" into two-stripe states by considering both infinite temperature (Section 4.2—A) and biased initial conditions (Section 4.2—B). We then offer an explanation of this relaxation process using an argument based on annihilating random walkers in Section 4.2—C.

4.2—A $T = \infty$ INITIAL CONDITION

To investigate the time scaling of the two-stripe states, we simulate 5×10^4 realisations on systems of size $16 \leq L \leq 1024$ from random initial conditions, storing only the subset of times from instances reaching frozen two-stripe states. To test if the relaxation to static two-stripe states is governed by a single timescale, we consider the extinction probability as a function of rescaled time for such realisations (see Figure 4.3). In
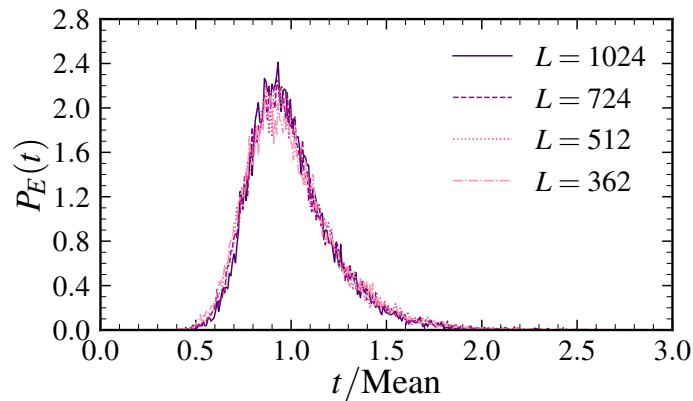
FIGURE 4.3 – Data collapse in extinction probabilities versus time for realisations reaching "frozen" two-stripe states. The distributions comprise the two-stripe state relaxation times from ensembles of 5×10^4 realisations from random initial conditions, and L denotes the system size.

each case, time is rescaled by the mean of the distribution. Although noisy, the data collapse in Figure 4.3 suggests the relaxation to two-stripe states is governed by a single timescale captured by the mean. The tail in Figure 4.3 is linear when viewed on a semi-logarithmic scale, which is suggestive of an exponential decay and indicative of a Poisson process.

The mean time to reach a two-stripe state T_S is plotted in Figure 4.4 (a) as a function of L, along with three fits: two power laws of form $\sim L^{\nu}$ (solid & dashed lines), and a fit of the form $\sim L^2 \log(L)$ (dotted line). Here it is reasonable for one to ask why we consider the $\sim L^2 \log(L)$ scaling form. In answer to this we include Appendix. C. The time taken to freeze into on-axis two-stripe states clearly grows faster than $\sim L^2$. At first glance, it's difficult to discern which of the fits to the T_S data are valid. One favourable feature of the $\sim L^2 \log(L)$ fit is that it requires only a single parameter, as opposed to the two parameters required by the power law. Technically, one could use two parameters by fitting $A \log(L/b)$, but in general it is best to use the fewer parameters when fitting.

The agreement between the data and the $\sim L^2 \log(L)$ fit is by no means conclusive, so we make the following argument. First, we assume $\sim L^2 \log(L)$ is the correct
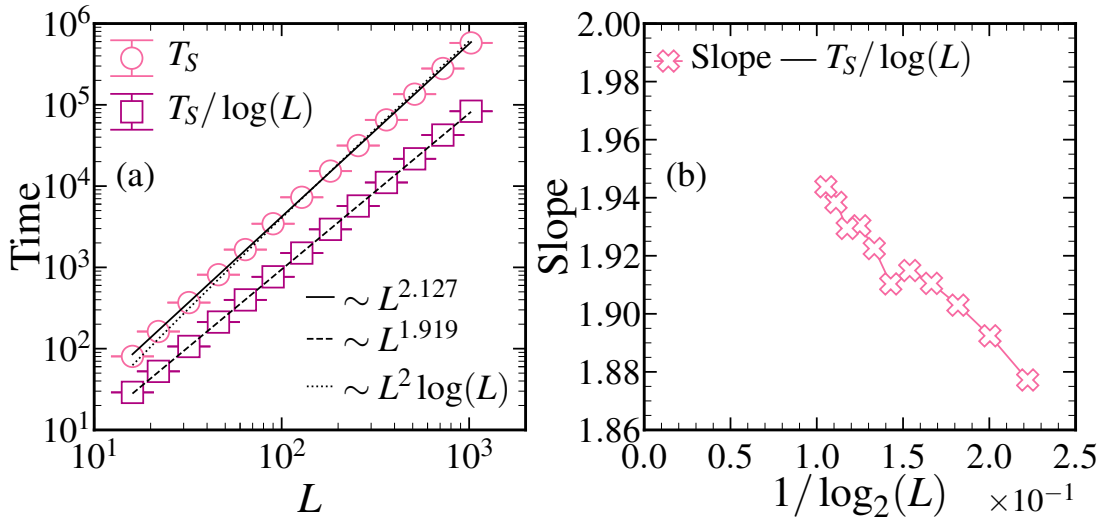
FIGURE 4.4 – (a) Two-stripe state freezing time T_S versus system size L and specified fits. (b) 3-point local slopes (see Appendix. A) in $T_S/\log(L)$ versus $1/\log_2(L)$. The data are based on the subset of realisations reaching two-stripe final states from ensembles of 5×10^4 realisations with random initial conditions, and the error bars are the standard deviation.

functional form, and thus expect that rescaling T_S by a factor of $1/\log(L)$ should yield a quantity that scales as

$$T_{\text{rsc}} = T_S/\log(L) \sim L^2. \tag{4.2}$$

In Figure 4.4 (a), we plot this quantity as a function of L and obtain a power law fit of exponent $\nu \approx 1.92$, which, although less than the desired exponent, only deviates from $\nu = 2$ by $\approx 4\%$.

Furthermore, the local slopes in the T_{rsc} data as a function of $1/\log_2(L)$ (see Figure 4.4 (b)) show hints of an asymptotic approach to power law scaling with an exponent of $\nu = 2$. However, from the data available to us this approach is not definitive. The main limitation on our data is that "frozen" two-stripe states only occur around 34% of the time, so studying them comes with an inherent inefficiency. This constrains the number of realisations we may obtain and necessitates that we explore the relaxation to frozen stripe states through other means.

4.2—B BIASED INITIAL CONDITION

The extinction time of static two-stripe states is dominated by late time events that occur when the system contains only two clusters, both of which wind in a single lattice direction only and have boundaries that are misaligned with the lattice axes. To capture this relaxation more efficiently, we consider the "wedding cake" (i.e. maximally tiered) initial condition given by Figure 4.5.
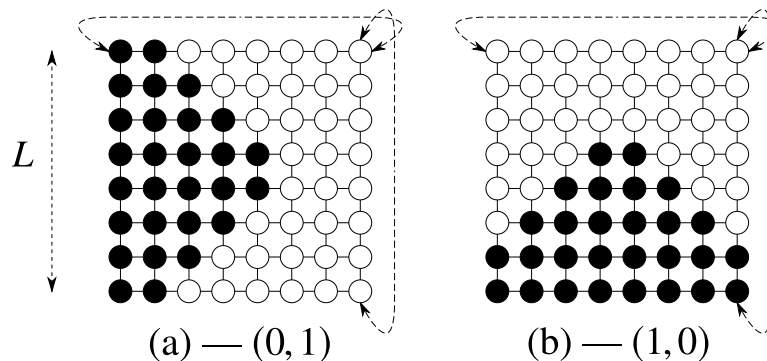
FIGURE 4.5 – Equivalent "wedding cake" initial conditions.

Simulating the dynamics from this initial condition is of greater convenience numerically compared to random initial conditions as the required CPU time is lesser. Furthermore, it eliminates the issue of rarity—and therefore efficiency—meaning we can now simulate 10^5 realisations per system size on the interval $16 \leq L \leq 2048$.

We plot the mean extinction time from this configuration as a function of system size in Figure 4.6 (a), and show the same fitted forms as in Figure 4.4 (a): two power laws of form $\sim L^\nu$ (solid & dashed lines) and $\sim L^2 \log(L)$ (dotted line). The scaling behaviour in Figure 4.6 (a) is congruent with that of Figure 4.4 (a), thus the "wedding cake" relaxation captures the mechanism behind the time scaling of the two-stripe states.

In Figure 4.6 (a), we also show the extinction time rescaled by $1/\log(L)$, and obtain a power law fit of exponent $\nu = 1.949$. Again, the exponent is less than desired value of $\nu = 2$, but in this instance the difference is less than 3%. Consider now the local slopes of the rescaled extinction time in Figure 4.6 (b). As L increases, the local slopes exhibit a suggestive approach to $\nu = 2$ that is not conclusive.
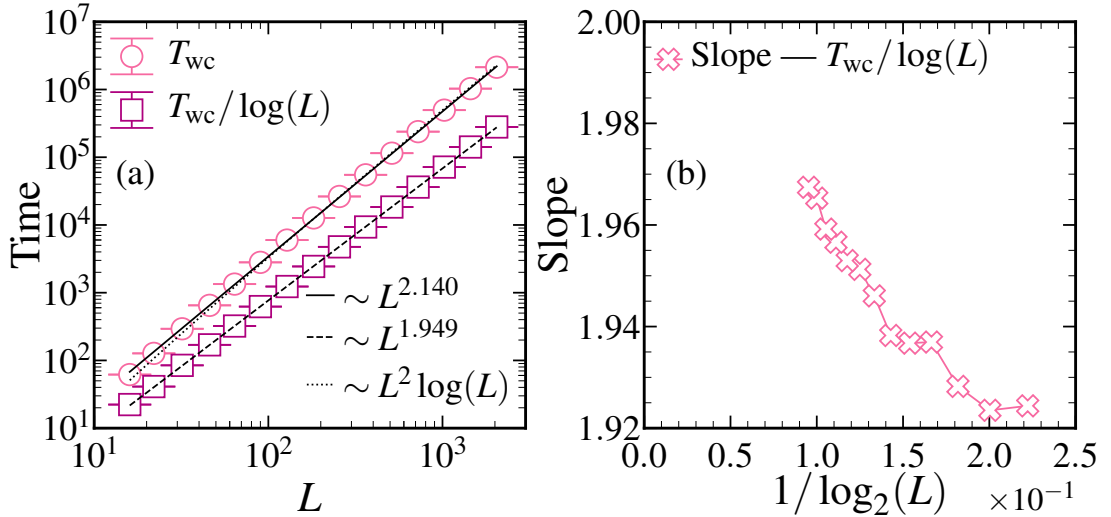
FIGURE 4.6 – (a) Freezing time T_{wc} versus system size L from the "wedding cake" initial condition (see Figure 4.5) and specified fits. (b) 3-point local slopes (see Appendix. A) in the T_{wc} data versus versus $1/\log_2(L)$. The data are based on 10^5 realisations and the error bars correspond to one standard deviation.

4.2—C HEURISTIC ARGUMENT FOR $\sim L^2\log(L)$

From simulation data alone we cannot conclusively show $\sim L^2\log(L)$ scaling, so we make the following case. In recent work—concerning the zero-temperature Potts model on the triangular lattice—we argued that the relaxation time of so-called "three-hexagon states" grew as $\sim L^2\log(L)$, and offered a simple argument to explain this scaling form [123].

The crux of this argument was that misaligned spin pairs moved along domain boundaries as random walkers on a one-dimensional interval. When a walker met a so called "T-junction", it was absorbed. To reach a frozen final state, all of the walkers had to be absorbed, at which point the domain boundaries aligned perfectly with the lattice axes.

The argument in Ref. [123] did not account for the changing timestep as the number of active sites reduced. However, the wedding cake initial condition serves as a simplistic model that allows us to probe the origin of this anomalous timescale without unnecessary complexity, so we now explain the logarithm in the scaling form by focusing on the wedding cake configuration only.

First, we cartoon the relaxation of the wedding cake. In the initial condition, each tier has two misaligned spin pairs forming domain-wall particles that behave as random walkers (see Fig. 4.7). The walkers may hop to the left or right with equal probability, and and reflected by the boundaries of their tiers. When two walkers meet: they annihilate—at which point the tier has relaxed and the number of active sites has reduced by four. The width of tier k is $L_k = L - 2(k-1)$, and the height of the wedding cake is $h = L/2 - 1$ (see Fig. 4.7).

The walkers on tier $k = 5$ are pinned between the positions of the walkers on tiers $k = 4$ and $k = 6$, so they cannot meet. However, the walkers on the topmost tier are unconstrained and therefore free to meet, so the entire structure relaxes "top-down".

Each of the tiers in the wedding cake can be modelled as annihilating random
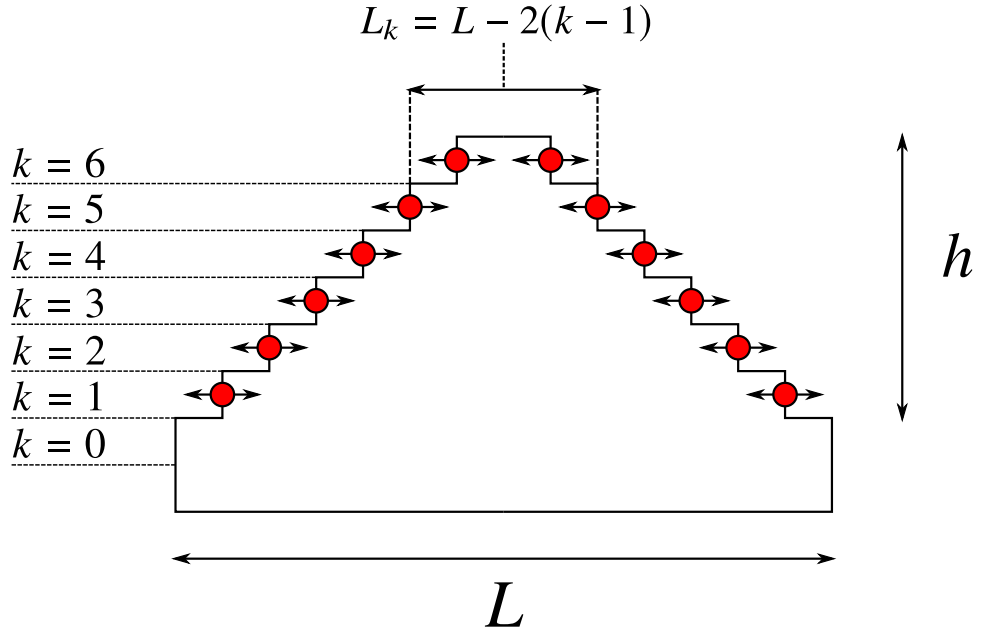
FIGURE 4.7 – Random walker picture of the "wedding cake" initial condition. The red circles cartoon misaligned spin pairs (domain-wall particles) as random walkers that may hop left or right with equal probability, and are reflected by the edges of their tiers.

walkers on intervals of length L_k. As the system relaxes from the top down, we assume the relaxation of the topmost tier occurs independently of the other tiers in the system. This is however a quasi-static approximation, because the location of the left- and right-hand boundaries of the topmost tier depends upon the positions of the walkers on the second top-most tier, which do fluctuate.

When a spin is flipped, the corresponding walker hops to the left or right. The *number of hops* required for two random walkers on an interval of length L_k to collide is of order L_k^2, ergo the total number of hops required for the entire structure to relax is

$$N_{\text{H}} \sim \sum_{k=1}^{k=h} L_k^2 \tag{4.3}$$

We count the number of flips in our simulations and find the same scaling as in Equation. 4.3, which is provides a strong validation of our argument.

Now that we have established the number of flips required for the structure to relax, we seek to relate this quantity to simulation time, which has units of Monte Carlo time

steps. Each spin in the system undergoes one microtrial per time step; that is to say, each site has the chance to flip once, on average, in a single time step. A successful microtrial is one in which the spin flip is accepted. As time progresses during a zero-temperature quench, the number of flippable spins decreases, so fewer and fewer spins flip in a given time step. Consequently, the time between successful microtrials—that is, the time between successful spin flips—increases. The mean *time between* successful microtrials is $\Delta t = 1/P$ [126, 130, 131, 153]. Δt is inversely proportional to the number of flippable spins in the system, which in the wedding cake is $4k$, so we denote the time increment as Δt_k [126, 130, 131, 153].

We know the number of flips required for the tiers to relax, and we have an expression for the time between individual flips, so we can write the total relaxation time as

$$t = \sum_{k=1}^{k=h} L_k^2 \Delta t_k, \tag{4.4}$$

i.e. the relaxation time is the sum of the total number of hops (successful flips) multiplied by the time step between each hop. As we use zero-temperature Glauber dynamics, the probability that a given *active site* in the wedding cake configuration should flip—which is an energy conserving move—is 0.5, except in the very rare exception where two walkers collide, which is energy lowering. Thus, $\Delta t_k = 1/(0.5 \times 4k)$, and Eqn. 4.4 becomes

$$t \sim \frac{1}{2}\sum_{k=1}^{k=h}\frac{1}{k}L_k^2, \tag{4.5}$$

$$\sim \frac{1}{2}\sum_{k=1}^{k=h}\frac{L^2}{k} + \frac{4L+4}{k} - 4L + 4k - 8.$$

This form is dominated by the first term in the sum, which asymptotically is

$$t \simeq L^2 \ln(L). \tag{4.6}$$

Although this argument *is* crude, in that it does not completely encapsulate the relaxation

process, it is compelling justification for $\sim L^2 \log(L)$ scaling.

4.3 ADDITIONAL TIMESCALES

Let us now explore the remaining timescales at play in the evolution of the zero-temperature Ising model. When the second coarsening timescale in the Ising model was first discovered, it was quantified by examining how reduced moments of the extinction probability scale with system size [53]. We repeat this analysis to obtain crude measures of the smallest and largest coarsening timescales present in $P_E(t)$.

First, recall that the k_{th} moment of a normalised distribution $P_E(t)$ is given by (see Ref. [154])

$$\langle t^k \rangle = \int_0^\infty P_E(t) t^k \, dt. \tag{4.7}$$

For small k, the reduced moments are dominated by the smallest times in $P_E(t)$, and conversely for large k they are dominated by the largest times present. To convert back into units of time, we use the reduced k_{th} moment: $M_k = \langle t^k \rangle^{1/k}$. Thus, by computing M_k as a function of L for various small and large k, we obtain estimates of the smallest and largest timescales associated with $P_E(t)$. Numerically we estimate $\langle t^k \rangle$ from ensembles of N realisations through

$$\langle t^k \rangle = \frac{1}{N} \sum_i^N (t_i)^k, \tag{4.8}$$

where k indexes the desired moment of the distribution and t_i the extinction times across the ensemble [154]. An example of how this procedure works is given in Appendix D.

Reduced moments of the extinction probability for $k \in \{0.05,\ 0.1,\ 10,\ 20\}$ are shown in Figure 4.8 as functions of L, along with two power laws (straight lines) of exponents 3.5 and 2. The power laws are merely guides to they eye, not fitted, giving rough measures of the maximum and minimum timescales at play. The magnitudes of the k values that one chooses here are important; if one uses smaller and smaller
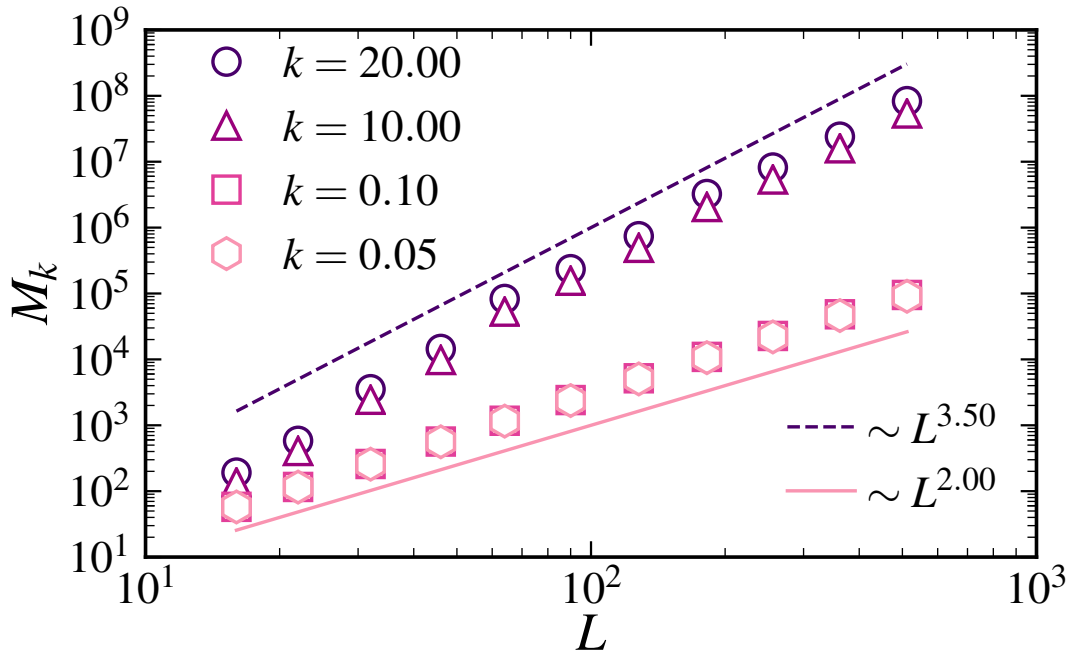
FIGURE 4.8 – Reduced moments of the extinction probability M_k versus system size L for specified k. The power laws are guides to the eye only, and the data are based on 10^4 realisations from random initial conditions.

k they will reach the limit where the numerical data are all essentially zero when raised to the power of k. Similarly, if the data are raised to the power of large k they become divergent to an unwieldy extent. A criticism of this technique is that the error propagation is large when raising to high or low powers, which is why it can only give one a tentative measure of the timescales.

4.3—A   GROUND STATE TOPOLOGY — $(0, 0)$

We recover the standard coarsening timescale of $O(L^2)$ by considering the biased initial condition in Figure 2.6 (a). From this initial state we expect no long-lived exotic timescales, and should find the coarsening time scales as $\sim L^2$. The mean extinction time from this initial condition T_G is plotted as a function of system size in Figure 4.9 (a), along with a power law fit of the form $\sim L^\nu$ (solid line).

The agreement between the data and the fit, while poor for small L, improves markedly as L grows. The power law exponent is $\nu \approx 2.025$, which is $\approx 1.25\%$ greater than the expected value of $\nu = 2$. The estimated exponent is not ideally close to
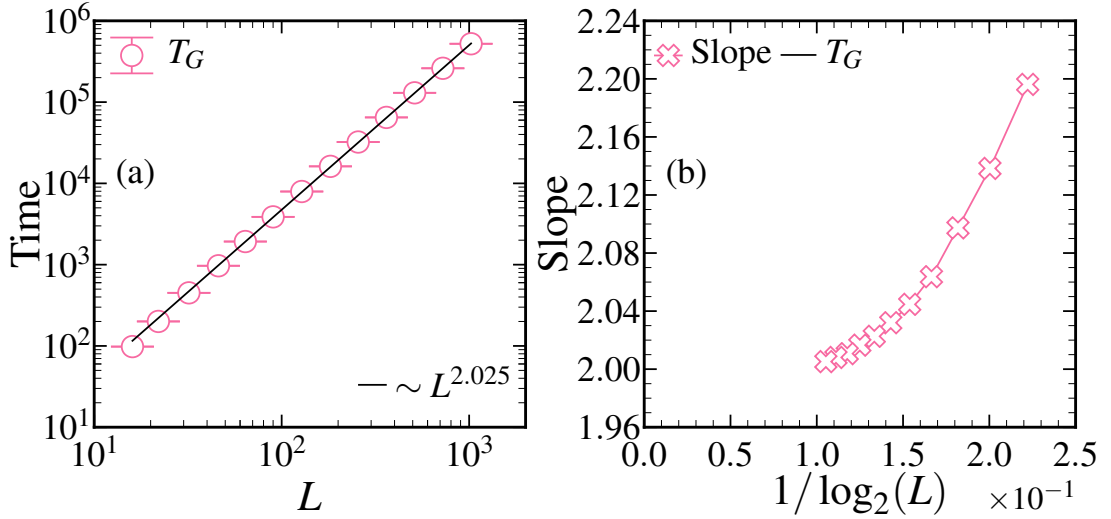
FIGURE 4.9 – (a) Extinction time T_G versus system size L with a power law fit of the form AL^ν. (b) 3-point local slopes (see Appendix. A) in T_G data versus $1/\log_2(L)$. The data are based on 10^4 realisations from the initial condition in Figure 2.6 (a) and the error bars correspond to one standard deviation.

$\nu = 2$ because of finite size effects, but as L increases there is a distinctive downwards curvature in the data, which is noticeable if one examines Figure 4.9 (a) carefully. This curvature is also obvious in Figure 4.9 (b), where the local slopes asymptotically approach $\nu = 2$. While trivial, this numerical experiment highlights the important influence of finite size effects; even in this simple case, the *correct* scaling form yields an *unsatisfactory fit* at small L.

4.3—B   DIAGONAL STRIPE TOPOLOGY — $(1, 1)$

We now turn to the first of the off-axis winding cases. The long-lived nature of these configurations makes it numerically challenging to precisely estimate their scaling behaviour with system size. This difficulty is accentuated by the rarity of the $(1, 1)$ stripe states, which occur with probability 0.04196 when the quench is from infinite to zero-temperature [57].

We assume the relaxation time of a diagonal stripe state is dominated by the time taken for it to collapse to the ground state after forming, and the formation time is comparatively negligible. To investigate the relaxation of these states, we consider the

initial condition shown in Figure 2.6 (c).

In Figure 4.10 (a) we plot the extinction time of realisations initialised in the $(1, 1)$ configuration (T_{D1}) as a function of system size along with a power law fit of the form $\sim L^\nu$ (solid line). If one examines these data "edge on", there is an obvious downward curvature in T_{D1} that reduces with increasing L. Ergo, one may easily overestimate the exponent when examining only smaller system sizes.

In Ref. [53] the authors provide a theoretical argument for the relaxation of "perfect" $(1, 1)$ winding configurations—i.e. the initial condition we employ—to scale as $\sim L^3$. This argument is based on a "particle deposition" and "evaporation" problem studied in Ref. [155], and says that the interface between two diagonal stripes should move a distance of $\sim L$ on a timescale of $\sim L^3$ [53].

The reducing curvature in Figure 4.10 (a) indicates a reducing exponent, but within the range of system sizes accessible to us we are unable to precisely estimate it as $L \to \infty$. However, despite initially growing, the local slopes shown in Figure 4.10 (b) obviously decay as $L \to \infty$. Perhaps this signals the approach to an exponent of $\nu = 3$ when $L \to \infty$ as predicted in Ref. [53]?
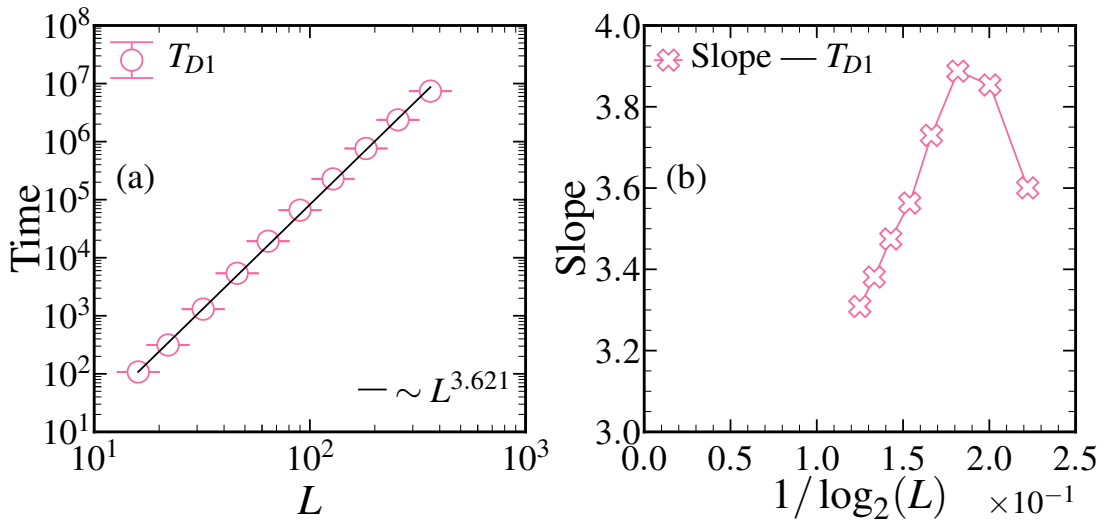
FIGURE 4.10 – (a) Extinction time T_{D1} versus system size L with a power law fit of form $\sim L^\nu$. (b) 3-point local slopes (see Appendix. A) in the T_{D1} data versus $1/\log_2(L)$. The data are based on 10^4 realisations using the initial condition shown in Figure 2.6 (c), and the errorbars correspond to the standard deviation of each estimate.

We also noticed that a small fraction of realisations initialised in the $(1, 1)$ configuration reached frozen two-stripe states rather than the ground state. For $L = 16$, this fraction was of order 10^{-2}, and had reached zero by $L = 32$. Our estimates of the time scaling are necessarily weak due to the fast growth with L, thus obtaining more than 10^4 realisations and estimating the exponent asymptotically is numerically impractical.

4.3—C DIAGONAL STRIPE TOPOLOGY — $(2, 1)$

In infinite to zero-temperature quenches, $(2, 1)$ winding configurations occur with a probability of 1.567×10^{-4} [57]. This scarceness negates any contribution they make to the timescales visible in Figure 4.1 (a). As a matter of curiosity, we estimate the time scaling of $(2, 1)$ windings using the initial condition in Fig 2.6 (d).
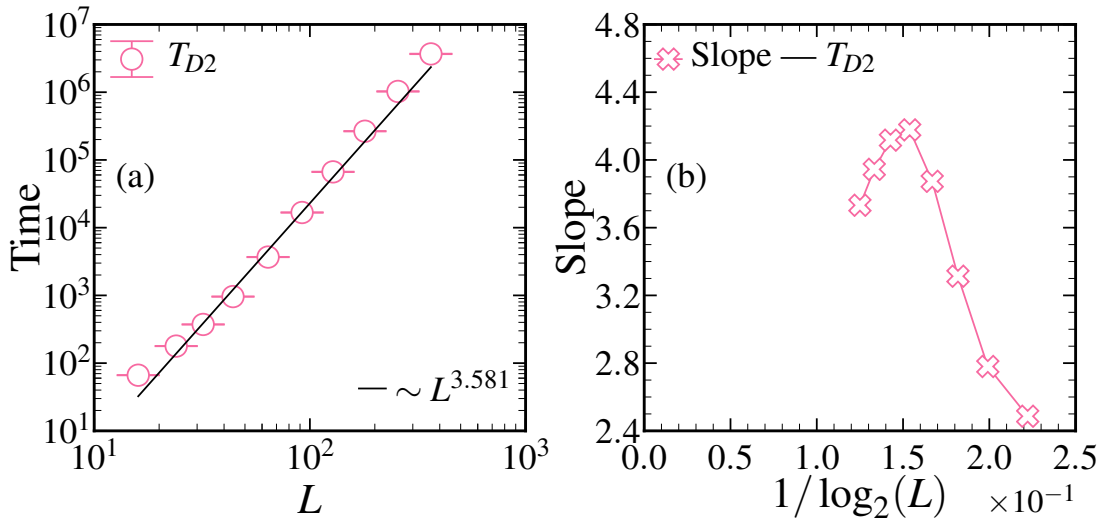
FIGURE 4.11 – (a) Extinction time versus L and a power law fit of form $\sim L^\nu$. (b) 3-point local slopes (see Appendix. A) in the T_{D2} data versus $1/\log_2(L)$. The data are based on 10^4 realisations, initialised in the $(2, 1)$ winding configuration shown in Figure 2.6 (d) and the error bars correspond the standard deviation of each estimate.

Figure 4.11 (a) shows the relaxation time from the $(2, 1)$ initial condition (T_{D2}), along with a power law fit of the form $\sim L^\nu$ (solid line). Naive power law fits to two significant figures give the same exponents for T_{D1} and T_{D2} (≈ 3.6), but the decay in the local slopes occurs at larger L for T_{D2}. In the regime of small L, finite size effects are clearly visible (see Figure 4.11 (a)), and as L increases the non-monotonicity in the

local slopes becomes obvious. In Figure 4.11 (b), the local slopes increase in the small L regime before decaying as large L is approached. Again, estimating this exponent as $L \to \infty$ is numerically impractical.

Additionally, when considering the relaxation from the biased $(2, 1)$ initial condition, a substantial fraction of the realisations reach frozen two-stripe states rather than the ground state. This fraction does however become negligible as L increases: for $L = 16$, it was ≈ 0.33, for $L = 32$ it was ≈ 0.14, and reached zero by $L = 180$. Though this fraction is considerably greater than it was in the $(1, 1)$ case, it plays no role in the scaling estimates at larger L.

4.3—D   DIAGONAL STRIPE TOPOLOGY — $(4, 1)$

The likelihood of observing $(2, 1)$ winding configurations was *just* significant enough to make them worth studying—though only as a matter of curiosity. Higher order winding configurations occur with such rarity (probability of 1.906×10^{-15} for $(4, 1)$ windings) that they have never been observed in the zero temperature Ising model [57]. The rarest behaviour reported is that of $(2, 1)$ windings [57]. Essentially for fun, I simulate higher order windings in order to see if any trend emerges in the scaling exponents as the number of windings increases.

As a numerical convenience, I keep my lattice sizes powers of two. To ensure each stripe is of equal width in the initial condition—which must be the case or the surviving phase will be biased—I skip $(3, 1)$ windings and examine the next case: $(4, 1)$ windings. If one considered the scaling behaviour of the $(2, 1)$ windings a little erratic, then the $(4, 1)$ behaviour certainly is (see Figure 4.12).

One could be forgiven for assuming these data would be well fitted by two power laws—i.e. a fit of form $\sim AL^{\nu} + BL^{\gamma}$—but such an approach also yields a poor description of the data. As large L is approached the local slopes seemingly increase, but given the behaviour in the previous two cases one could easily believe that they plateau. The only obvious trend from this data is that the extinction time of $(4, 1)$
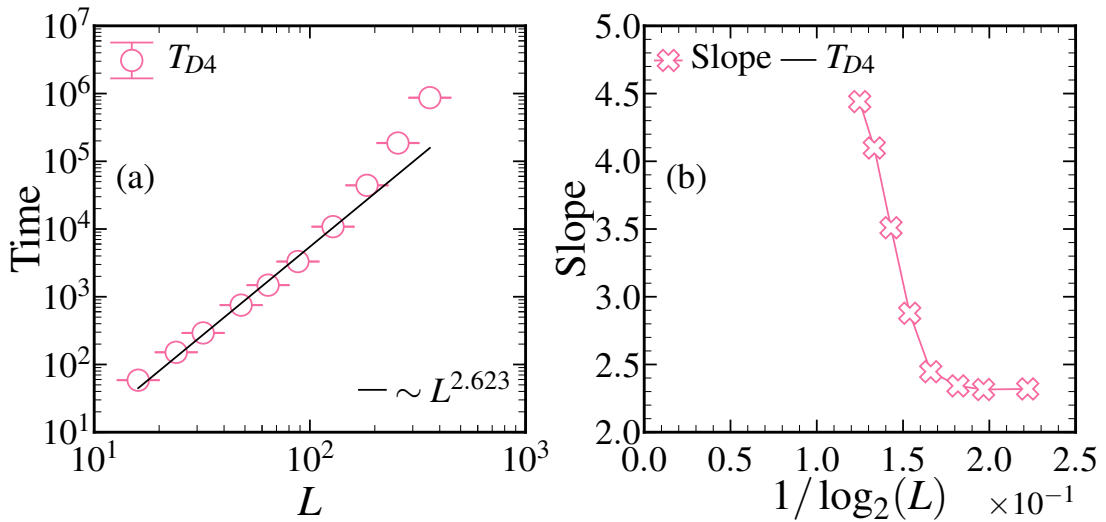
FIGURE 4.12 – Extinction time $\langle E_t \rangle$ versus system size L with a power law fit of form $\sim L^\nu$ and (b) 3-point local slopes in the $\langle E_t \rangle$ data versus the inverse logarithm of the system size. The data are based on 10^4 realisations from the "perfect" $(4, 1)$ winding initial condition.

configurations grows faster than in all previous cases. It is on this note that I conclude my time scaling studies of the zero-temperature Ising model. I review my time scaling studies in Section 4.4.

4.4 SUMMARY

In this chapter I presented studies of a square lattice Ising ferromagnet that was quenched to zero-temperature from both random and biased initial conditions. My *primary* result was the discovery of an overlooked coarsening timescale—which appeared to grow as $\sim L^2 \log(L)$—that emerges at zero-temperature and originates from relaxations reaching on-axis two-stripe states.

I confirmed the mechanism behind this anomalous timescale by using biased initial conditions to mimic the late time ordering dynamics of frozen two-stripe states, and explained its origin using an argument based on annihilating random walkers and a simplified interpretation of the relaxation process.

I also examined the relaxation timescales associated with off-axis winding configurations. The first of these configurations—denoted by the winding numbers $(1, 1)$ and

off-axis by $\pi/2$—was reported in the literature to scale as roughly $\sim L^{3.5}$, but predicted to scale as $\sim L^3$ [53, 57]. Interestingly, from my data I was able to show that the growth of this timescale is not a straightforward power law of fixed slope, but perhaps a scaling form exhibiting an asymptotic approach to $\sim L^3$ scaling. I also found qualitatively similar behaviour in my study of higher order off-axis winding configurations, namely $(2, 1)$ and $(4, 1)$ configurations.

Before the turn of the millennium, the tacit assumption of the zero-temperature Ising ferromagnet, at least in two dimensions, was that the ground state should *always* be reached, and on a timescale of order L^2. Although this assumption has already been shattered by the work of Spirin *et al.* (see Refs. [53, 57]), I have further contributed to our understanding of this system here by revealing the presence of an additional coarsening timescale that grows as $\sim L^2 \log(L)$. I also showed the anomalous timescale discovered by Victor Spirin does not exhibit a straightforward power law dependence with the system size, but instead displays a curvature that is perhaps indicative of an asymptotic approach to the predicted growth of $\sim L^3$.

FREEZING THE TRIANGULAR POTTS MODEL

In this chapter I present my studies of the late-time final states that persist when the Potts model is quenched from infinite to zero temperature on the triangular lattice geometry. Remarkably, the complexity that arises on the square lattice all but vanishes, making the triangular-lattice Potts model considerably more tractable from a numerical standpoint. This chapter is comprised of work from a bittersweet rejection from *Phys. Rev. Lett.*, in which a third referee was required to intervene. We ultimately elected to take the path of least resistance and published in *Phys. Rev. E.* [123].

We begin this chapter by recapping a study of zero-temperature coarsening in the square lattice Potts model by Olejarz *et al.*, which, after the surprising findings from the Ising model, aimed to ascertain the final state of a square-lattice Potts model that undergoes a deep quench to zero temperature [122]. Applying the tacit assumption that the ground state should always be the final result of a zero-temperature quench to the square-lattice Potts model is somewhat tenuous at best; mainly because this system has already been studied in greater detail that the Ising model and people have hinted that the late-time configurations are non-trivial (see review in Section 2.3—B).

The main surprises of the most recent examination of the zero-temperature square-lattice Potts model were as follows: the ground state is only reached 10% of the time;

there also exist a plethora of metastable final states that can either be static or non-static, and some even more peculiar configurations which appear to be trapped at constant energy for orders of magnitude in time, before suddenly undergoing macroscopic declines in energy [122]. Characterising these configurations was of extreme numerical expense, and it was ultimately unfeasible to definitively classify the final states [122].

In this study, the authors speculated that one might find a greater affinity between a system of three degenerate ground states and a lattice geometry with six-fold coordination, because the number of spin states is an integer multiple of the coordination number [122]. The obvious candidate for such an experiment is the triangular-lattice geometry, and this is precisely where my work enters the picture.

This chapter is organised as follows: I first review the model and simulation method in Section 5.1—along with some other important aspects of my simulations. I then present my studies of the late time "frozen" final states that arise when the triangular lattice Potts model is quenched to zero-temperature in Section 5.2. I characterise these final states, estimate the probability of finding of them and present the distributions of the domain areas in relevant cases. I detail my time scaling studies of this system in Section 5.3. I then give a preview of some behaviours that arise in $q > 3$ Potts models. Finally, I review and summarise the material presented in this chapter in Section 5.5.

5.1 MODEL & METHOD: RECAP

A full description of the methodology may be found in Chapter 3, but before we delve into my results and their significance, we shall briefly recap the simulation rules for the Potts model—which are a bit trickier than those of the Ising model. In the Ising model, one flips a spin by simply reversing its orientation—up spins flip to down and vice versa—so long as the flip is allowed by the dynamics. In the case of the Potts model, life is slightly more complicated as there is often more than one permissible orientation that a spin may flip to. Suppose we have a spin of state $S_i = 1$ that is surrounded by

three spins of state 2 and three spins of state 3. The spin may flip to any of the $(q-1)$ spin states that are different from itself. So, not only must one select a spin to flip, but they also must determine which of the allowed orientations it should flip to.

In simulating the Potts model, we employ zero-temperature Metropolis dynamics: energy lowering and conserving flips are accepted with unit probability, while energy raising flips are forbidden [130, 131, 153]. The reason for this choice of dynamics is numerical simplicity. Consider a spin that may flip two ways; one way would lower the energy and the other would conserve it. If we were to use Glauber dynamics, we would need to first select a spin to flip, and then probabilistically decide if it should flip to an energy lowering or energy conserving state. This is numerically cumbersome compared to Metropolis dynamics, where one need only select a spin to flip and then draw randomly from the list of permissible states it may flip to.

Throughout this chapter I initialise my simulations in the antiferromagnetic configuration (see Section 3.1), where no spin in the system has any aligned neighbours, but later in this thesis I will show that random and antiferromagnetic initial conditions yield virtually identical results. In each case, the lattice sizes used are $L = q \times 2^n$ with $n = 1, 2, 3 \ldots$. Finally, in the simulation method we use the time step for each flip should carry a factor of $(q-1)$, which we ignore in this chapter as the time properties we present are independent of it.

5.2 FINAL STATES

Now that we are acquainted with our method of simulation, let us ask the following simple question: when a triangular lattice Potts ferromagnet endowed with nearest-neighbour metropolis dynamics is quenched to zero temperature, what are the long time final states that persist?

5.2—A   EXAMPLES

In short, we find three main categories of final state: ground states, three-hexagon states, and on-axis stripe states. Before we examine the probability of finding each of these configurations, let us first introduce them by examining examples of each case.

5.2—A.i   *Ground state*

We begin with ground state realisations, where every spin is aligned and there are no permissible flips. An example of a ground state realisation is given by Figure 5.1. As the realisation progresses the number of domains decays from L^2 to unity. Each of the spin states compete to survive the ordering dynamics and ultimately a single domain spans the system in all lattice directions before engulfing it completely and becoming the sole survivor.

$$t = 0.001L^2 \qquad t = 0.01L^2 \qquad t = 0.1L^2 \qquad t = 0.1676L^2$$
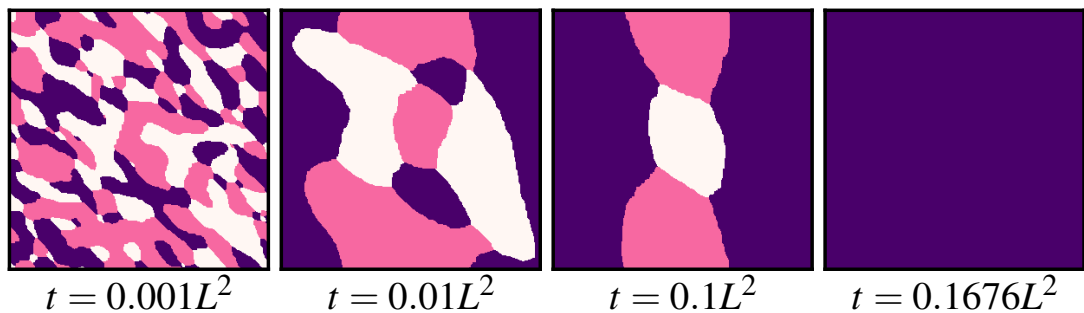
FIGURE 5.1 – A ground state realisation of zero-temperature coarsening in a three-state Potts ferromagnet of 300^2 spins on the triangular lattice geometry. Each distinct colour represents spins in one of the $q = 3$ possible orientations.

5.2—A.ii   *Three-hexagon state*

The next most common member in our family of final states is the so called three-hexagon state, which was unimaginatively named by me. [123]. In such realisations, all spin states survive the ordering dynamics (when $q = 3$ at least) and the final states consist of three colour tessellations where the domain boundaries align with the lattice axes. An example of a three-hexagon state realisation is shown in Figure 5.2.

$$t = 0.001L^2 \qquad t = 0.01L^2 \qquad t = 0.1L^2 \qquad t = 0.3244L^2$$
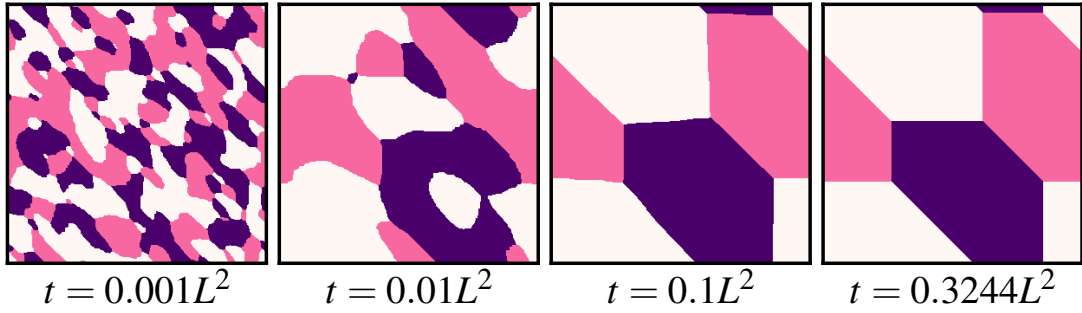
FIGURE 5.2 – A three-hexagon state realisation of zero-temperature coarsening in the triangular lattice Potts with $q = 3$. Each distinct colour represents spins in one of the $q = 3$ possible orientations.

Recall from the Potts Hamiltonian (see Figure 5.3): aligned neighbouring spins contribute zero to the total energy and misaligned spins pairs yield a positive energy contribution of $+2J$. Thus, once a spin has aligned with the majority of its nearest neighbours, it is no longer flippable. Consider now the "zoom-in" on the meeting of the three domains in in Figure 5.3. Each interfacial spin is aligned with the majority of its nearest-neighbours and is thus forever trapped in this configuration. We now understand why the three-hexagon states are *frozen* and therefore *final* states: flipping any spin in the right-hand panel in Figure 5.2 would raise the system's energy, which is forbidden.

Another interesting feature of the three-hexagon state is that the final state energy is always a constant value of $24L$, regardless of the individual hexagon sizes. If one examines the final panel in Figure 5.2, they should notice that the total length of the interface in the system is $3L$, meaning there are $6L$ boundary spins. In the Potts

$$H = 2J \sum_{i,j} \left(1 - \delta(S_i, S_j)\right)$$
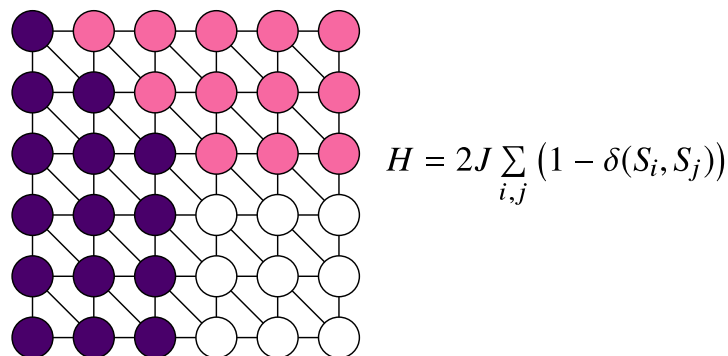
FIGURE 5.3 – Zoom in on the meeting of three domains in a frozen three-hexagon configuration. Every spin on a domain boundary is aligned with the majority of its nearest-neighbours, thus cannot flip.

Hamiltonian we use, each misaligned spin-pair contributes $+2J$, where $J = 1$ is the coupling strength. Recalling that each boundary spin has two misaligned neighbours, the total energy of the system is $E = 6L \times 4 = 24L$. Note: in these units we count each "bond" twice.

5.2—A.iii   *Two-stripe states*

The next most common configuration is the on-axis two-stripe state, however, I also found on-axis *three*-stripe configurations with a probability on the order of 10^{-5}. For now we shall focus on the two-stripe cases only. An example of such a realisation is given by Figure 5.4. There are three possible orientations for on-axis stripe states. Their

$t = 0.001L^2$	$t = 0.01L^2$	$t = 0.1L^2$	$t = 0.2761L^2$
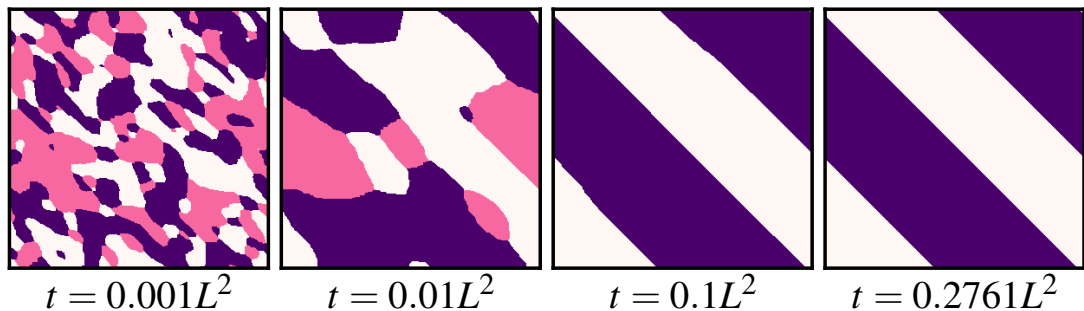
FIGURE 5.4 – A two-stripe state realisation of zero-temperature coarsening in the triangular lattice Potts model with $q = 3$. Each distinct colour represents spins in one of the $q = 3$ possible orientations.

boundaries may run in parallel which each of the three lattice / bond directions. We have now completed our visual introduction to the main categories of final states that arise when the three-state Potts ferromagnet is quenched to zero-temperature on the triangular lattice.

5.2—B   PROBABILITIES

Now that we are acquainted with the main categories of final state associated with the zero-temperature Potts model on the triangular lattice, let's answer the following simple question: how often do we find them? Estimates of the final state probabilities are

shown in descending order (from top to bottom) as function of the inverse logarithm of the system size in Figure 5.5.

The ground state probability P_G exhibits a non-monotonic approach to the continuum limit in a similar fashion to that of the ground state probability estimates in both the square lattice Ising and Potts models at zero-temperature (and also the triangular lattice Ising model) [53, 54, 122]. Frustratingly, this peculiar aspect of nature somewhat encumbers one's efforts to extend estimates of P_G to the continuum limit. As a result of this, we simply say that in the triangular lattice Potts model roughly
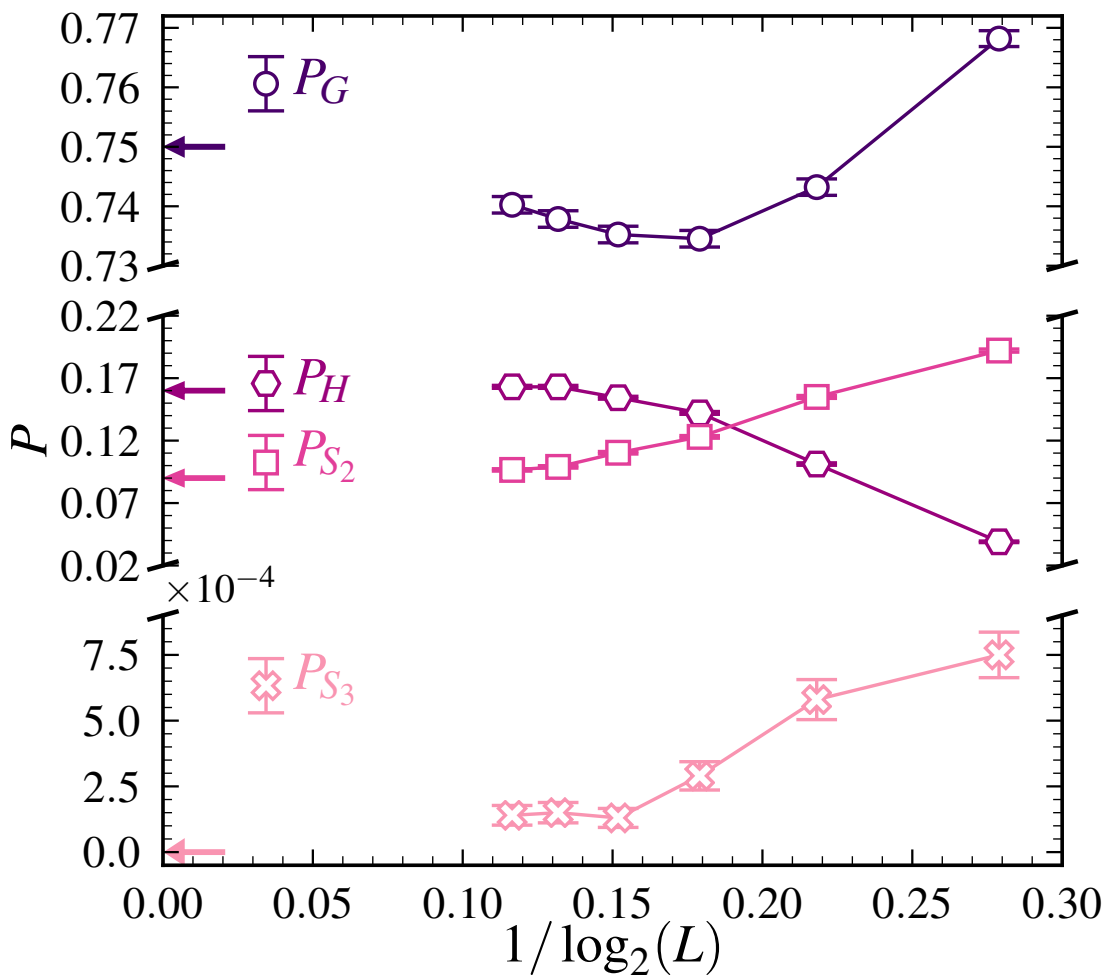
FIGURE 5.5 – Probability of freezing into ground (circles), three-hexagon (hexagons), two-stripe (squares) and three-stripe (crosses) states versus the inverse logarithm of the system size L. The data are based on 10^5 realisations initialised in the antiferromagnetic configuration. The arrows represented the final state probabilities on the largest system sizes when roughly rounded.

75% of all realisations relax to the ground state—our actual estimate for $L = 384$ was $P_G = 0.74025$.

In the case of the three-hexagon state, the probability P_H exhibits a much clearer approach to the infinite lattice case, which we take to be roughly 16%. While initially rarer than the two-stripe state, the three hexagon state increases in prevalence as it approaches the asymptotic limit, thus making it the second most common final state.

While the two-stripe states initially appear as the second most-common final states, they decay in probability as the large L limit is approached, meaning they are the third most common final state. The probability of observing three-stripe final states is seemingly negligible as $L \to \infty$, and is roughly $\sim 10^{-5}$.

5.2—C   DOMAIN AREAS

One simple and obvious question we can ask of the three-hexagon and two-stripes is: what is the distribution of the cluster areas within these configurations? We define the domain area, A, as simply the number of spins in each cluster. A cluster, or domain, is simply a series of aligned spins that are all connected through nearest neighbour bonds.

The cluster areas from the three-hexagon and two-stripe states are shown in Figure 5.6. For each case we fit a normal distribution of form

$$P_A = \frac{1}{\sqrt{2\pi\sigma_A^2}} \exp\left(-\frac{1}{2}\left(\frac{A - \mu_A}{\sigma_A}\right)^2\right), \tag{5.1}$$

with mean μ_A and standard deviation σ_A (see dashed lines in Figure 5.6 (a)–(b)). The means for each case—whether estimated directly from the data or from the fits—are essentially exactly $1/3$ and $1/2$ of the total system area. Upon close inspection of the tails in Figure 5.6 (a)–(b), one can see the agreement between the data and fit becomes poor. Perhaps formally these data do not satisfy normal distributions, but to a rough approximation it is an acceptable fitted form. The distribution of domain areas in the two-stripe states is consistent with what one might expect from similar work examining
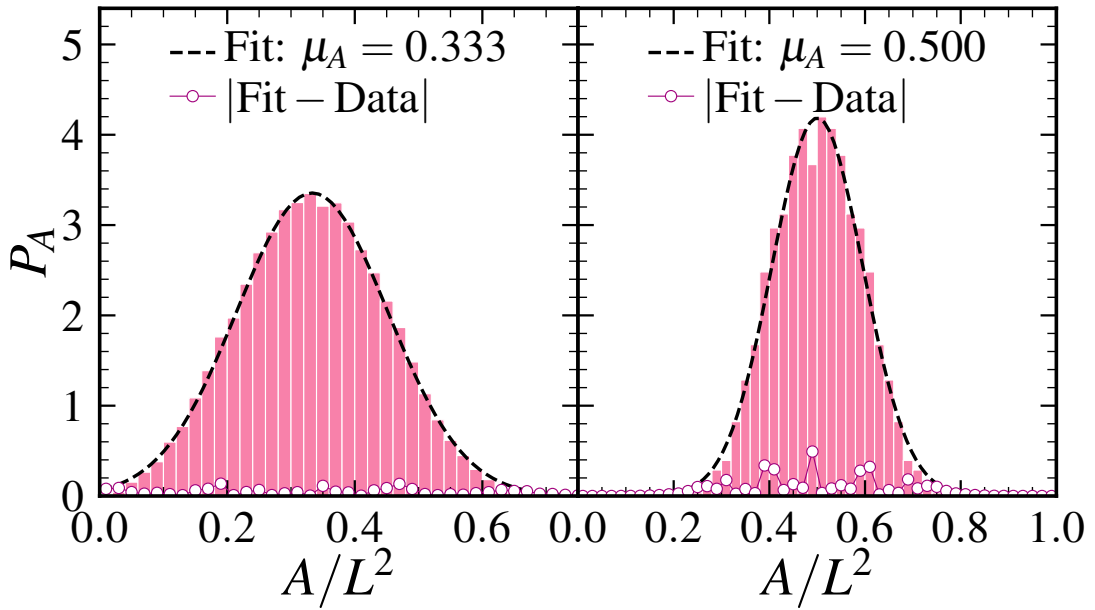
FIGURE 5.6 – Cluster area distributions in (a) three-hexagon and (b) two-stripe states with normal distribution fits (dashed lines). The data are based on the cluster areas from subsets of instances reaching three-hexagon and two-stripe states from an ensemble of 10^5 realisations.

the final magnetisation distribution in the zero-temperature Ising model [53–55].

5.3   ANOMALOUS TIMESCALES

Another intriguing feature of zero-temperature coarsening in the triangular lattice Potts model is the existence of multiple relaxation timescales. While this notion is less surprising now that we know of multiple timescales in the Ising model, it is a further indication that there are rich aspects of the Potts model that remain unanalysed. We again begin our analysis of the timescales with the extinction and survival probabilities.

5.3—A   EXTINCTION AND SURVIVAL

The two main quantities of interest are the distribution of the extinction time—the extinction probability $P_E(t)$—and the survival probability $S_P(t)$. Recall: the survival probability is simply one minus the cumulative of the extinction probability. We will use these quantities to perform an analysis of the timescales similar to that used for the
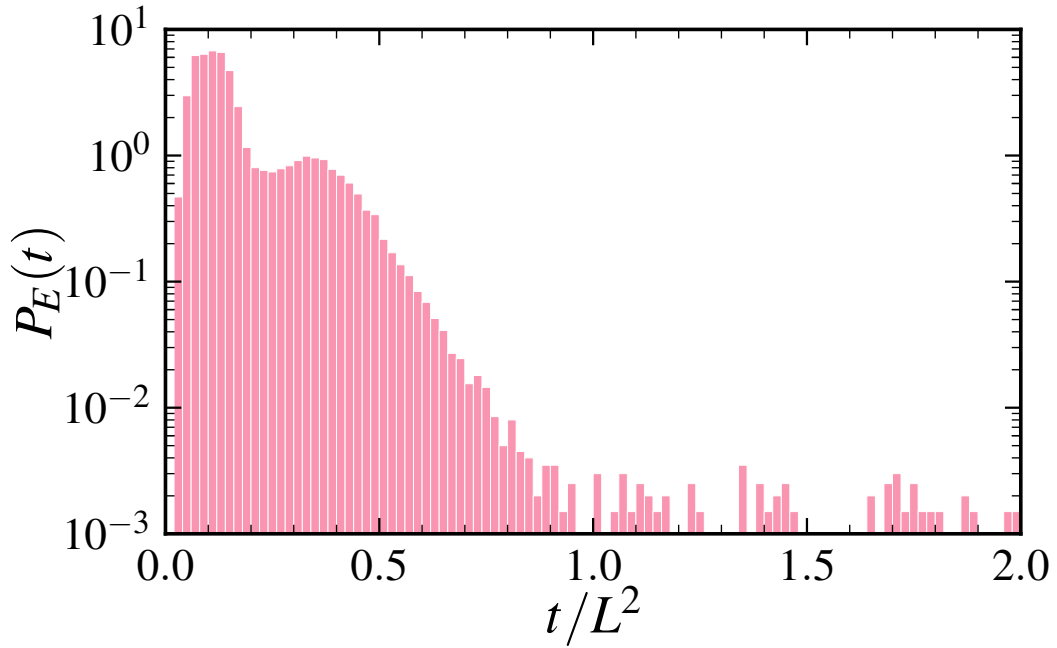
FIGURE 5.7 – Extinction probability versus time for the zero-temperature Potts model on the triangular lattice. The data are based on 10^5 realisations from antiferromagnetic initial conditions with $L = 384$.

Ising model in the previous chapter, and begin with the extinction probability shown in Figure 5.7.

It is clear from Figure 5.7 that there are multiple relaxation timescales play. If we adopt the same rationale as in our Ising analysis, then we should expect the various timescales to be clearly visible in the survival probability, which we plot in Figure 5.8. In Figure 5.8 (a), we focus on shorter times ($0 \leq t \leq 2L^2$), thus highlighting three linear regions corresponding to exponential decays (note the semi-logarithmic scale). These decays correspond to three timescales: the first is standard $\sim L^2$ coarsening, the second—which happens to be the original piece of evidence that prompted the Ising studies in the previous chapter—is $\sim L^2 \log(L)$, and the third is roughly $\sim L^3$. Figure 5.8 (b) shows the slow decay of $S_P(t)$, ultimately reaching zero at $t \approx 29.99L^2$.
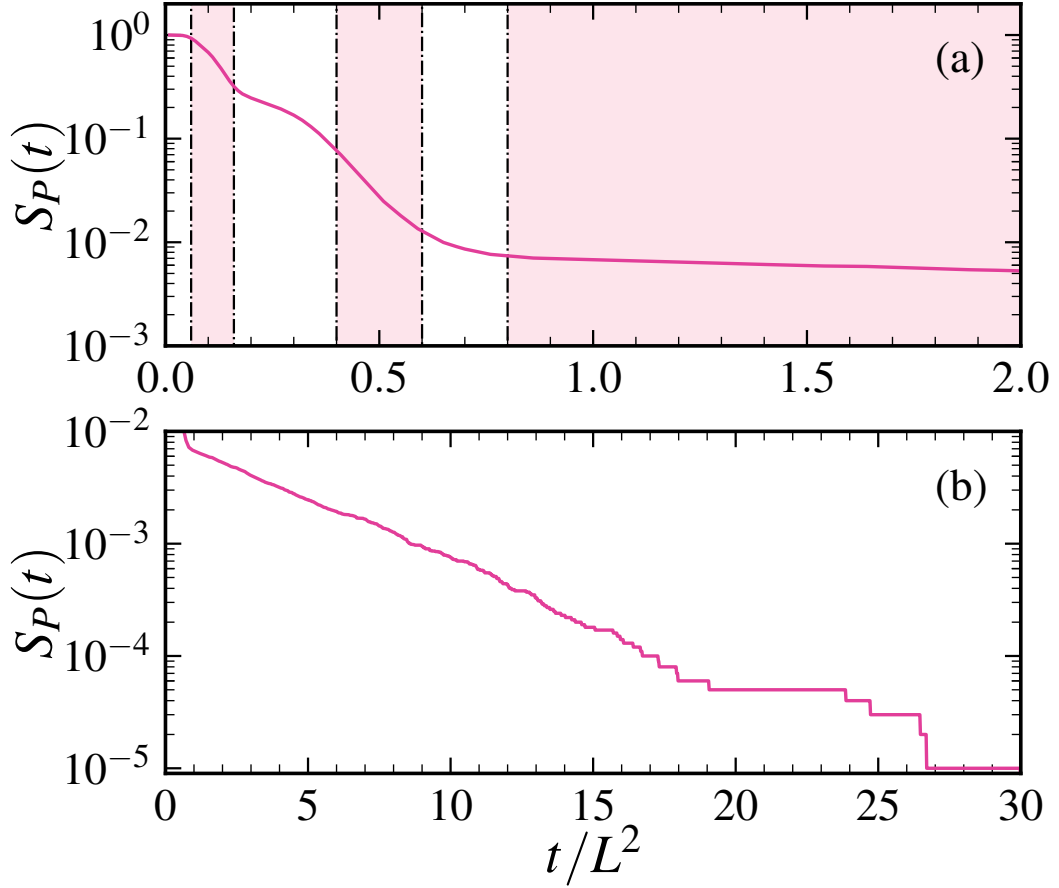
FIGURE 5.8 – Survival probability versus time for the zero-temperature Potts ferromagnet on the triangular lattice geometry. The data are based on 10^5 realisations from random initial conditions.

5.3—B   REDUCED MOMENTS

The notion of multiple timescales is interesting but thus far we have not quantified them, so we continue our analysis by examining the reduced moments of the extinction probability, which have already proven useful in approximating the maximum and minimum timescales present. Briefly restated, the k_{th} moment of a data set containing N times t_i is (see Ref. [154])

$$\langle t^k \rangle = \frac{1}{N} \sum_{i=1}^{i=N} (t_i)^k. \tag{5.2}$$

For small k, $\langle t^k \rangle$ is dominated by the smallest times in the data, and for large k the reverse is true. To convert back into a quantity that has units of time we consider the reduced k_{th} moment: $M_k = \langle t^k \rangle^{1/k}$. An example of this procedure is shown in

Appendix D.

Reduced moments of the extinction probability for $k \in \{0.05, 0.1, 10, 20\}$ are given by Figure 5.9. For small k, the reduced moments clearly scale as $\sim L^2$, as expected, and are dominated by realisations that proceed directly to the ground state. Most interestingly, for large k, the reduced moments appear to grow as *roughly* $\sim L^3$. This finding sparks and immediate and interesting question: from where does this large timescale originate?

It turns out that the ground state is generally reached through two routes. Firstly, most ground state realisations coarsen directly to ground state on a timescale of order L^2. Secondly, realisations fall into off-axis configurations similar to three hexagon states—i.e. three-cluster configurations that do not span the system—but different in that their domain boundaries are misaligned with the lattice axes.

An example of such a realisation is given by Figure 5.10. The dominant late time configuration has established itself by around $t = 0.01L^2$, and from this point forward the system remains visually unchanged until just after $t \approx 9.43L^2$—which is a huge
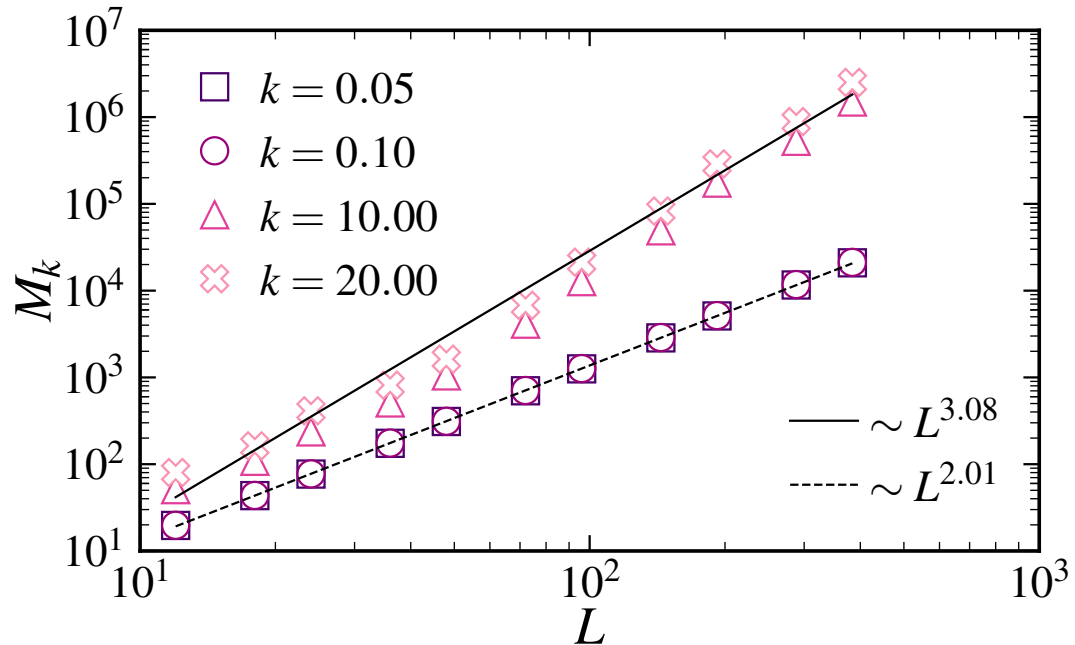
FIGURE 5.9 – Reduced moments M_k versus system size L for specified k. The straight lines are power law fits to the $k \in \{0.05, 20\}$ cases and the data are based on 10^5 realisations from the antiferromagnetic initial condition.

time gap relative to the time steps between the first few frames—where the purple cluster erodes the pink, thus winding in the "horizontal" direction. The white and pink clusters then continue to be eroded by the purple, before it ultimately engulfs the system. The example configuration in Figure 5.10 is representative of the realisations that give rise to this long-lived timescale of roughly $\sim L^{3.1}$. At this point in time we have no theoretical understanding of this timescale.

| $t = 0.001L^2$ | $t = 0.01L^2$ | $t = 0.1L^2$ | $t = 9.0L^2$ |

| $t = 9.43L^2$ | $t = 9.44L^2$ | $t = 9.5L^2$ | $t = 9.5438L^2$ |
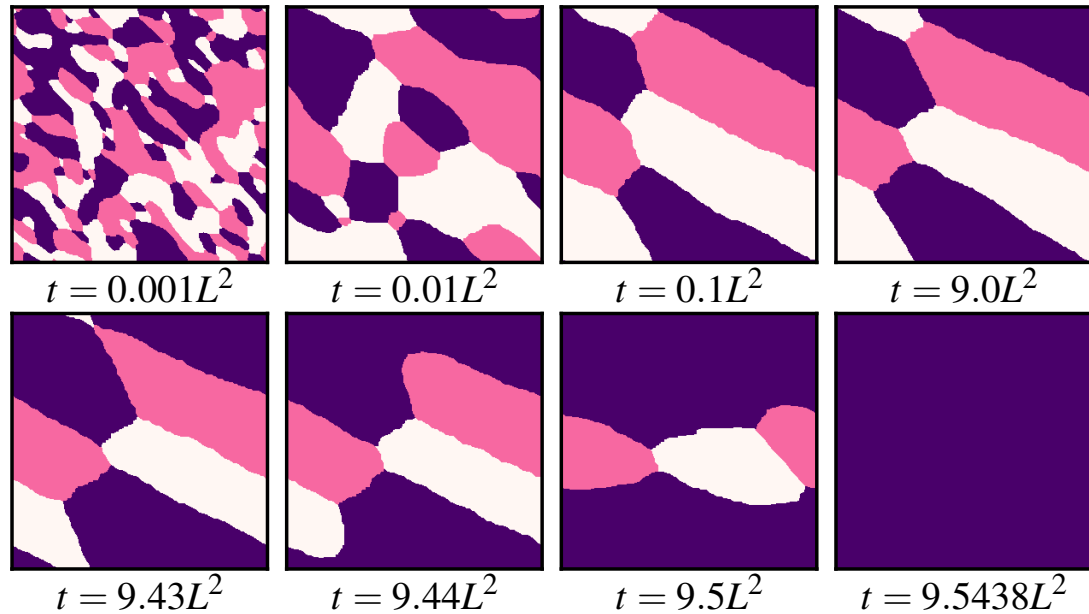
FIGURE 5.10 – Snapshots of a realisation evolving through a long-lived off-axis configuration at specified points in time (left–right). Note the varying timesteps between snapshots.

Now that we have explored the origin of the shortest and longest coarsening timescales that arise, the main remaining question is that of the intermediate timescale: what is it, and from where does it originate?

5.3—C THREE-HEXAGONS: TIME SCALING

So far we have acquainted ourselves with the smallest and largest coarsening timescales at play—$O(L^2)$ and $O(L^{3.1})$. Now we shall explore the origin of the intermediate timescale: $\sim L^2 \log(L)$. Let us begin our examination of the three-hexagon scaling time by inspecting Figure 5.11 (a), where we plot the three-hexagon state relaxation time

T_H as a function of the system size L, as well as the same data rescaled by the inverse logarithm of the system size.

We suspected this scaling form was $L^2 \log(L)$ when we initially examined it, but some peer reviewers suggested that it was difficult to distinguish between a fit of the form $L^2 \log(L)$ and a power law of form $\sim L^\nu$. However, there are actually some telltale signs that distinguish the two (see Appendix. C). At first glance, T_H appears to grow as a power law of exponent $\nu \approx 2.167$, yet these data exhibit a downward curvature that is characteristic of a power law multiplied by a logarithm (on a double logarithmic scale). Another hint of the logarithm is that the power law exponent is close to an integer value.

The first and most obvious step is to eliminate the logarithm by simply dividing it out, as shown in Figure 5.11 (a). In doing this, the *obvious* curvature in the data vanishes, and we obtain a power law fit of exponent $\nu \approx 1.93$. If the form was purely $L^2 \log(L)$, then this exponent would be ideally close to $\nu = 2$, but the estimate is off by 3.5%. The next most obvious issue in recovering the scaling form is finite size effects—which we have yet to discuss in the context of this model.

To explore finite size effects in the scaling form, we employ the same analysis as in the previous chapter and examine the local-slopes in the rescaled relaxation time
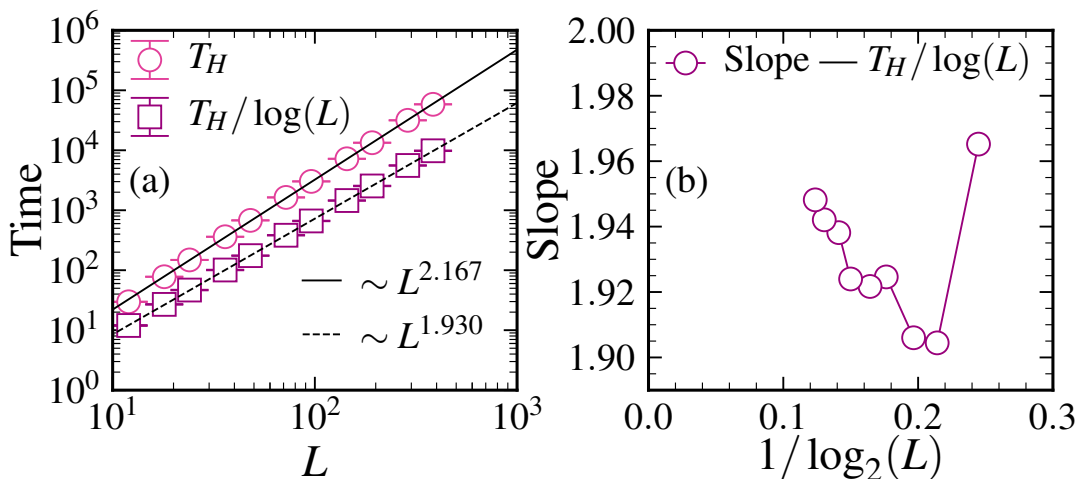
FIGURE 5.11 – (a) Three-hexagon state relaxation time T_H versus system size L with power law fits of specified form. (b) 3-point "local slopes" in the $T_H/\log(L)$ data versus the inverse logarithm of the system size.

(see Figure 5.11 (b)). If the leading term in the scaling form is $\sim L^2 \log(L)$, then the local slopes in $T_H/\log(L)$ should asymptotically approach $\nu = 2$ as $L \to \infty$. Upon examination of Figure 5.11 (b) one can see that the local slopes exhibit a nonmonotonic approach to the asymptotic limit, but with the data available to us we cannot predict what this limit is. It could well be $\nu = 2$ based on the behaviour in Figure 5.11 (b), but the approach is certainly not conclusive. In order to convince oneself of $\sim L^2 \log(L)$ scaling, one needs a demonstrable physical mechanism that predicts this form.

It is worth noting that at the time of the reviewers concern regarding the scaling form of T_H we had not considered the progression of the local slopes (shown in Figure 5.11 (b)). The behaviour of these data, I argue, helps solidify our claim that $T_H \sim L^2 \log(L)$.

5.3—C.i *Random walker argument*

In order to understand the argument we first used in the case for $L^2 \log(L)$ scaling, we must be able to solve the problem of an absorbing random walker on a one-dimensional interval. This problem is very simple to formulate. Consider a random walker on an interval $\{0, 1, 2, \ldots, N\}$. From a given initial condition, the walker may hop one "step" to the left or right with equal probability in a single timestep.

Imagine now that the boundaries are absorbing: if the walker lands on site 0 or N it is absorbed. Thus, the mean "exit time" of the system t_n, from initial position n, obeys the recursion relation

$$t_n = \frac{1}{2}\left(1 + t_{n-1}\right) + \frac{1}{2}\left(1 + t_{n+1}\right), \quad n = 1, 2, \ldots, N - 1, \tag{5.3}$$

with $t_0 = t_N = 0$ [156]. This equation is actually the discreet Poisson equation

$$\nabla^2 t_n = -2, \tag{5.4}$$

which has general solution $t_n = A + Bn - n^2$ [156]. Using $t_0 = t_N = 0$, the solution
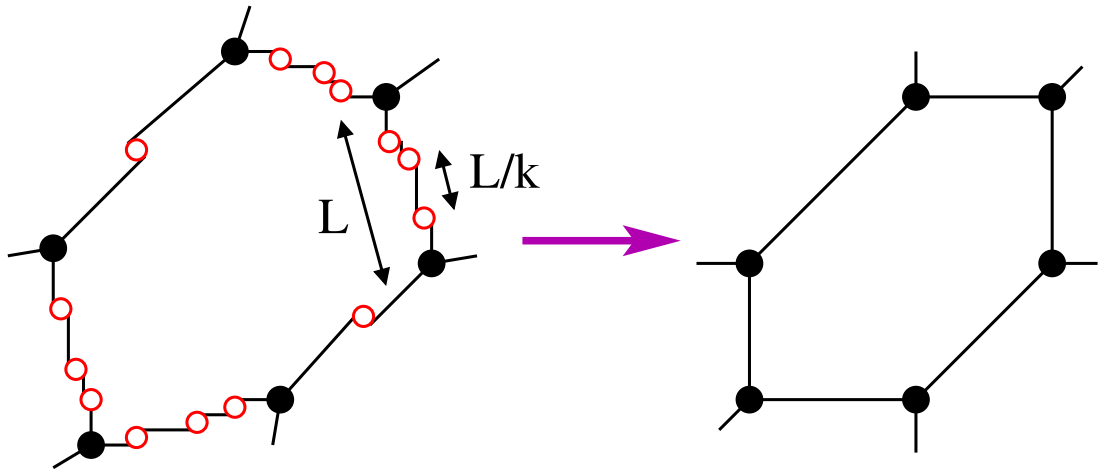
FIGURE 5.12 – Schematic relaxation to a three-hexagon state; the red circles correspond to random walkers on the interfaces and as the walkers are absorbed the interfaces straighten out and align with the lattice axes.

becomes $t_n = n(N - n)$. Now, let us imagine the interval has length L. If the initial condition is some fraction of L, αL, then the absorption time is

$$t_n = (\alpha - \alpha^2)L^2 \sim L^2. \tag{5.5}$$

Now that we follow this basic example, we are ready to examine the argument for $T_H \sim L^2 \log(L)$. Note: the following argument is that which we gave in Ref. [123], but this argument does not account for the variable time step in the relaxation process. We will discuss this point after first understanding the argument.

The dependence of T_H on L appears to have a simple geometrical origin. To reach a frozen three-hexagon state, an initial realisation first has to condense to a state that consists of three clusters, none of which span the system (shown in the third panel of Figure 5.2 and schematically in Figure 5.12). This three-cluster state contains geometric distortions whereby the six T-junctions—points where three interfaces meet—are out of registry compared to the aligned T-junctions in the frozen three-hexagon state (third panel of 5.2).

Each of the interfaces between pairs of adjacent T-junctions is thus tilted with respect to a triangular lattice direction. This means that a substantial fraction of the spins on

each such interface are freely flippable. Each freely flippable spin on an interface is equivalent to an independent random walker that can hop along the interface [156].

The tilted interfaces must gradually straighten for the configuration to reach the frozen three-hexagon state. This straightening process occurs by the motion of the equivalent random walkers. When a random walker reaches a T-junction, the position of the latter moves by one lattice spacing. This displacement corresponds to the random walker being absorbed at the T-junction. Thus we can view the process of interface straightening as equivalent to the successive absorption of the order of L independent random walkers on a finite interval whose length is also of the order of L.

When there are k walkers in an interval, their typical separation is L/k; this is also the distance between the end of the interval and the closest walker to the interval end [123]. The first passage time until this closest walker reaches the end of the interval and is absorbed there is given by $t_k = \frac{L}{k}(L - \frac{L}{k})$. When all the walkers along the interfaces have been absorbed, the final, frozen three-hexagon state has been reached. By adding these individual absorption times until all walkers have been absorbed (see Ref. [123]), the time to reach the frozen three-hexagon state is (ignoring constants of order 1)

$$
\begin{aligned}
\tau &= t_L + t_{L-1} + \cdots + t_1 = \sum_{k=1}^{L} \frac{L}{k}\left(L - \frac{L}{k}\right) \\
&\simeq L^2 \log(L).
\end{aligned}
\tag{5.6}
$$

While crude, this argument appears to capture the mechanism behind the slower-than-expected approach to the three-hexagon state. However, it fails to account for the fact that the time between spin flip events grows as the number of active sites decreases, so it is flawed. In light of our explanation behind the $\sim L^2 \log(L)$ time scaling in the Ising model—which actually accounted for the growing time step as the number of active sites decreased—in Chapter 4.2—C, it is likely this argument is not actually appropriate. Nevertheless, it still remains important to understand, both for posterity and

because it was an important step in the development of the argument in Chapter 4.2—C, which we now believe is the correct way to explain this ordering process.

5.4 HIGHER q—A BRIEF LOOK

In this work we also briefly examined higher q Potts models. Apart from finding more exotic tilings—hexagonal final states with more than three-clusters—we noticed an interesting feature in the late time evolution of the density of surviving spin states.

The density of each of the spin types in the system P_n is simply the count of the number of sites in each orientation divided by the total number of spins L^2. At fixed
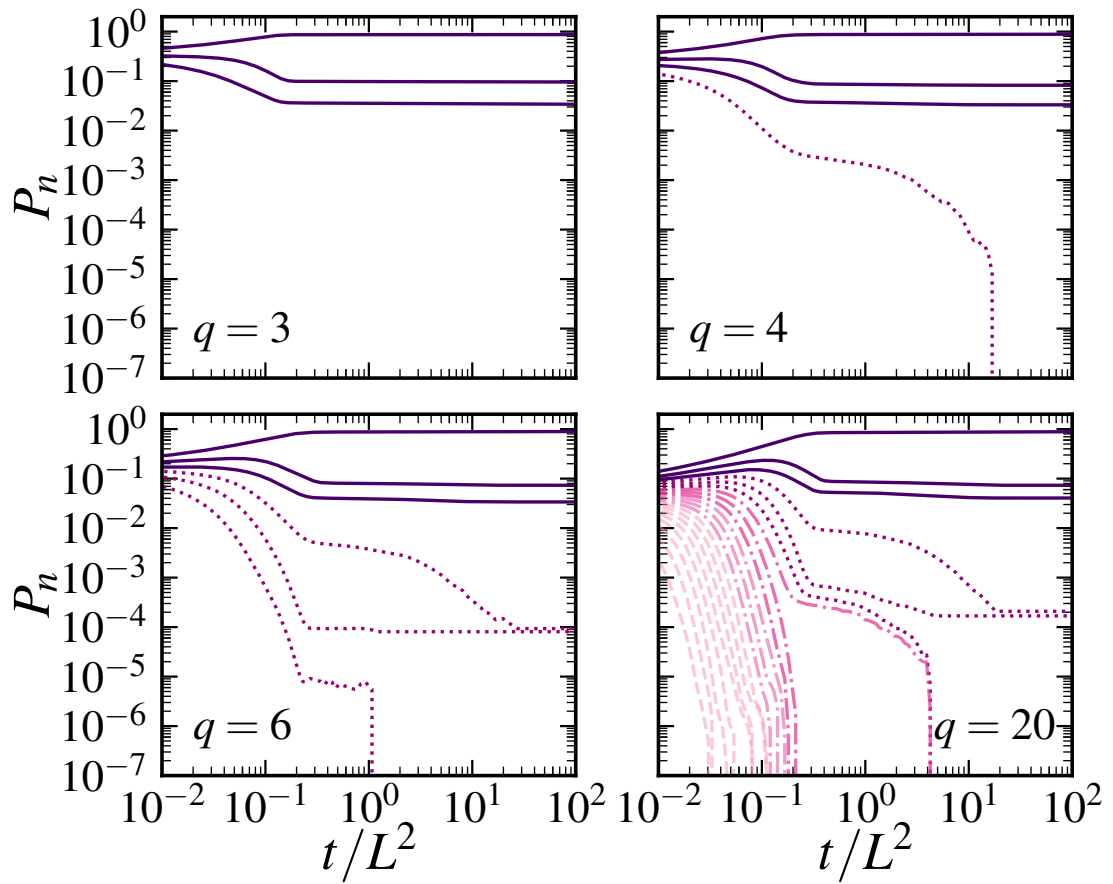
FIGURE 5.13 – Mean population density of each spin type P_n versus time for specified degeneracy q. At each point in time the number of spins in each distinct state are sorted in ascending order. The dominant populations (solid lines) are roughly constant at late time regardless of q. The data are based on 10^4 realisations from antiferromagnetic initial conditions with $L = 240$.

points in time we compute this quantity—ranked in descending order—and plot the average density as a function of time in Figure 5.13. The main point in Figure 5.13 is that the densities of the top three surviving spin states at late time are essentially identical regardless of the initial degeneracy q. Furthermore, it suggests the "top three"— ground, three-hexagon and two-stripe states—are still vastly the most abundant final states even at higher q.

5.5 SUMMARY

In this chapter I presented studies of the late-time phase ordering kinetics of a triangular lattice Potts model that was quenched to zero-temperature by way of metropolis dynamics. I first introduced the categories of final states: ground states, stripe states and hexagon states in Section 5.2. To our knowledge these final states have neither been realised nor quantified on the triangular lattice Potts model in the literature. I then estimated the probability of finding each of the final states as a function of system size, and analysed the domain areas in two-stripe and three-hexagon configurations.

Surprisingly, I also found a variety of coarsening timescales associated with various relaxation properties in Section 5.3. While observing the standard coarsening time of $O(L^2)$, there is also an anomalous relaxation timescale associated with three-hexagon states which I claim grows as $\sim L^2 \log(L)$—or at least approaches this scaling form as the system size increases. I also gave an argument in favour of this scaling form based on absorbing random walkers, but with hindsight the argument in Section 4.2—C better explains the origin of this scaling form because it accounted for the non-fixed timestep in the relaxation process. I also found a long-lived timescale that grew as roughly $\sim L^{3.1}$, which arose from ground state relaxations that first evolved through off-axis three-cluster configurations.

Finally, I briefly examined how the density of surviving spin states varied as a function of time for various initial q. Here the main finding was that these densities

appear to be vastly dominated by the three most abundant spin states, which are roughly equal in density at late time regardless of the initial degeneracy.

CHAPTER

SIX

POTTS MODEL: INCREASED DEGENERACY

After the surprising findings in the previous chapter—which showed the Potts model to be considerably more tractable from a numerical standpoint on the triangular lattice—one obvious question arises: what happens when the degeneracy of the system is increased—do more exotic final states arise?

In the previous chapter, we saw that the triangular lattice Potts model seemingly always reaches frozen final states that are easy to characterise. We also saw, somewhat briefly, that increasing the degeneracy—i.e. the number of spin states—gave rise to final states with more than three clusters. In this chapter we will examine what happens when a Potts ferromagnet with more than three spin states is quenched to zero-temperature, and see how the provisional findings I present are motivation for further research.

In Section 6.1, we explore the role played by the initial condition in the final state probabilities. We then visually introduce the richer final states that arise when $q > 3$ in Section 6.2. We examine the final state probabilities as a function of L for various q in Section 6.3, and then as functions of q with L fixed in Section 6.4. Finally, we shall summarise my findings in Section 7.4.

6.1 CHOICE OF INITIAL CONDITION

Before we examine and discuss the data from higher q Potts models, we must first revisit the question of the initial condition. For small q, the antiferromagnetic initial condition seems like a natural choice. With random initial conditions, there are a huge number of initial configurations to average over, whereas with the antiferromagnetic configuration one need only average over the possible trajectories from a constant initial condition. However, as we approach the regime where $q \sim L$, it seems prudent to check that the final state probabilities remain the same when one uses either randomly ordered or antiferromagnetic initial conditions.

The first test we perform is as follows: we fix the number of spin states and investigate the final state probabilities as a function of the system size L for both randomly ordered and antiferromagnetic initial conditions. Note: we obtain random initial conditions by taking an antiferromagnetic configuration—where each spin state is equal in concentration—and rearranging the configuration in a random order.

We plot the resulting data for the ground, three-hexagon and two-stripe final state cases in Figure 6.1 (a)–(c). In each case we use three spin-states, and the corresponding probability estimates for the random and antiferromagnetic cases are within error bars of each other.

Now that we have checked the probability estimates for fixed q as a function of L, the next most logical step is to examine the final state probabilities in fixed system sizes and vary the number of spin-states. We consider a system of $L = 60$ and simulate 3×10^5 realisations for each q. In order to ensure that each spin type is equal in population in the initial condition, we keep the lattice size an even integer multiple of q over the range $3 \leq q \leq L$; Specifically, we set $L = q \times 2^n$ with $n \in \{1, 2, 3 \ldots\}$.

We plot the resulting probability estimates for the ground, three-hexagon and two-stripe final states in Figure 6.2 (a)–(c). Again, the corresponding estimates from the antiferromagnetic and random initial conditions are within error bars of each other.
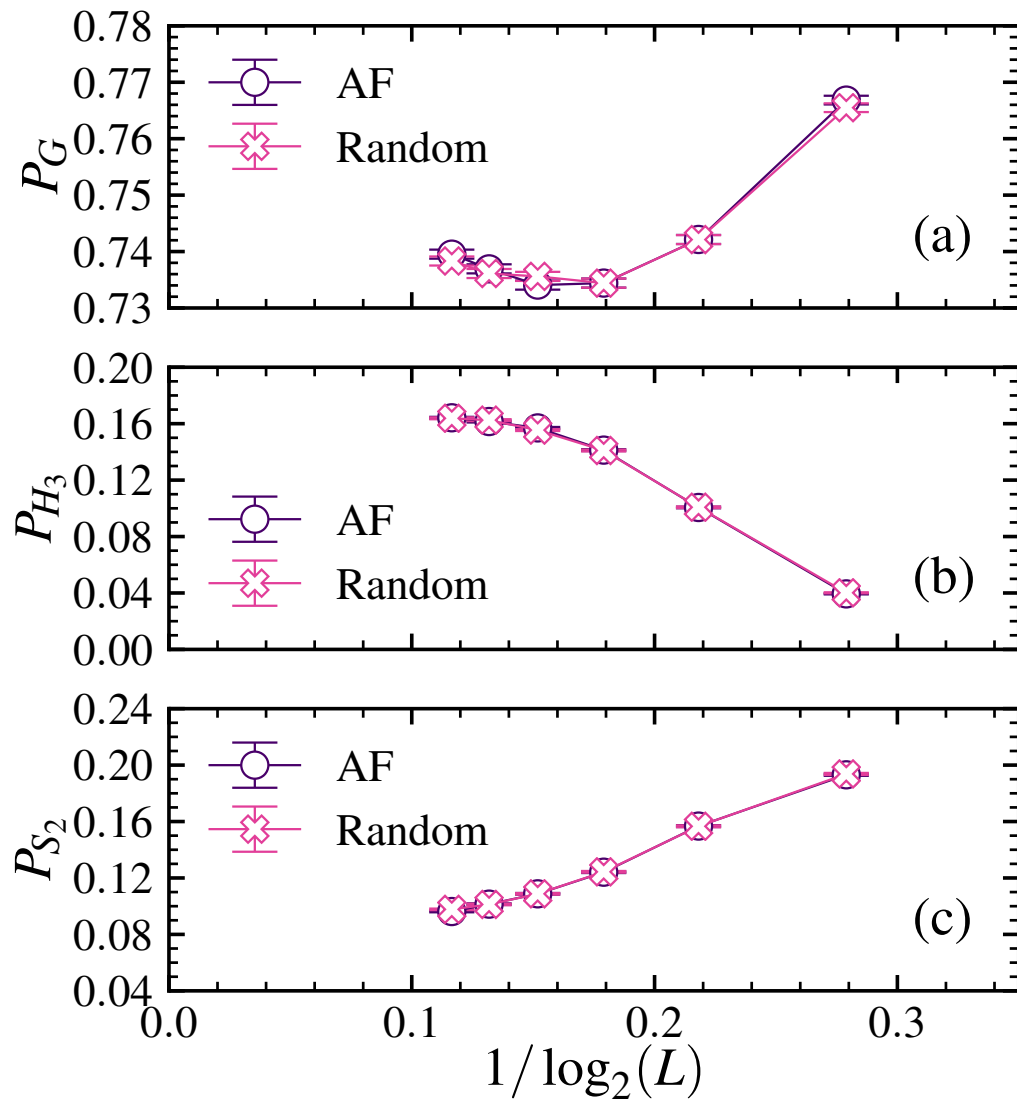
FIGURE 6.1 – Probability of freezing into (a) the ground, (b) a three-hexagon and (c) a two-stripe final state versus the inverse logarithm of the the system size from both antiferromagnetic (circles) and random (crosses) initial conditions. The data are based on 3×10^5 realisations and $q = 3$.

Therefore, it seems that one may safely use either random or antiferromagnetic initial conditions without fear of biasing the final state probabilities. We shall discuss the behaviours in Figure 6.2 in greater detail Section 6.4—for now now pay no mind to how the probabilities vary with q.
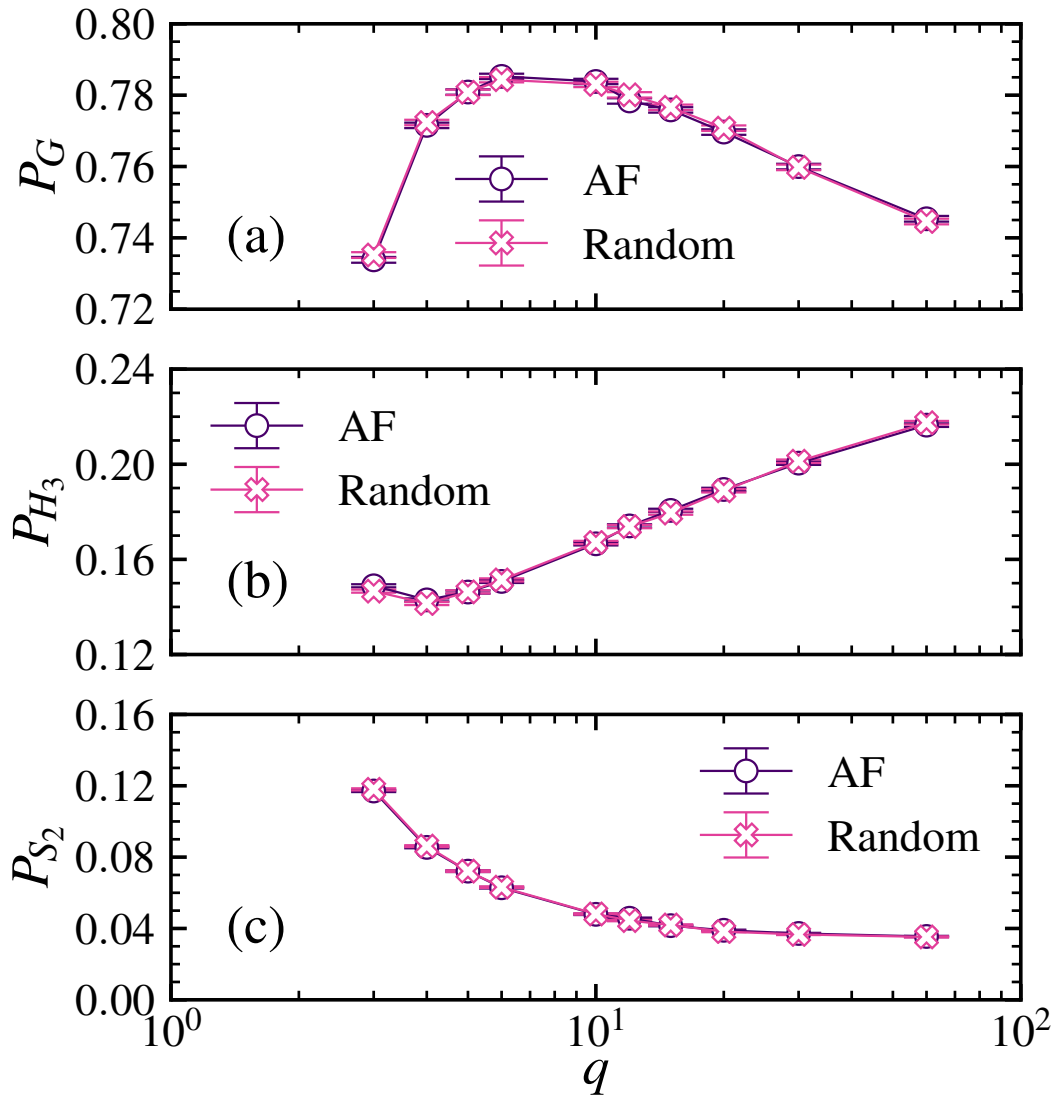
FIGURE 6.2 – Probability of freezing into (a) the ground, (b) a three-hexagon and (c) a two-stripe state versus the degeneracy q for both antiferromagnetic (circles) and random (crosses) initial conditions. The data are based on 3×10^5 realisations on a system of length $L = 60$.

6.2   RICHER FINAL STATES

Let us now visually introduce the "richer" final states that we have already hinted arise when one considers more than three spin-states. Essentially the main thing that happens when the number of spin states is increased is that two "new" varieties of final state emerge: hexagon states with more than three clusters and "blinkers". In comparison to the most common final states that we are already familiar with, these new states occur

with negligible probabilities—particularly the blinkers.

6.2—A HEXAGONAL TILINGS

The most abundant of the higher order tilings is the five-hexagon state; an example

of which is shown in Figure 6.3 (a). As was the case in the three-hexagon state, the

domain boundaries run parallel to the lattice axes, making the configuration stable. In

the five-hexagon state, the total length of the interface is $4L$, thus giving $8L$ boundary

spins. If one "looks along" each of the interfaces in the system, they should note that

each spin has 2 misaligned neighbours—each contributing $+2J$ to the energy—so the

total energy of the configuration is $32L$. Remarkably, the energy of an n-hexagon final

state does not depend on the individual areas of the hexagons, but rather the total length

of interface in the system—which is fixed. I also observed eight- and twelve-hexagon

final states (Figure 6.3 (b)–(c)). Surprisingly, it is possible to have a twelve-hexagon

tiling with *only* three spin-states—as shown in Figure 6.3 (c)—which is a "three-colour"

tiling.

Using the same reasoning as before, we can easily determine the energy of these

tilings. In the eight-hexagon state, the total length of the interface is $5L$, which gives

$10L$ boundary spins and a total energy of $40L$. Similarly, in the twelve-hexagon state
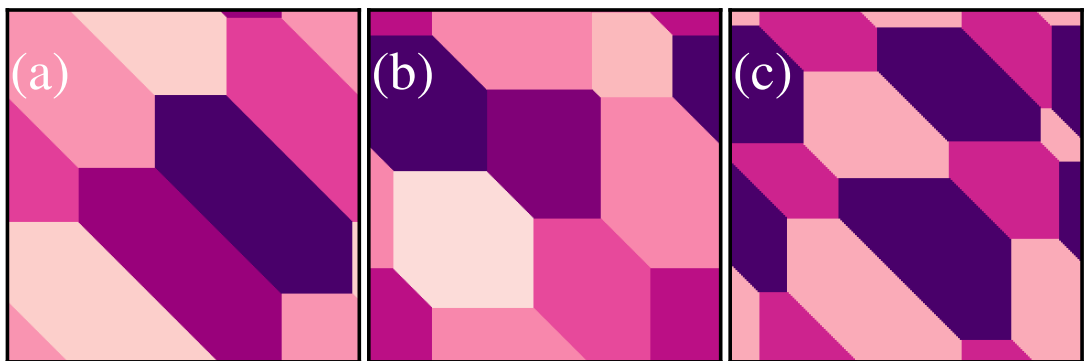
FIGURE 6.3 – (a) A five-hexagon state in a $q = 10$ Potts model of $L = 320$. (b) An eight-hexagon state in a $q = 10$ Potts model of $L = 320$. (c) A twelve-hexagon state in a $q = 3$ Potts model of $L = 192$. The energy of the final states in (a)–(c) are $32L$, $40L$ and $48L$ respectively.

Clusters	Interface length	Interface spins	Energy
3	$3L$	$6L$	$24L$
5	$4L$	$8L$	$32L$
8	$5L$	$10L$	$40L$
12	$6L$	$12L$	$48L$

TABLE 6.1 – Final state energies in frozen hexagon configurations. Note: in these units each "bond" is counted twice".

the total length of the interface is $6L$, so the total energy is $48L$. An overview of the energies of these configurations are given in Table. 6.1.

6.2—B   BLINKERS

Blinkers are configurations in which the system is *forever* trapped in a *local* energy minima, but *always* has flippable spins. In other words, the system wanders on an iso-energy surface ad infinitum.

In both the cubic lattice Ising model and the square lattice Potts model, blinker configurations have proven difficult to identify. [54, 98, 99, 122]. There can be huge time steps between energy lowering moves in configurations that resemble blinkers, so it is difficult to discern if the system is genuinely trapped at constant energy or on an ultra-slow approach to an energy lowering move. The triangular lattice Potts model apparently stands in contrast to this; here blinkers seemingly only occur with $q \geq 5$, and consist of merely a few active sites that are well separated from each other. These active sites are typically surrounded by 4 unique spin states.

Consider the example realisation shown in Figure 6.4. This configuration has only a single blinker spin—marked by the black cross—that is surrounded by a nearest neighbour configuration of $S_j = \{1, 1, 2, 3, 4, 4\}$. The West and North-West neighbours are of spin-type $S_j = 1$, and the East and South-East neighbours are of spin-type $S_j = 4$. Consequently, the blinker spin may always flip between spins states $S_i = 1$ and $S_i = 4$ with no energy cost, and may never align with the North or South sites without incurring an energy cost. This representative example explains both the geometric and infinitely

$$t = 1.0L^2 \qquad t = 10.0L^2 \qquad t = 100.0L^2 \qquad t = 1000.0L^2$$
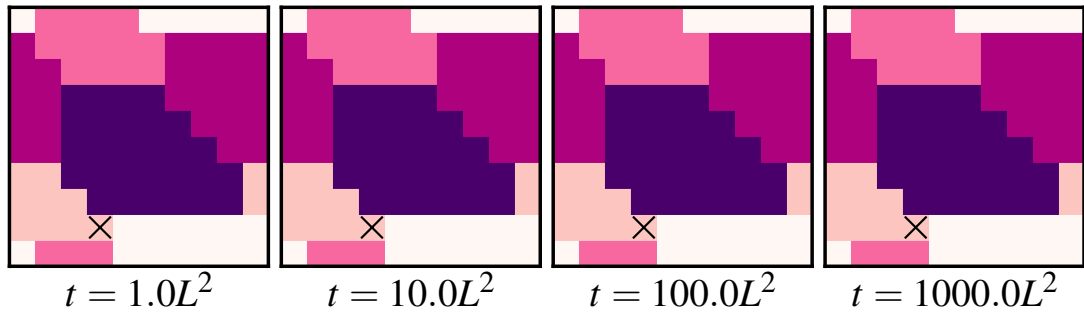
FIGURE 6.4 – A realisation of zero-temperature coarsening in a ten-state triangular lattice Potts model of $L = 10$ that is forever trapped in a *blinker* configuration. This configuration has only a single active site that is marked by the black cross. Note the exponentially growing timestep between the frames.

long-lived nature of blinkers on the triangular lattice.

Blinkers occur with probabilities of order 10^{-3} for only $q \geq 5$ and in the smallest of system sizes. They decay in prevalence such that they do not appear in my data for $L \geq 60$, and thus contribute negligibly to the coarsening dynamics. Consequently, I don't address them any further in this Section.

6.3   PROBABILITIES WITH q FIXED

Now that we are familiar with the other kinds of final states that arise when $q \geq 3$, let us examine the following simple question: how do the final state probabilities vary with system size L for different values of q? We begin with the ground state.

6.3—A   GROUND STATE

In the three-state Potts model we saw that roughly 3/4 of all realisations reached the ground state. In Figure 6.5, we show the probability of freezing into the ground state as a function of the inverse logarithm of the system size for various initial q. At first glance, it appears that increasing the degeneracy of the system increases the likelihood of reaching the ground state. However, when $q = 20$ we see a reduction in P_G with respect to $q = 5$ and $q = 10$; for the largest system sizes, $P_G \approx 0.80$ when $q = 10$ and $P_G \approx 0.78$ when $q = 20$. Perhaps this signals a non-monotonicity in P_G as a function

of q. This idea is consistent with the data shown in Figure 6.2 (a).
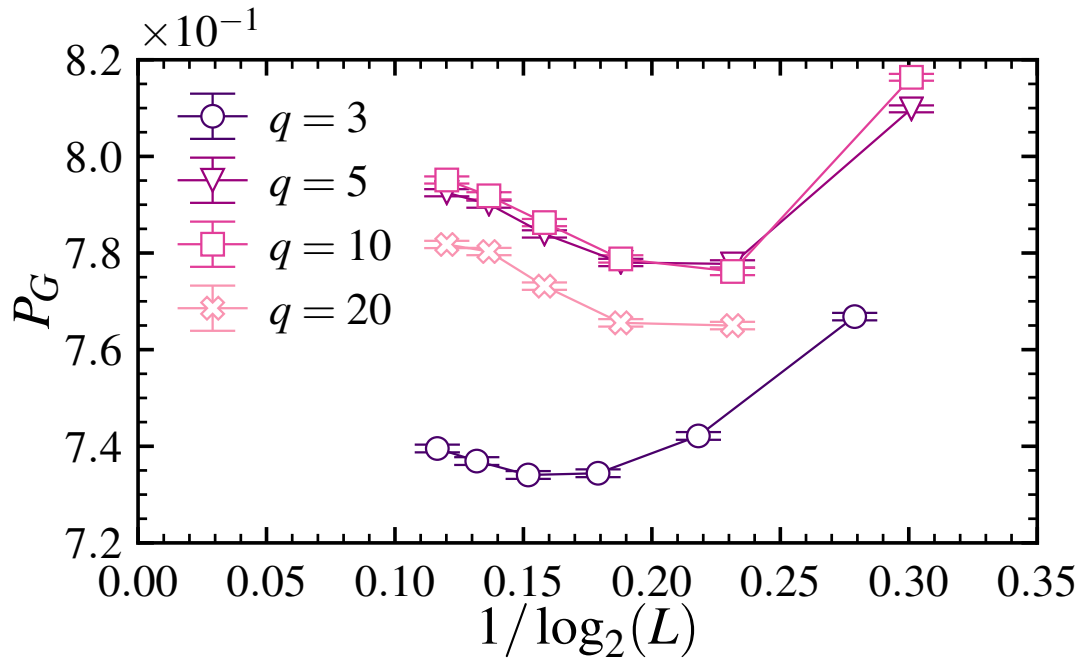
FIGURE 6.5 – Ground state probability P_G versus the inverse logarithm of system size L for specified q. The data are based on 3×10^5 realisations from the antiferromagnetic initial condition, and the lattice sizes are $L = q \times 2^n$ with $n = 1, \, 2, \, 3 \ldots$.

6.3—B   HEXAGON STATES

Let us now examine the three-hexagon state probability P_{H3}—note the slight notation change from P_H in the previous chapter—as a function of $1/\log_2(L)$ for various q. Recall that in the three-state Potts model, we said that roughly 16% of all trajectories resulted in a three-hexagon state.

We plot the probability of reaching a three-hexagon state against the inverse logarithm of the system size in Figure 6.6. Again, we see hints of non-monotonicity: P_{H3} seem to decrease—regardless of L—between $q = 3$ and $q = 5$, after which it begins to increase. This is consistent with the data presented in Figure 6.2 (b). I also found five-, eight- and twelve-hexagon configurations, which occur with probabilities of order 10^{-3}, 10^{-5} and 10^{-5} respectively.
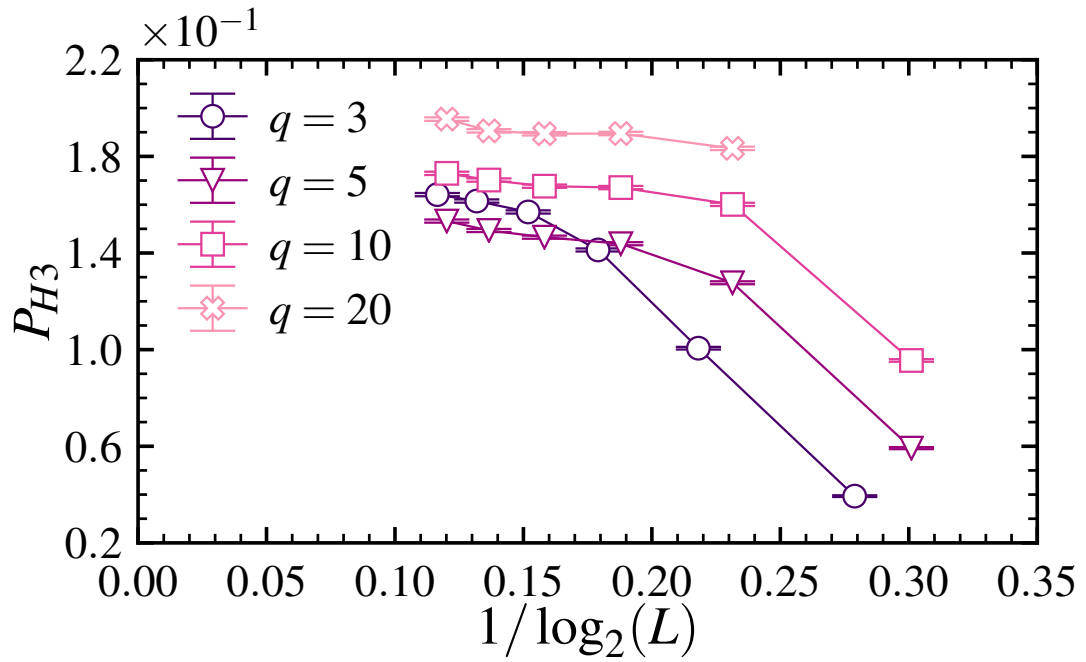
FIGURE 6.6 – Three-hexagon state probability P_{H3} versus $1/\log_2(L)$ for specified q. The data are based on 3×10^5 realisations from the antiferromagnetic initial condition, and the lattice sizes satisfy $L = q \times 2^n$ with $n = 1, 2, 3 \ldots$.

6.3—C   STRIPE STATES

Here we examine the probability of freezing into two- (P_{S2}) and three-stripe (P_{S3}) states as a function of L for various initial q. For three spin states, we saw that the probability of finding two-stripe states was roughly 9% with $L = 384$, and the three-stripe state probability (P_{S3}) was essentially negligible—on the order of 10^{-5}—at high L. In Figure 6.7, we plot the probability of freezing into a two-stripe state as a function of the inverse logarithm of the system size for $q \in \{3, 5, 10, 20\}$.

In Figure 6.7 we see that P_{S2} seemingly decays to zero as $L \to \infty$ regardless of the degeneracy of the system. It is also clear that increasing q has the general effect of lowering the two-stripe state probability. In Figure 6.8 we see that with increasing q, the probability of freezing into a three-stripe state remains negligible, and the same general effect of lowering the probability with increasing q is also present. Conjecturally, the salient point here is that the likelihood of finding on-axis stripe states—with any number of clusters—seemingly decays when increasing either L or q.
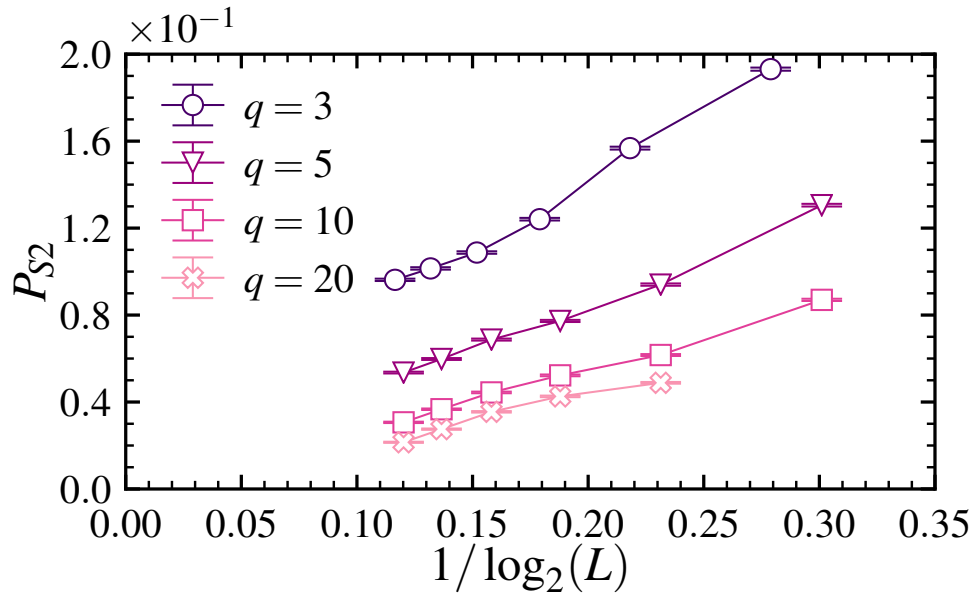
FIGURE 6.7 – Two-stripe state probability P_{S2} versus $1/\log_2(L)$ for specified q. Here P_{S2} decays monotonically with increasing q regardless of L. The data are based on 10^5 realisations from the antiferromagnetic initial condition and the lattice sizes satisfy $L = q \times 2^n$ with $n = 1, 2, 3 \ldots$.
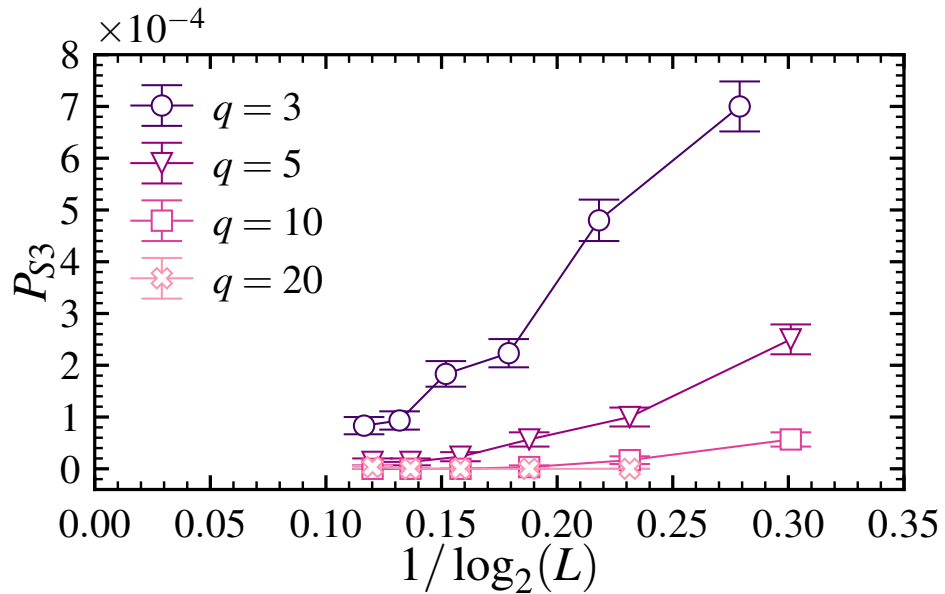
FIGURE 6.8 – Three-stripe state probability P_{S3} versus $1/\log_2(L)$ for specified q. The data are based on 10^5 realisations from the antiferromagnetic initial condition and the lattice sizes satisfy $L = q \times 2^n$ with $n = 1, 2, 3 \ldots$.

6.4   PROBABILITIES WITH L FIXED

Now that we have explored how the final states vary with L for various initial q, it seems

natural to fix the system size and investigate the final state probabilities as a function of

the degeneracy itself. We show estimates of the ground, three-hexagon and two-stripe state probabilities as function of q for $L = \{60, \ 120, \ 240\}$ in Figure 6.9 (a)–(c).
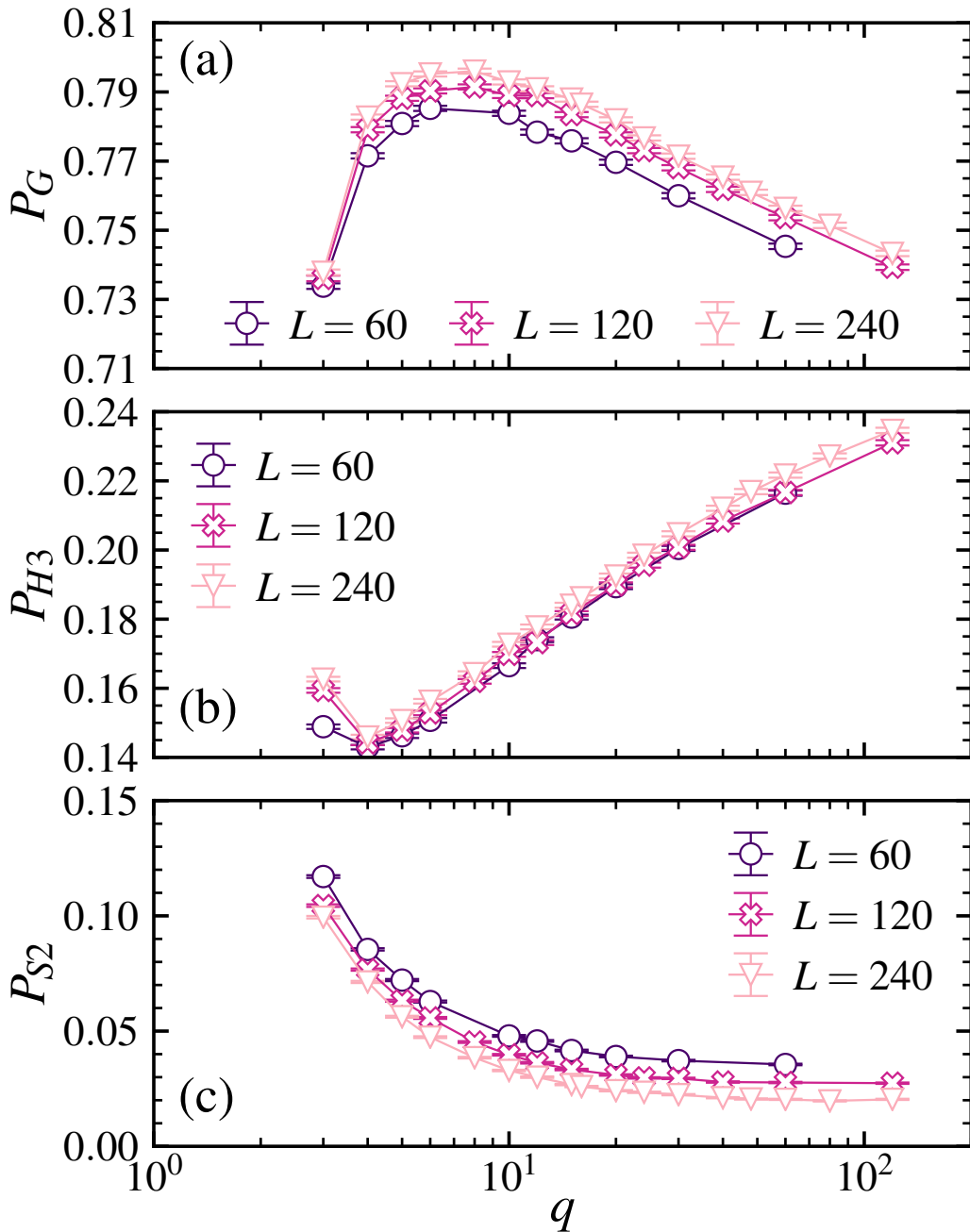
FIGURE 6.9 – Probability of freezing into (a) the ground, (b) a three-hexagon and (c) a two-stripe state as a function of the degeneracy q for specified system size L. The data are based on 3×10^5 realisations from antiferromagnetic initial conditions and use only q values that divide L.

In Figure 6.9 (a), the ground state probability initially grows with the number of spin states, and yet, at around eight spin states, it begins to decay. In Figure 6.9 (b), the
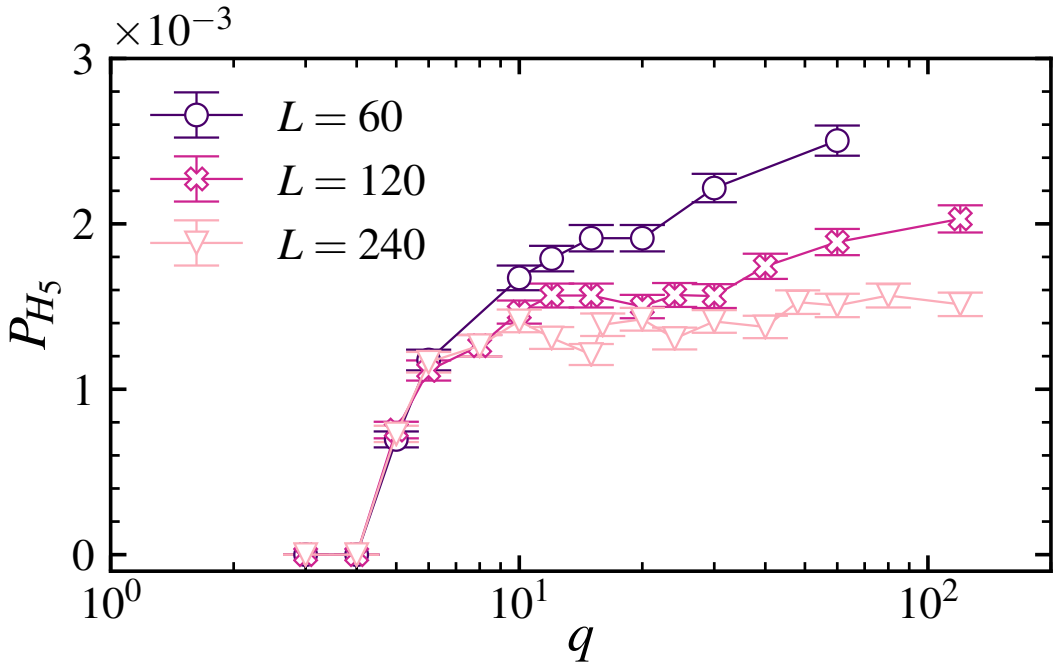
FIGURE 6.10 – Probability of freezing into a five-hexagon final state P_{H5} versus q for specified lattice sizes L. The data are based on 3×10^5 realisations from the antiferromagnetic initial condition.

probability of freezing into a three-hexagon state decays between $q = 3$ and $q = 4$, then oddly, increases for $q > 4$. The two-stripe state probability in Figure 6.9 (c) is the only one of these three cases that seems to approach the large q limit monotonically, though it is not clear if P_{S2} is on an asymptotic approach to some non-zero limit as $q \to \infty$.

While the ground state probability initially grows with q, the three-hexagon and two-stripe states decay in abundance. However, as the three-hexagon states begin to increase in likelihood, the growth of P_G slows until around $q = 8$, where it begins to decay. Thus, with increasing q, the ground and two-stripe state probabilities decay, while the probability of reaching a three-hexagon state grows. Qualitatively, these behaviours do not seem to depend on the lattice size.

Since P_{H3} grows with q, it seems natural to ask how the probability of observing hexagon states with more than three clusters behaves with q. The next most abundant hexagonal tiling has five clusters. P_{H5} is plotted as a function of q in Figure 6.10. In Figure 6.10, the probability of finding five-hexagon configurations is of order 10^{-3} for $q \geq 5$, and, at high q, seemingly decreases with L. Other hexagonal configurations

occur with probabilities on the order of 10^{-5}, but with only 3×10^5 realisations it is not helpful to plot them. This concludes my examination of the final states that emerge when the triangular-lattice Potts model that has $q > 3$ spins states, and we now move on to the square lattice.

6.5   SUMMARY

In this chapter I examined the final states that emerge when a triangular lattice Potts model undergoes a zero-temperature quench with $q \geq 3$ spin states. I demonstrated that the choice of initial condition does not influence the final state probabilities in Section 6.1, and then showed examples of the richer final states that arise when the degeneracy increases—namely higher order hexagonal tilings and blinker configurations—in Section 6.2. I investigated the final state probabilities in two situations: first as a function of the system size with q fixed in Section 6.3, and then as a function of the number of spin states with the system size fixed in Section 6.4.

My main findings are summarised in the following: the choice of the supercritical initial condition plays little role in the final state probabilities so long as it has net zero magnetisation—i.e. no significant regions that are ferromagnetically ordered. When the number of spin states is increased, two main things happen:

i. Frozen hexagon states with more than three clusters arise; namely, five-, eight- and twelve hexagon states with probabilities of order 10^{-3}, 10^{-5} and 10^{-5} respectively.

ii. Blinker configurations emerge on small lattice sizes where $L \sim 10$ with probabilities of $\sim 10^{-3}$, and decay in prevalence such that I never observed any at all regardless of q for $L \geq 60$.

The final state probabilities vary in peculiar non-monotonic fashions when expressed as functions of either the system or the number of spin states. In general, no significant new coarsening phenomenology emerges when $q < 3$. One interesting question that

emerges is: what happens if one consider the maximally degenerate case of $q = L^2$, i.e. if each lattice site is initialised with a unique spin state.

POTTS MODEL: SQUARE LATTICE

As we have seen that the Potts model is more tractable, at least from a numerical standpoint, on the triangular lattice, one might wonder what happens on the square lattice with second-nearest-neighbour interactions? If we build the triangular lattice by adding two diagonal bonds to each site in the square lattice, and this makes the system more tractable, it is reasonable to speculate that second-neighbour interactions might unveil an underlying simplicity in the square lattice Potts model.

In this chapter we explore this basic question. The chapter is organised as follows: we first examine interesting features of the second-nearest-neighbour Ising model in Section 7.1, which serves as an excellent numerical test of the simulations. Next, we examine the final state probabilities of the three-state Potts model with nearest-neighbour interactions only in Section 7.2, and then probe the second-nearest-neighbour Potts model in Section 7.3. Finally, we shall summarise my findings in Section 7.4.

The $q = 2$ Potts model is the Ising model. Interestingly, in the Ising model, when one considers a zero-temperature quench with non-zero second neighbour interactions—of *any* magnitude—$(1, 1)$ diagonal stripe configurations become stable: it is possible for the system to freeze into $(1, 1)$ stripe states [57]. This simplifying feature is rather interesting as it allows for the easy identification of $(1, 1)$ winding configurations, and in

a sense reduces the complexity of the system. It also begs the following simple question: does considering non-zero second neighbour interactions in the square lattice Potts model unveil any underlying simplicity in the final states? The late-time final states that persist in the nearest-neighbour case are challenging numerically and difficult to identify [122]. Let us first begin answering this question by considering the simplest case: the Ising model.

7.1   ISING CASE

As we seen in Chapter 4, one essentially finds three main behaviours when the Ising model undergoes a zero-temperature quench from above criticality. The system may freeze into a ground state ($P_{(0, 0)} \approx 0.62$), an on-axis stripe state ($P_{(1, 0)} + P_{(0, 1)} \approx 0.34$), or reach the ground state after first evolving through an off-axis diagonal winding configuration ($P_{(1, \pm 1)} \approx 0.04$) [79]. We ignore $(2, 1)$ winding configurations in this section as they occur with a tiny probability (1.567×10^{-4}) [57].

Here, we shall demonstrate the influence of second neighbour interactions in the Ising model to provide a foothold in understanding what might happen in the Potts model. We begin with the ground state; in the absence of second neighbour interactions, there are two topologically distinct categories of evolution reach the ground state: $(0, 0)$ and $(1, \pm 1)$. This means the total ground state probability is (see Ref. [79])

$$
\begin{aligned}
P_G &= P_{(0, 0)} + P_{(1, \pm 1)} \\
&= 0.61908 + 0.04196 \\
&= 0.66104.
\end{aligned}
\tag{7.1}
$$

However, $(1, \pm 1)$ windings become stable when the second-neighbour interaction strength $J_2 \neq 0$, so the ground state probability simply becomes $P_{(0, 0)}$. We plot the ground state probability of the second-neighbour Ising model in Figure 7.1 for specified
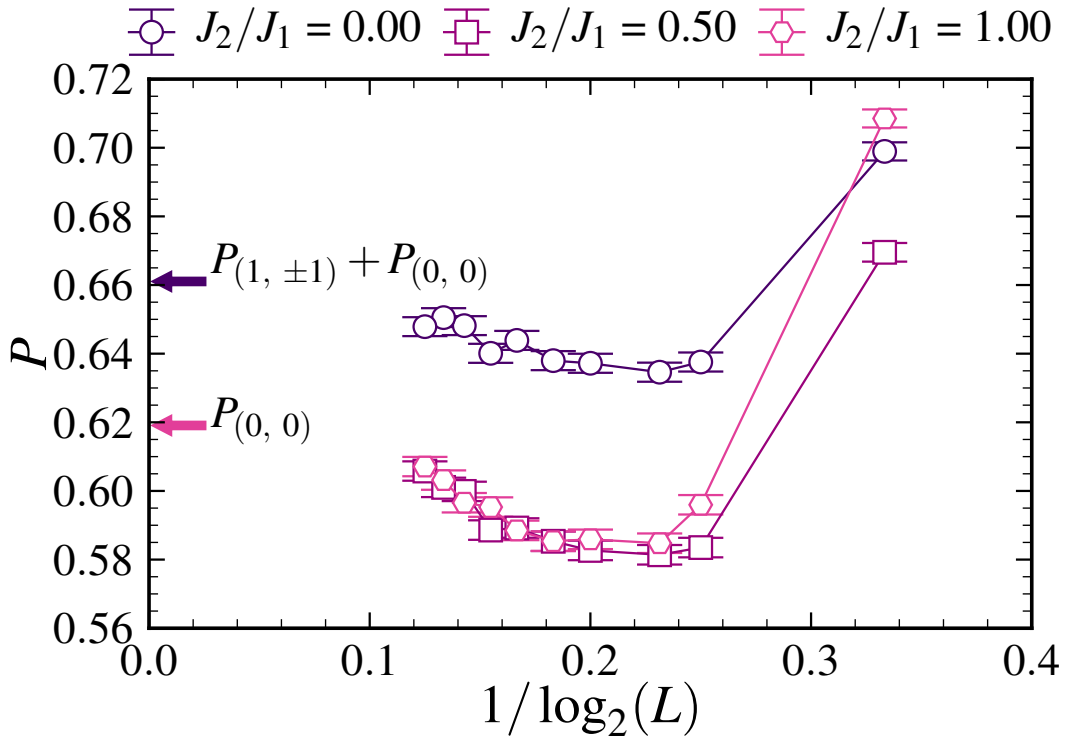
FIGURE 7.1 – Ground state probability versus $1/\log_2(L)$ in the zero-temperature Ising model for specified ratios of the first- and second-neighbour interaction strength J_2/J_1. The marked arrows indicate the asymptotic predictions from continuum percolation theory as quoted in Ref. [79]. The data are based on 3×10^4 realisations from random initial conditions.

ratios of $J_2 : J_1$. Despite the non-monotonic approach to the asymptotic limit, one can easily see the qualitative influence of having non-zero second-neighbour interactions: the ground state probability drops from $P_{(0,\, 0)} + P_{(1,\, \pm1)}$ to $P_{(0,\, 0)}$ when $J_2 \neq 0$.

It is also interesting to visualise this phenomenon by considering the probability of finding a frozen "off-axis"—or $(1,\ \pm1)$—winding configuration with various zero and non-zero second-neighbour interaction strengths. We plot this quantity in Figure 7.2: when $J_2/J_1 = 0$, the probability of freezing into a $(1,\ \pm1)$ configuration is zero, and when $J_2/J_1 \neq 0$, the probability approaches the asymptotic limit of $P_{(1,\, \pm1)} = 0.04196$. Note, the approach to the asymptotic limit is not definitive here because we use only 3×10^4 realisations.
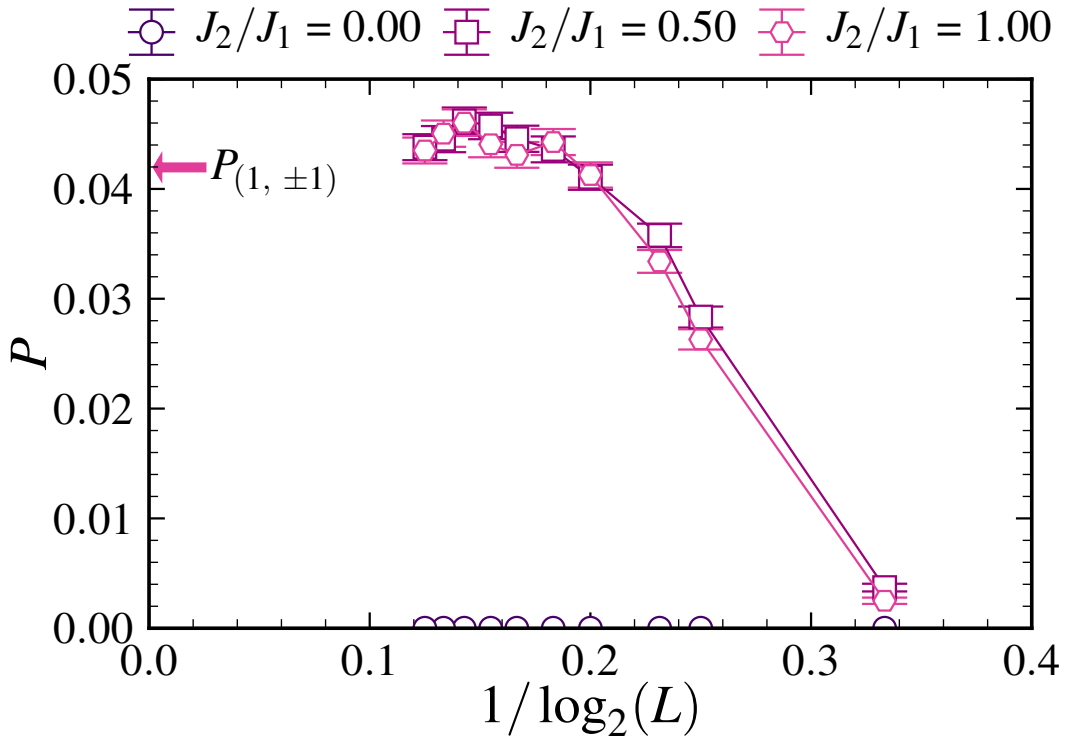
FIGURE 7.2 – Probability of freezing into a $(1, \pm 1)$ winding configuration in the zero-temperature Ising model for specified ratios of first- to second-neighbour interactions. The data are based on 3×10^4 realisations from random initial conditions and the arrow indicates the asymptotic prediction from percolation theory given in Ref. [79].

7.2   NEAREST-NEIGHBOUR POTTS MODEL

Discerning the final state of the nearest-neighbour Potts model at zero-temperature has proven itself a considerable challenge [122]. The main issue: blinkers—or at least, "pseudo blinkers". Configurations that strongly resemble blinkers persist for exorbitant periods of time before a single energy lowering flip triggers a sudden "energy avalanche", where the system globally reorders and undergoes a macroscopic decline in energy. [122]. Determining if a realisation has fallen into a genuine blinker configuration or is merely on an ultra-slow approach to an energy lowering move is the source of this difficulty [122].

Although the authors of Ref. [122] proposed a scheme to determine if a given microstate is genuinely in a blinker configuration, such tests are still numerically cumbersome. Since the purpose of my investigation here is to probe for qualitative

differences in the final state when considering non-zero second-neighbour interactions, we avoid this scheme and simply say that any configuration still active by $t = 100L^2$ is in a blinker configuration. With this in mind, we shall briefly examine the final states one finds when $J_2 = 0$ before examining the situation when $J_2 \neq 0$. Firstly however, we must examine the source of the complexity on the square lattice: T-junctions.

7.2—A   T-JUNCTIONS ON THE SQUARE LATTICE

The increased complexity in the nearest-neighbour Potts model, with respect to the Ising model, originates from so called "T-junctions" [122]. A "T-junction" is a stable three colour tiling that becomes possible when there are more than two spin states (Figure 7.4). When these configurations arise, they underpin non-spanning metastable
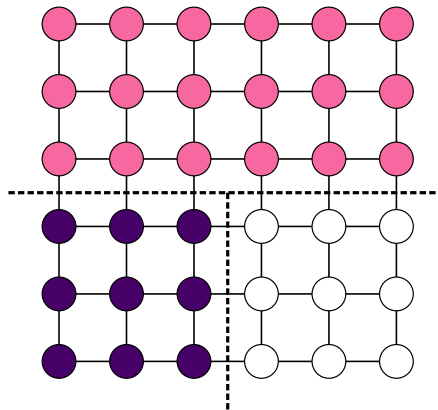
FIGURE 7.3 – A "T-junction" in the square lattice Potts model with nearest-neighbour interactions. Each spin in the junction is aligned with the majority of its neighbours, and is thus frozen.

tilings that have no flippable spins, and also give rise to blinker configurations; unstable interfaces become pinned between two T-junctions and are thus forever trapped. An illustration of a T-junction is shown in Figure 7.3, where one can see that each spin around the junction is aligned with the majority of its neighbours and is therefore frozen. An example of a static metastable final state realisation relying on eight T-junctions is plotted in Figure 7.4; each meeting point between three clusters is made stable by the T-junction formation.

$$t = 0.001L^2 \qquad t = 0.01L^2 \qquad t = 0.1L^2 \qquad t = 0.5125L^2$$
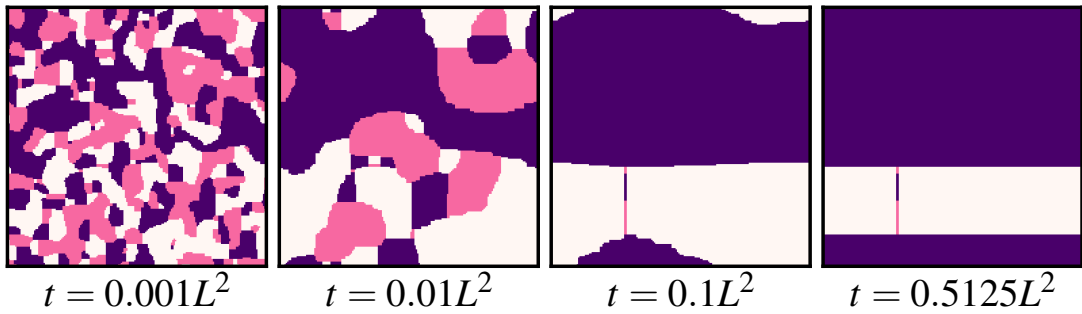
FIGURE 7.4 – A metastable final state realisation at zero-temperature in the three-state Potts model with $L = 192$. The final state has five clusters and eight "T-junctions".

Another configuration that is underpinned by T-junctions is the blinker configuration; an example of which is shown in Figure 7.5. In such configurations, unstable interfaces between domains are pinned in place by two T-junctions—e.g. see the off-axis interfaces in the final panel of Figure 7.5—thus the configuration is infinitely long lived.

$$t = 0.01L^2 \qquad t = 0.1L^2 \qquad t = 1.0L^2 \qquad t = 100.0033L^2$$
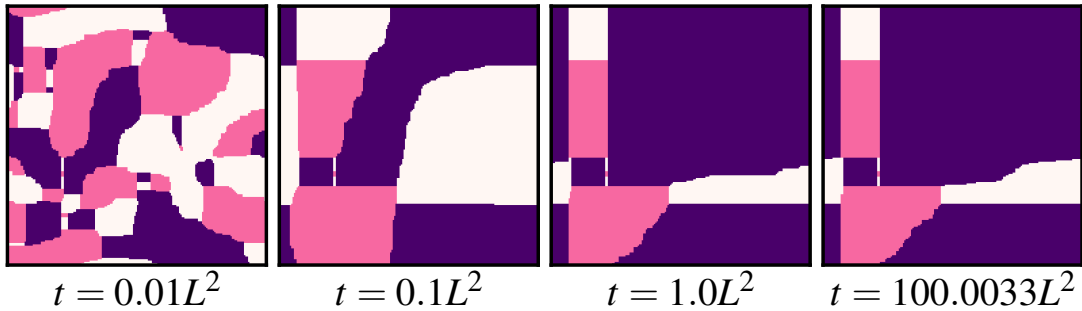
FIGURE 7.5 – A blinker state realisation of zero-temperature coarsening in a square-lattice Potts model with $q = 3$ and $L = 192$. Note how the off-axis interfaces in the final panel are pinned between "T-junctions".

7.2—B ROUGH PROBABILITY ESTIMATES

The probability of reaching a ground, on-axis two-stripe, non-spanning metastable and blinker configuration is plotted in Figure 7.6 (a)–(d). In Ref. [122], the authors plot the probability of reaching the ground state before $t = 2L^2$, which is consistent with my findings in Figure 7.6 (a)—in the regime of $L \geq 192$, the ground state probability is roughly 10%. The probabilities plotted in Figure 7.6 (b)–(d) have not been presented in the literature; in Figure 7.6 (b), the probability of freezing into an on-axis two-stripe state seemingly approaches zero as $L \to \infty$. Static non-spanning metastable configurations
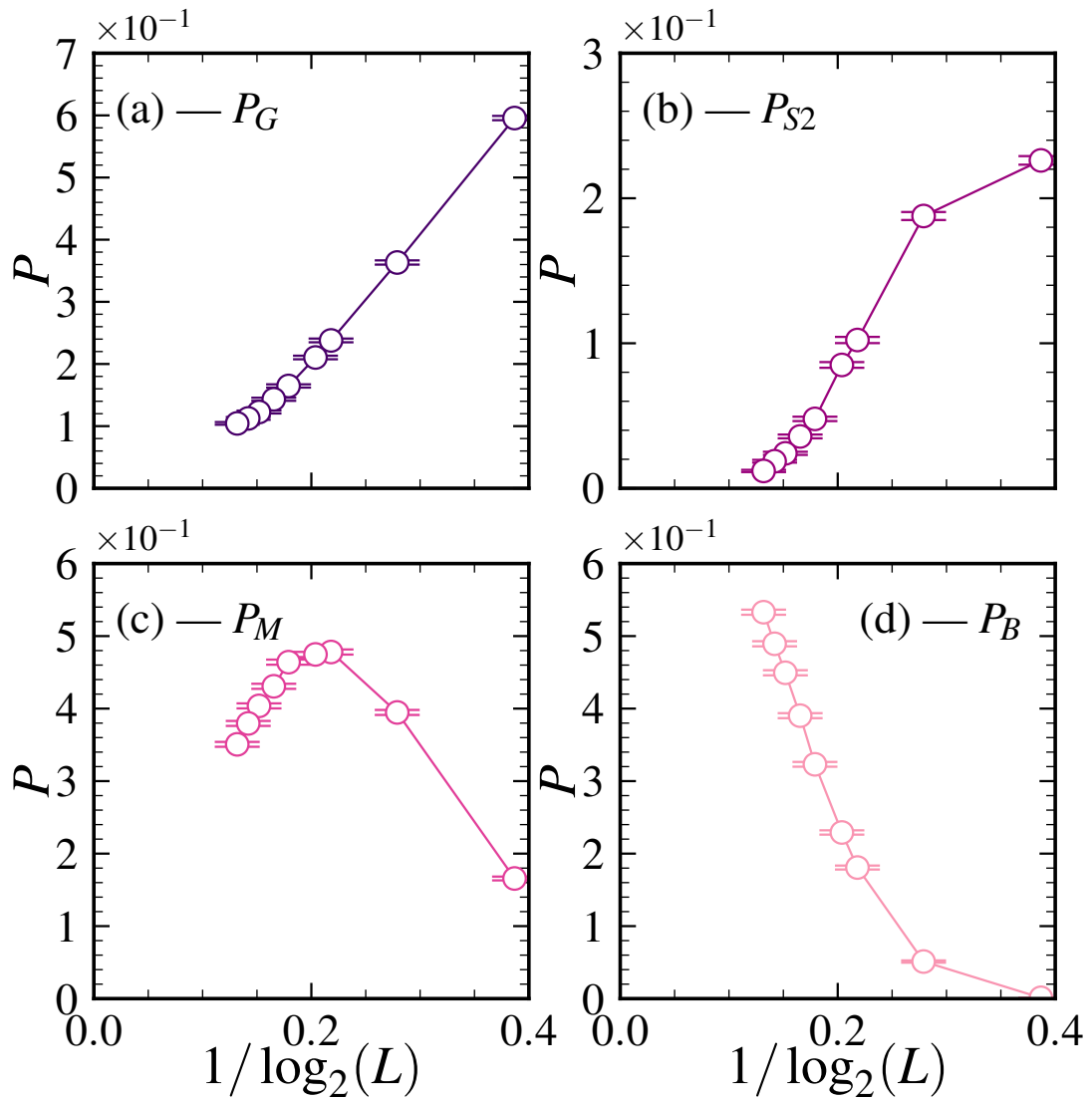
FIGURE 7.6 – Probability of freezing into (a) the ground state, (b) an on-axis two-stripe state, (c) a non-winding metastable tiling and (d) a blinker configuration in the nearest-neighbour Potts model on the square lattice with $q = 3$. The data are based on 2×10^4 realisations from random initial conditions.

initially increase in abundance with L, before decaying on the approach to large L (see Figure 7.6 (c)). In Figure 7.6 (d), the probability of reaching a blinker configuration—or specifically, the probability that flippable spins remain at $t = 100L^2$—seems to diverge as $L \to \infty$. It is important to note that the probability estimates in Figure 7.6 are rough, and based on only 2×10^4 realisations.

Interestingly, in Ref. [122], the probability of reaching the ground state before $t = 2L^2$ showed hints of a increasing for $L \geq 384$ and $q \geq 3$, however here I focus only

on a three-state Potts model.

7.3   SECOND-NEIGHBOUR POTTS MODEL

Before turning to simulations with $J_2 \neq 0$, there is some simple and obvious reasoning one can employ to help understand what might happen. Firstly, the inclusion of second-neighbour interactions makes $(1, \pm 1)$ winding configurations stable, so it is reasonable to expect such final states—though it's worth noting that these configurations were not found by Olejarz *et al.* [122]. Secondly, one should make the obvious realisation that T-junctions become unstable when $J_1 = J_2$.

   If we look closely at Figure 7.3, one can see that the upper right purple spin becomes flippable when $J_1 = J_2$ because the energy contribution from its three purple neighbours is equal to that of its three pink neighbours. It is therefore reasonable to expect materially different behaviour from the system in this special case.

   We begin our exploration of non-zero second-neighbour interactions with the ground state case. In Figure 7.7 (a), the ground state probability estimates are not materially different for $J_2 < J_1$, however, when $J_2 = J_1$ we see a sudden contrast to the former case. For $L = 192$, the ground state probability is around 10% for $J_2 < J_1$, and jumps to roughly 72% when $J_2 = J_1$. Immediately this suggests that our expectation of different behaviour for $J_1 = J_2$ is correct: when T-junctions become unstable the final state probabilities are markedly different.

   The next quantity of interest is P_{S2}: the probability of reaching an on-axis two stripe state. In Figure 7.7 (b), we again see that for $J_2 < J_1$ there is no material difference in the final state probability, but as soon as $J_2 = J_1$ the probability suddenly jumps from around 1% to 14%—with $L = 192$. If T-junctions become unstable when $J_2 = J_1$, then probability of finding metastable tilings with non-spanning domains should also change drastically in this special case—which is exactly what we see in Figure 7.7 (c). In Figure 7.7 (c), the P_M estimates are indistinguishable for $J_2 < J_1$, and despite being
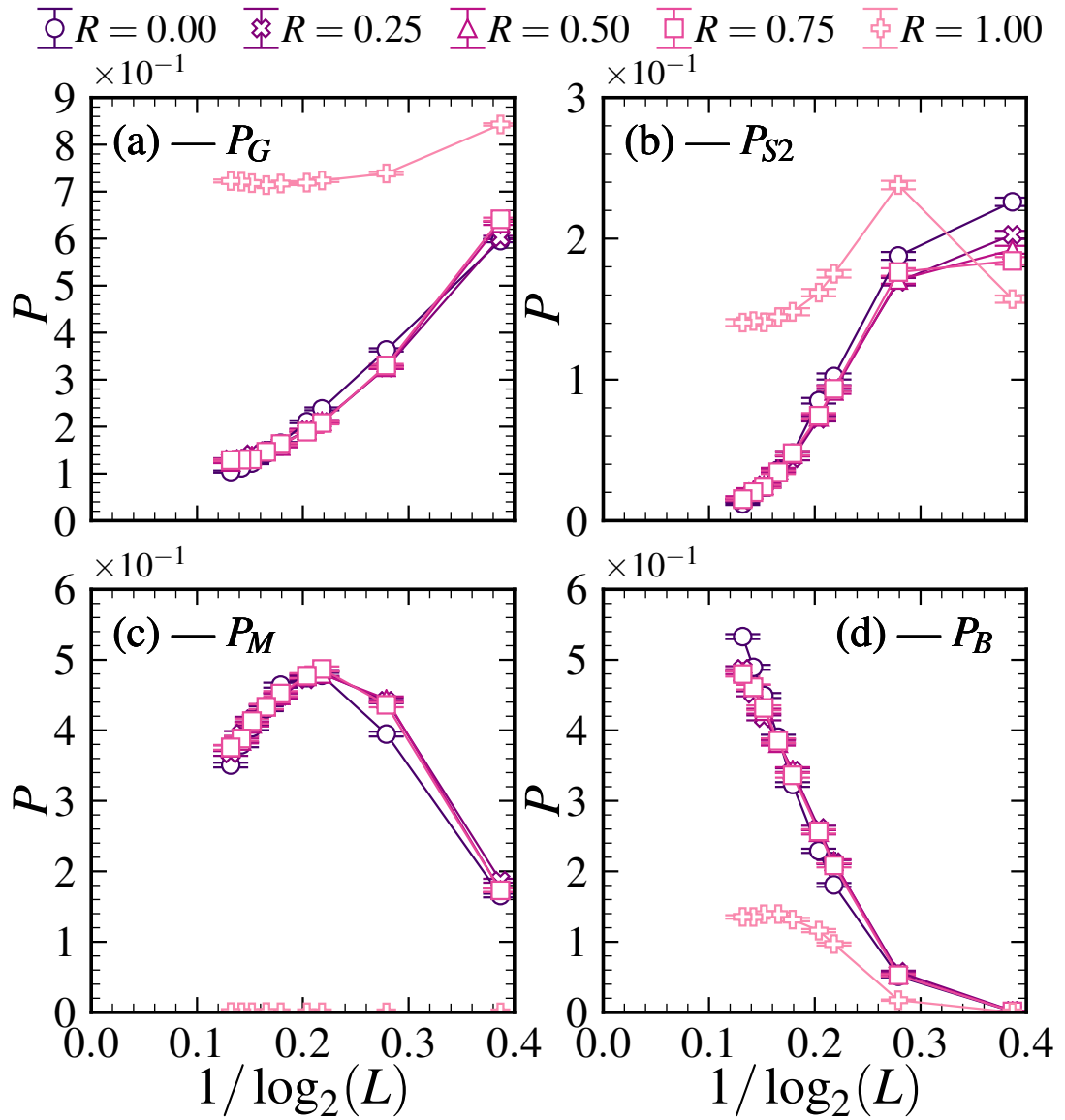
FIGURE 7.7 – Probability of freezing into (a) the ground, (b) an on-axis two-stripe, (c) a non-spanning metastable and (d) a blinker state for specified ratios $R = J_2/J_1$ in the square lattice Potts model at zero temperature. The data are based on 2×10^4 realisations.

considerably different when $J_2 = J_1$, they are *non-zero*, and actually $\sim 10^{-4}$. This suggests another metastable tiling is possible when $J_2 = J_1$; an example of which we show in Figure 7.8. Note how the T-junction nature of the domain interfaces has changed.

The final quantity we address in Figure 7.7 (d) is the probability of reaching a blinker configuration, which we take to be the probability of finding flippable spins at
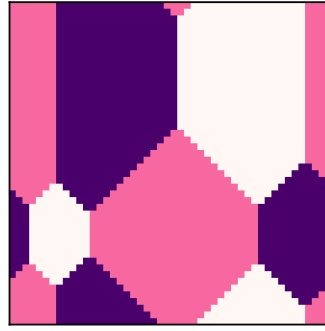
FIGURE 7.8 – A metastable final state tiling in a square lattice Potts model of $L = 48$ with three spin states. This configuration has six clusters and no flippable spins, and the energies due to the first- and second-neighbour bonds are $23.875L$ and $32L$.

$t = 100L^2$. Again, the estimates of P_B remain seemingly unchanged when $J_2 < J_1$, and are considerably different when $J_2 = J_1$. One might even argue that in the approach to large L, P_B actually decays when $J_2 = J_1$; however, this claim is hardly rigorous when the number of realisations is only $\sim 10^4$. A representative example of a blinker configuration is plotted in Figure 7.9.

At first glance it is not easy to discern if the realisation in Figure 7.9 is genuinely trapped at constant energy, or simply stuck in an extremely long lived configuration. As an initial test to probe the long-lived nature of these realisations, I ran two separate batches of 10^4 simulations with $L = 24$ and a long time cut off of $t = 100L^2$ and $t = 10000L^2$. In each case the number of active realisations at the long time cut off was 146 and 144 respectively. This is suggestive that these configurations are infinitely long lived, but not conclusive.

$t = 0.1L^2$ $t = 1.0L^2$ $t = 10.0L^2$ $t = 1000.01L^2$
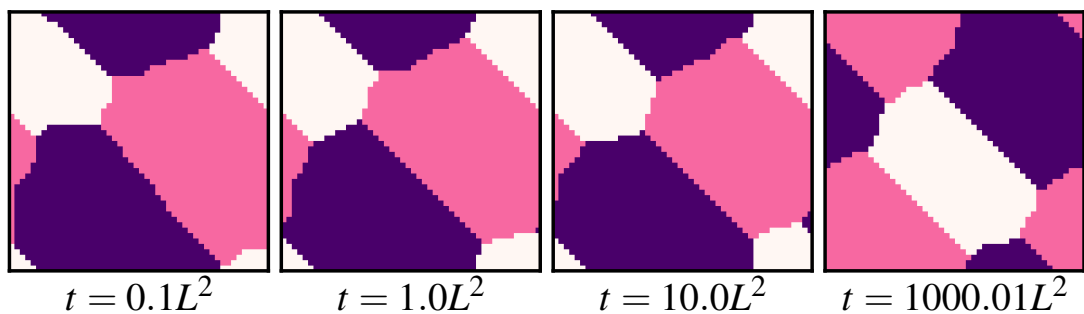
FIGURE 7.9 – A blinker state realisation of zero-temperature coarsening in a square lattice Potts model with $L = 48$ and $q = 3$. This configuration always has flippable spins but is seemingly trapped at constant energy.

To further labour this point, I ran a batch of 10^4 simulations and tracked the energies as functions of time, using an even longer cut off time of $t = 10^5 L^2$. I never detected any energy lowering moves for $t \geq 0.85 L^2$. This is a stronger suggestion that these configurations are genuine blinkers.

7.4   SUMMARY

In this chapter I investigated the late-time final states that arise in the square-lattice Potts model with second-neighbour interactions. I first showed how the inclusion of second-neighbour interactions influenced the final states that persist in the Ising model in Section 7.1. I then introduce the various complexities that arise in the zero-temperature coarsening of the nearest-neighbour Potts model on the square lattice as motivation for exploring the next-nearest-neighbour case in Section 7.2. In Section 7.3, I presented the late-time states that persist in the Potts model for non-zero second-neighbour interaction strengths and compared their probabilities to the case of no second-neighbour interactions. I outline my main conclusions in the following.

The final states that arise in square-lattice Potts model with only nearest-neighbour interactions are difficult to characterise due to "ultra-slow" relaxation features. It essentially not possible—or at the very least, not numerically feasible—to estimate the largest timescales at play in the nearest-neighbour Potts model at zero-temperature. The phenomenology of the dynamical scaling hypothesis seemingly doesn't apply here; domains don't grow in size as $\sqrt{t}$ until they reach the linear dimension of the system, but instead smaller domain structures persist.

The final state probabilities are not materially different with the inclusion of second-neighbour interactions, except in the special case where the second- and first neighbour interaction strengths are equal. In this case, T-junctions—the origin of the increased complexity in the square-lattice Potts model—become unstable, meaning the system can escape more complicated long-lived configurations—infinite or otherwise—and

reach final states that are easier to characterise.

"Blinker" configurations still persist when the second- and first-neighbour interaction strengths are equal, though they occur only around 12% of the time and have a considerably different geometric nature to the nearest-neighbour case. It is not clear if such configurations are genuinely infinitely long-lived, or on an incredibly slow approach to lower energy configurations. Provisional evidence suggests the former is the case.

The authors of Ref. [122] speculated that the Potts model on the square lattice was a "bad model" because of the complexity that stems from it—particularly in comparison to simple final states that arise in the nearest-neighbour Ising model—but the provisional findings I present here suggest that increasing the strength of the second-neighbour coupling strength gives rise to simpler dynamical features and final states, making the model more tractable from a numerical standpoint. One question that is sparked by this work is the definition of second-neighbour interactions. Here I have used Euclidan distance [I], but if one uses the Manhattan metric [II] the final states might be materially different yet again, and perhaps even more tractable.

[I]By Euclidian distance, I mean that the separation between two points $(0, 0)$ and (x, y) is $\sqrt{x^2 + y^2}$. In other words: one may move in a straight line between the points.

[II]The Manhattan metric whimsically refers to the grid-like nature of the streets of Manhattan, where the distance between positions $(0, 0)$ and (x, y) is $|x| + |y|$. In other words: one can move in "on-axis" directions only, and not diagonally.

SUMMARY AND FUTURE WORK

8.1 SUMMARY

As I presented my results in four chapters, I divide the summary of my findings into four parts: Section 8.1—A, Section 8.1—B, Section 8.1—C and Section.8.1—D—that is, one for each results chapter. I then discuss potential lines of enquiry for future work in Section 8.2.

8.1—A ANOMALOUS ISING FREEZING TIMES

The zero-temperature Ising model provides an excellent framework for studying coarsening systems. Since the universal characteristics of coarsening should depend little on the particular model of choice, and any artefacts of the system that do impose on the coarsening evolution can generally be viewed as nuances, it is convenient to study a simple model. If in Physics one should always strive to understand the dominant mechanisms at play using as simple a model as possible, then the Ising model is in some ways ideal.

Although the Ising model *is* simple in nature, its non-equilibrium behaviour at zero-temperature has proven somewhat enigmatic—the rich aspects of zero-temperature

Ising coarsening that have come to light in the past decades could easily have remained overlooked. After the work of Roy Glauber in the one-dimensional Ising model, and the extensive studies by Alan Bray in two-dimensions, the zero-temperature dynamics was thought fully understood.

In one-dimension, the ground state is invariably reached on a timescale of $O(L^2)$. In two-dimensions, there was a seemingly tacit assumption that large domain structures would ultimately engulf the system causing the ground state to always be reached. Then, the discovery of non-ground final states and multiple relaxation timescales triggered, in a roundabout way, considerable research interest in the zero-temperature coarsening of the two-dimensional Ising model. Although the findings presented by Spirin *et al.* in Ref. [53] were initially viewed as unexpected and overlooked aspects of Ising coarsening, there was and a deep and fundamental explanation underlying them: a connection to critical continuum percolation [56, 57]. In three dimensions, and most likely beyond, the ground state is only reached in the smallest of system sizes [54, 98–101].

My own studies of the zero-temperature Ising model involved a more extensive examination of the various timescales that arise in the phase ordering process. My main finding was that of an anomalous coarsening timescale that originates from relaxations reaching on-axis two-stripe states.

While close to a power law of form $\sim L^\gamma$, this timescale apparently grows as $\sim L^2 \log(L)$ (see Appendix. C for a comparison). I explored this unexpected relaxation time by examining zero-temperature quenches using both infinite temperature and biased initial conditions. This biased initial condition confirmed the mechanism behind the anomalous timescale and allowed me to formulate an explanation for it based on annihilating random walkers—thus solidifying my claim. I had reason to believe in the existence of this timescale because of similar behaviour observed in the Potts model, and due to some very subtle hints in the so-called survival probabilities presented in the literature [53, 57].

I also examined other relevant timescales at play in the zero-temperature Ising model. I tested the simulations by recovering $\sim L^2$ time scaling using a biased initial condition configured in the ground state topology. I then investigated the relaxation times of off-axis winding configurations; I found these times to scale roughly in the same way as Victor Spirin found when fitting naïve power laws (see Ref. [53]), but an inspection of the local slopes in these data showed a reducing exponent with increasing L. This feature of the scaling lead me to speculate that perhaps the relaxation times asymptotically approach $\sim L^3$ as predicted in Ref. [53].

While larger scale numerical studies could make it easier to identify the asymptotic limits of these timescales, it seems like such a venture would at the very least be numerically impractical.

8.1—B   FREEZING THE TRIANGULAR POTTS MODEL

In Chapter. 5 I investigated the "fate" of a three-state Potts ferromagnet that was quenched to zero-temperature on the triangular lattice geometry. Before this work little effort had been devoted to understanding the final states that arise when a Potts ferromagnet undergoes a zero-temperature quench; the only specific investigation of the final states was a study by Jason Olejarz *et al.* that focused exclusively on the square lattice with nearest-neighbour interactions [122]. This work showed that simulating the late-time dynamics of the Potts ferromagnet on the square lattice to be hugely cumbersome and essentially numerically intractable at zero-temperature. The difficulty originated from the surprising late-time configurations that emerged, which we shall now briefly recap.

The first revelation involved the rarity with which the ground state was reached: only around 10% of all realisations reached the ground state at large L. Instead, the authors of Ref. [122] found that the system can freeze into on-axis stripe states or reach static metastable tessellations that are underpinned by so-called "T-junctions". Additionally, blinker configurations emerged, which were also underpinned by "T-junctions". Here

the system becomes forever trapped on an iso-energy surface with perpetually "blinking" spins.

However, the strangest and most perplexing feature was that of "pseudo-blinkers". After exorbitant time periods strongly resembling blinkers, pseudo-blinkers undergo energy lowering flips that trigger sudden "energy avalanches", where the system undergoes a macroscopic decline in energy as it reorders. Identifying these configurations was the main source of the numerical expense because their total relaxation time grew exponentially with system size [122].

In Ref. [122], the authors hinted that lattice effects impose less strongly on the ordering process if one uses a triangular geometry. This prompted them to question the extent of the universality between the square- and triangular-lattice Potts models. In 2018, I entered a collaboration with an author of Ref. [122], S. Redner, where we sought to investigate and characterise the final state of the zero-temperature Potts ferromagnet on the triangular lattice.

Our findings were indeed surprising and stand in contrast to many of the behaviours on the square lattice [123]. On the triangular lattice, roughly 75% of all realisations reach the ground state. Around 9% of the time, the system freezes into a host of metastable stripe states which span the linear dimension of the system. Most interestingly, the system can freeze into a myriad of so-called three-hexagon states, where the domain boundaries are parallel to the three directions of lattice symmetry.

We found that there were two timescales associated with realisations that reach the ground state: the first was standard $\sim L^2$ coarsening; the second was anomalously large and grew with the system size as roughly $\sim L^{3.5}$. In such instances, the first reached a three-hexagon configuration where the domain boundaries misaligned with the lattice axes. This boundary misalignment prohibited the system from reaching a final state in a similar way to the diagonal stripe interfaces in the nearest-neighbour Ising model. The hexagons met at "T-junctions", but, unlike on the square lattice, the positions of the junctions were free to move. This enabled the system to slowly escape

this configuration; domains slowly "breathed" and when interfaces of the same spin type met, the system rapidly collapsed the ground state.

We also discovered that the relaxation time of the three-hexagon states grows as roughly $\sim L^2 \log(L)$. We tried to explain this anomalous time scaling using an argument based on absorbing random walkers, but upon reflection feel the argument used in Chapter 4 better explains this phenomenon. We also found that the domain areas in the two-stripe and three-hexagon states were broadly well fit by Guassians—specifically normal distributions—which is expected based on known findings from the Ising model (see Refs. [53–55]).

8.1—C POTTS MODEL: INCREASED DEGENERACY

In Chapter 6 I continued my examination of the zero-temperature Potts model on the triangular lattice. I explored how the final state probabilities vary in response to different ground state degeneracy. When investigating the final state probabilities with q fixed for various L, I found, broadly speaking, that the ground state probability increased with q in the regime of large L; the same was also true of the three-hexagon state, and the converse was true of the two-stripe states, which decayed in probability with both increasing q and L.

I also investigated how the final state probabilities varied as a function of the number of spin states for fixed system sizes. The ground state probability initially increased with q, before exhibiting a non-monotonicity by starting to decrease at around $q = 7$. In the case of the three-hexagon state, the probability decays from $q = 3 \rightarrow 4$ before increasing with q. This increase seemingly remains consistent with increasing q after $q > 4$. The two-stripe states again decrease in likelihood with either increasing q or L. As q increases, it is not only the three hexagon states that grow in prevalence; five-, eight- and twelve hexagon states also appear with probabilities of order 10^{-3}, 10^{-5} and 10^{-5} respectively.

Furthermore, when the number of spins states is greater than four, blinker config-

urations arise. On the triangular lattice, blinkers are trivial and consist of only a few active sites that are well separated from each other. Generally speaking, no new coarsening phenomenology arises when studying higher q triangular-lattice Potts models at zero-temperature.

8.1—D POTTS FURTHER: SQUARE LATTICE

I also investigated zero-temperature coarsening in a square lattice Potts model with second-neighbour interactions. I first showed the *known behaviours* of the final states of the zero-temperature Ising model—that is, the $q = 2$ Potts model—with non-zero second-neighbour interactions in order to understand how they might influence a $q = 3$ Potts model. My main findings are summarised in the following.

When the ratio of second- to first-neighbour interaction strengths is less than unity, there is essentially no material difference in the final states of the $q = 3$ Potts model compared to those found in Ref. [122]. The only *slight* difference is that off-axis stripes occur with a probability of order 10^{-4} when the second-neighbour strength J_2 is non-zero.

However, when $J_2 = J_1$, "T-junctions"—the source of increased complexity on the square lattice—become unstable and the final states are significantly different. The ground state probability at large L shifts from $\approx 10\%$ to around 72%. Non-spanning metastable tessellations essentially vanish (probability of $\approx 4.5 \times 10^{-4}$), and the geometrical nature of the small fraction that persist is considerably different to the case where $J_2 < J_1$. Frustratingly, incredibly long-lived configurations still persist. Whether these are *genuine* or *psuedo*-blinkers is not yet clear. For example, in one batch of 10^4 simulations with $L = 24$, 146 were still active at $t = 100L^2$ and in another batch of the same size 144 were active at $t = 10^4 L^2$. The ratio of these probabilities are sufficiently close to unity that it seems these realisations don't reach frozen final states at late times. Another test for long lived realisations involved tracking the energy of these configurations as functions of time. In doing this I found no energy lowering flips

for $0.85L^2 \leq t \leq 10^5 L^2$

8.2   OUTLOOK AND FUTURE WORK

Here I discuss possible lines of enquiry for future research with respect to coarsening in Ising and Potts models.

8.2—A   ISING MODEL

It is generally surprising when new findings emerge from the zero-temperature Ising model, purely because it has been *extensively* studied. In one- and two-dimensions it is unlikely that any new aspects of coarsening phenomenology will arise, but one never knows. Even in recent months, in a *Phys. Rev. Lett.*, the two-dimensional Glauber-Ising model was used to demonstrate how a pre-cooling strategy allows exponentially faster heating of a system [157]. It seems more likely that Ising model will be used to demonstrate ideas or understand them through universality rather be studied purely for interest in the model itself.

With respect to the number of timescales that exist in the zero-temperature Ising relaxation, it seems there is little more to be learned. In one-dimension, there is only a single timescale at play; in two dimensions the multitude of timescales has been intensively studied; in three-dimensions, the characteristic relaxation time is more complicated due to the intricacies of the approach to the final states, and apparently grows exponentially with the linear dimension of the system [98].

My claim of $\sim L^2 \log(L)$ scaling comes from a seemingly convincing argument, but it is also possible that there are other subtleties to this relaxation process that I have not considered. It does however seem that even in such a case, $L^2 \log(L)$ would still to be the *dominant* term in the scaling form.

8.2—B   POTTS MODEL

With the Potts model there are a number of open questions sparked, at least in part, by my work. For example: is it possible to compute the final state probabilities of the zero-temperature Potts model on the triangular lattice? The mapping between critical percolation and the two-dimensional Ising model proved decisive in understanding the various stripe topologies. Perhaps there is another mapping between the triangular-lattice Potts model and the yet-to-be-understood three colour percolation model [158, 159]. Another open question is to understand the area or perimeter distribution of the three-hexagon state; although the area is seemingly well fit by a normal distribution, we do not know why this phenomenon should be normally distributed.

The fact that the final states are simply characterised on the triangular lattice (six-coordinated lattice) but not the square lattice (four-coordinated) also raises the question: what are the final states of the three-state Potts ferromagnet on the simple cubic lattice, which is also six-coordinated? Perhaps there is an underlying simplicity when the lattice coordination number is an integer multiple of the number of Potts states.

In the case of the square-lattice with second-neighbour interactions I have shown that, perhaps, in the special case of equal first- and second-neighbour couplings the final states become more tractable and generally simpler to view. Potts models with equal first- and second-neighbour couplings have been used to explore coarsening in soap froths so it seems reasonable to explore the final states with these interactions [103]. The provisional studies of this system that I have presented motivates a more in-depth study to identify whether or not the blinker like configurations that arise are truly trapped at constant energy, or merely or ultra-slow energy lowering trajectories. These features have not been explored in the literature.

LOCAL SLOPES

We obtain three-point local slopes as follows: let $x = \{x_1,\ x_2,\ x_3\}$, $y = \{y_1,\ y_2,\ y_3\}$ and say $y \sim x^\nu$. We fit a straight line to $\log(y)$ versus $\log(x)$ and obtain a slope ν that corresponds to the power law exponent in linear space. We then plot ν against $M_P = \exp(\log(\sqrt{x_1 x_3}))$—i.e. the linear value of the middle of the x-range in logarithmic space. We apply this procedure to every three consecutive data.

THE HARMONIC SUM AND THE LOGARITHM

Throughout this thesis I rely on the approximation that the natural logarithm and harmonic sum are asymptotically equivalent. However, the harmonic series and the natural logarithm are actually related through

$$\sum_{k=1} \frac{1}{k} = \log(k) + \frac{1}{2k} + \gamma \tag{B.1}$$

where $\gamma \approx 0.57721$ is the Euler-Mascheroni constant and $\log(k)$ is the natural logarithm of k. Therefore the harmonic sum, H_n, is of $O(\log(k))$, and they are asymptotically indistinguishable.

To illustrate this graphically, consider the functions plotted in Figure. B.1 (a). The harmonic sum clearly exhibits a logarithmic divergence, but is not exactly equal to the natural logarithm without the inclusion of the correction terms [1].

Alternatively, one can visualise this by recalling that the Euler-Mascheroni constant is defined as the asymptotic limit of the difference between the harmonic series and the natural logarithm, which is plotted in Figure. B.1 (b). Here one can easily visualise the asymptotic approach to γ.

---

[1]For more info see "Weisstein, Eric W. "Harmonic Series." From MathWorld–A Wolfram Web Resource. http://mathworld.wolfram.com/HarmonicSeries.html", Accessed: February 13, 2020.
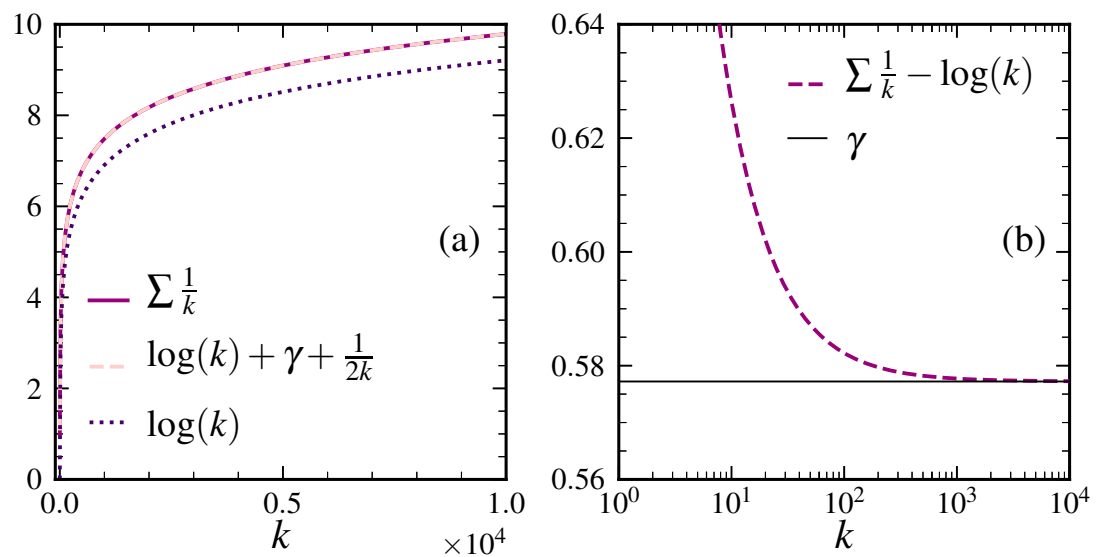
FIGURE B.1 – (a) Harmonic series (solid line), the natural logarithm with correction terms (dashed line) and the natural logarithm (dotted line). (b) Harmonic series minus the natural logarithm (dashed line) and Euler-Mascheroni constant γ (solid line).

POWER LAW WITH A LOGARITHM

On a double logarithmic scale a power law appears as a straight line; if one takes the logarithm of both sides of a power law they obtain a straight line with a slope that is equal to the exponent. What is *perhaps* less obvious is how a logarithmic factor influences the form (see Figure. C.1).
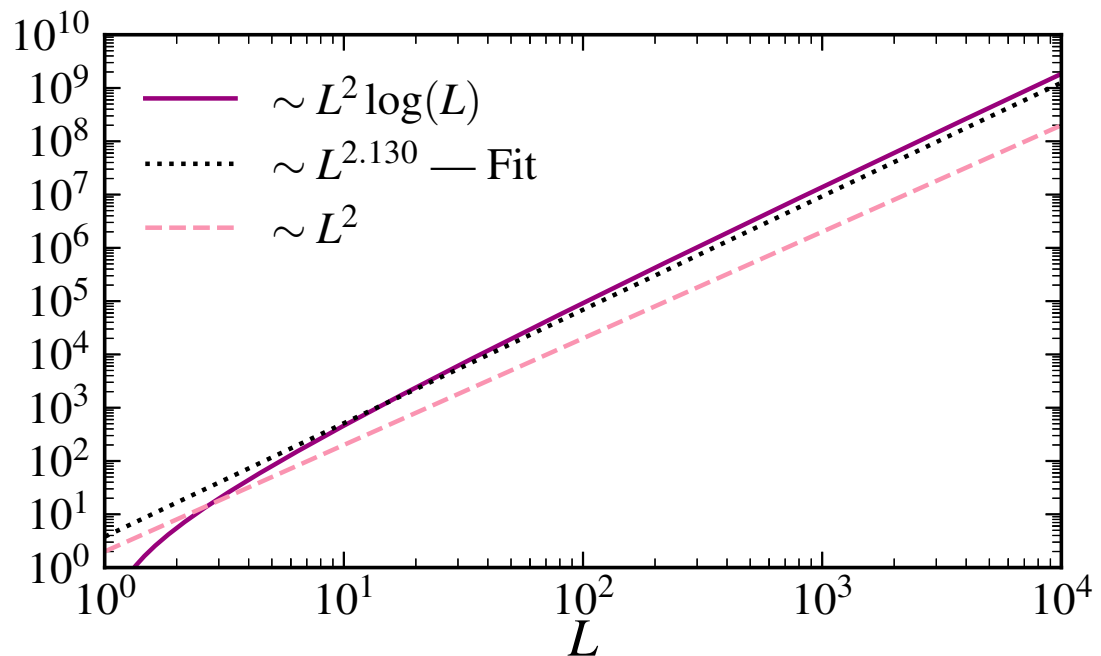
FIGURE C.1 – Plots of $L^2 \log(L)$ (solid line), a power law fit of exponent $\nu = 2.130$ (dotted line) and L^2 (dashed line) versus L. These plots serve to illustrate the influence of a logarithmic factor on a power law.

If one tries to fit a power law, say L^ν, to data of the form $\sim L^\eta \log(L)$, where η is some integer exponent, they estimate ν to be an irrational exponent that is near to η (see Figure. C.1). Moreover, the logarithm introduces a curvature in the data that would otherwise appear as a straight line if it were a pure power law. These telltale signs should generally prompt one to consider the presence of a logarithm in a scaling form. Even though $\log(k)$ is divergent, its influence at large k is extremely subtle.

SEPARATING TIMESCALES: REDUCED MOMENTS

Suppose a large ensemble of cars embark upon a long journey. 90% of the cars have enough fuel to travel for a time of $\sim L^2$, and the remaining 10% have extra fuel such that they can travel for an even longer time of $\sim L^3$. Imagine now that this experiment is repeated for various, well-separated, values of L.

If one is given the list of times at which the cars ran out of fuel for each value of L, and is tasked with identifying the two timescales, how could one do it? This question is directly analogous with separating the smallest and largest relaxation timescales in the zero-temperature Ising model, where we have a list of times for each L and need to identify the smallest and largest timescales at play.

In this problem, we essentially have a mixture of two distributions: one with mean $\sim L^2$ and the other $\sim L^3$. To illustrate how we can separate and identify each timescale, we draw times from two normal distributions of the form

$$P = \frac{1}{\sqrt{2\pi\sigma^2}} \exp\left(-\frac{t - \langle t \rangle}{2\sigma^2}\right), \tag{D.1}$$

where $\langle t \rangle$ is the mean and σ the standard deviation. For each L, we draw 90% of the times from a normal distribution of mean $\sim L^2$, and the remaining 10% from a normal distribution of $\sim L^3$.
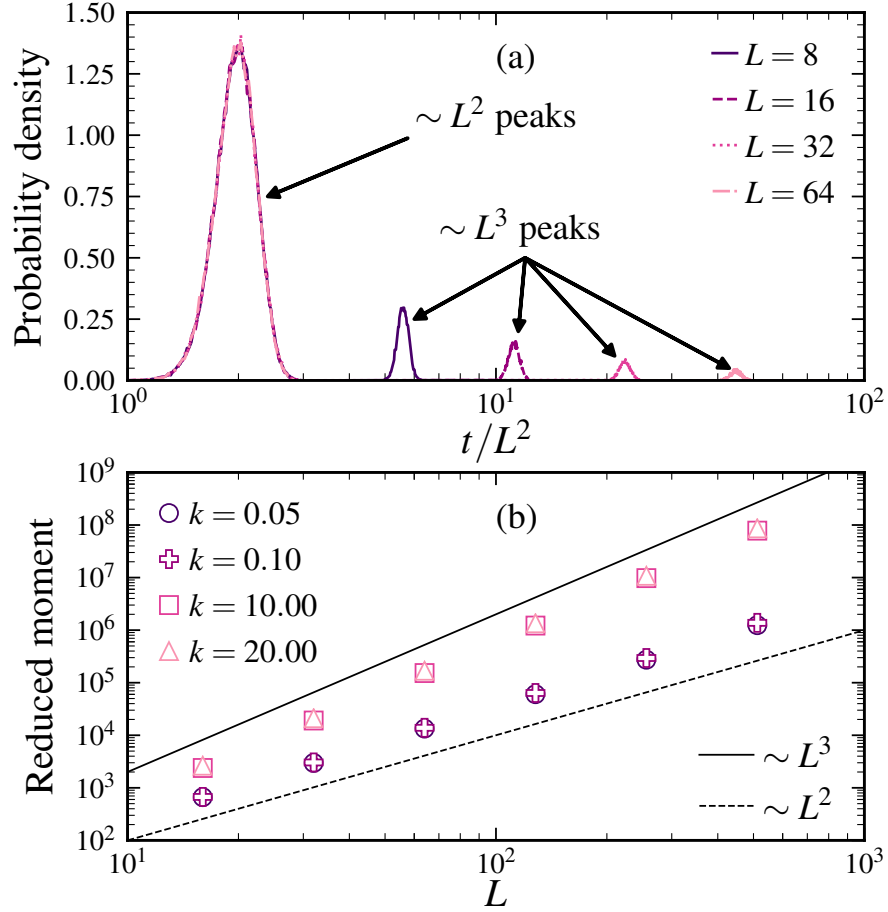
FIGURE D.1 – (a) Multi-scale distributions where 90% of the data is of order L^2 and 10% of order L^3. (b) Reduced moments for specified k and two power laws of exponents $\nu = 2$ and $\nu = 3$.

We plot some examples of the resulting distributions in Figure D.1 (a). By rescaling the time by $1/L^2$, we see the $\sim L^2$ peaks remain fixed in their horizontal position, and the $\sim L^3$ peaks move to the right and widen with increasing L.

The k_{th} raw sample moment of a data set containing N times is

$$\langle t^k \rangle = \frac{1}{N} \sum_{i}^{N} t_i^k, \tag{D.2}$$

where k is the order of the moment. If we compute the moments for large values of k (say $k \in \{10, 20\}$) the quantity will be dominated by the largest numbers present in the set, and conversely, for small k (say $k \in \{0.05, 0.1\}$) the quantity will be dominated by the smallest times in the set. Consequently, we can use this approach to filter out either

small or large times from the data by selecting appropriate values of k.

In order to recover the timescales, we need to convert back into units of time. To do this, we compute the reduced k_{th} moments $M_k = \langle t^k \rangle^{1/k}$. Computing M_k as a function of L for various small and large k provides us with a measure of how each of the timescales grows with L. We plot an example of these computations in Figure D.1, and show two power laws (straight lines) of exponents $\nu = 2$ and $\nu = 3$.

BIBLIOGRAPHY

[1]   E. Ising. "Beitrag zur theorie des ferromagnetismus". In: *Zeitschrift für Physik* 31.1 (1925), pp. 253–258. DOI: 10.1007/BF02980577.

[2]   A. Taroni. *Statistical Physics: 90 years of the Ising model*. 2015. DOI: 10.1038/NPHYS3595.

[3]   E. Ibarra-García-Padilla, C. G. Malanche-Flores, and F. J. Poveda-Cuevas. "The hobbyhorse of magnetic systems: the Ising model". In: *European Journal of Physics* 37.6 (2016), p. 065103. DOI: 10.1088/0143-0807/37/6/065103.

[4]   R. Peierls. "On Ising's model of ferromagnetism". In: *Mathematical Proceedings of the Cambridge Philosophical Society* 32.3 (1936), pp. 447–481. DOI: 10.1017/S0305004100019174.

[5]   L. Onsager. "Crystal statistics. I. A two-dimensional model with an order-disorder transition". In: *Physical Review* 65.3-4 (1944), pp. 117–149. DOI: 10.1103/PHYSREV.65.117.

[6]   L. P. Kadanoff. "Scaling laws for Ising models near T_c". In: *Physics Physique Fizika* 2 (6 1966), pp. 263–272. DOI: 10.1103/PHYSICSPHYSIQUEFIZIKA.2.263.

[7]   L. P. Kadanoff. "Spin-spin correlations in the two-dimensional Ising model". In: *Il Nuovo Cimento B* 44 (2 1966), pp. 276–305. DOI: 10.1007/BF02710808.

[8] C. Domb, M. F. Sykes, and J. T. Randall. "On the susceptibility of a ferromag-
     netic above the Curie point". In: *Proceedings of the Royal Society of London.*
     Series A. Mathematical and Physical Sciences 240.1221 (1957), pp. 214–228.
     DOI: 10.1098/RSPA.1957.0078.

[9] B. Widom. "Surface tension and molecular correlations near the critical point".
     In: *The Journal of Chemical Physics* 43.11 (1965), pp. 3892–3897. DOI: 10.
     1063/1.1696617.

[10] B. Widom. "Equation of state in the neighborhood of the critical point". In: *The*
     Journal of Chemical Physics 43.11 (1965), pp. 3898–3905. DOI: 10.1063/1.
     1696618. eprint: HTTPS://DOI.ORG/10.1063/1.1696618.

[11] K. G. Wilson. "Renormalization group and critical phenomena. I. Renormaliza-
     tion group and the kadanoff ccaling picture". In: *Physical Review B* 4 (9 1971),
     pp. 3174–3183. DOI: 10.1103/PHYSREVB.4.3174.

[12] K. G. Wilson. "Renormalization group and critical phenomena. II. Phase-space
     cell analysis of critical behavior". In: *Physical Review B* 4 (9 1971), pp. 3184–
     3205. DOI: 10.1103/PHYSREVB.4.3184.

[13] H. J. Maris and L. P. Kadanoff. "Teaching the renormalization group". In:
     American Journal of Physics 46.6 (1978), pp. 652–657. DOI: 10.1119/1.11224.

[14] H. Chen-Hsi and M. Jaime. "A generalized Ising model for studying alloy
     evolution under irradiation and its use in kinetic Monte Carlo simulations". In:
     Journal of Physics: Condensed Matter 28.42 (2016), p. 425201. DOI: 10.1088/
     0953-8984/28/42/425201.

[15] B. Liu, Y. Zou, S. Zhou, L. Zhang, Z. Wang, H. Li, Z. Qu, and Y. Zhang.
     "Critical behavior of the van der Waals bonded high T_c ferromagnet Fe_3GeTe_2".
     In: *Scientific Reports* 7 (1 2017). DOI: 10.1038/S41598-017-06671-5.

[16] D. Stauffer. "Social applications of two-dimensional Ising models". In: *Ameri-*
     can Journal of Physics 76.4 (2008), pp. 470–473. DOI: 10.1119/1.2779882.

[17]   T. Kazuyuki. "Statistical-mechanical approach to image processing". In: *Journal of Physics A: Mathematical and General* 35.37 (2002), R81–R150. DOI: 10.1088/0305-4470/35/37/201.

[18]   A. E. Noble, J. Machta, and A. Hastings. "Emergent long-range synchronization of oscillating ecological populations without external forcing described by Ising universality". In: *Nature Communications* 6 (1 2015). DOI: 10.1038/NCOMMS7664.

[19]   C. Yoshimura, M. Yamaoka, M. Hayashi, T. Okuyama, H. Aoki, K. Kawarabayashi, and H. Mizuno. "Uncertain behaviours of integrated circuits improve computational performance". In: *Scientific Reports* 5 (1 2015). DOI: 10.1038/SREP16213.

[20]   H. Suzuki, J. Imura, and K. Aihara. "Chaotic Ising-like dynamics in traffic signals". In: *Scientific Reports* 3 (1 2013). DOI: 10.1038/SREP01127.

[21]   T. Inagaki, K. Inaba, R. Hamerly, K. Inoue, Y. Yamamoto, and H. Takesue. "Large-scale Ising spin network based on degenerate optical parametric oscillators". In: *Nature Photonics* 10 (6 2016). DOI: 10.1038/NPHOTON.2016.68.

[22]   G. Torlai and R. G. Melko. "Learning thermodynamics with Boltzmann machines". In: *Physical Review B* 94 (16 2016), p. 165134. DOI: 10.1103/PHYSREVB.94.165134.

[23]   L. Wang. "Discovering phase transitions with unsupervised learning". In: *Physical Review B* 94 (19 2016), p. 195105. DOI: 10.1103/PHYSREVB.94.195105.

[24]   W. Hu, R. P. Singh Rajiv, and R. T. Scalettar. "Discovering phases, phase transitions, and crossovers through unsupervised machine learning: a critical examination". In: *Physical Review E* 95 (6 2017), p. 062122. DOI: 10.1103/PHYSREVE.95.062122.

[25]   J. Carrasquilla and R. G. Melko. "Machine learning phases of matter". In: *Nature Physics* 13 (5 2017), pp. 431–434. DOI: 10.1038/NPHYS4035.

[26] E. P. L van Nieuwenburg and Y. H. Liu. "Machine learning phases of matter". In: *Nature Physics* 13 (5 2017), pp. 435–439. DOI: 10.1038/NPHYS4037.

[27] M. M. Barry and T. W. Tai. *The two-dimensional Ising model*. 2. Dover, 2014. Chap. 1.

[28] R. M. Potts. "Mathematical investigation of some cooperative phenomena". PhD thesis. Oxford University, 1950.

[29] J. Ashkin and E. Teller. "Statistics of two-dimensional lattices with four components". In: *Physical Review* 64 (5-6 1943), pp. 178–184. DOI: 10.1103/PHYSREV.64.178.

[30] T. Kihara, Y. Midzuno, and T. Shizume. "Statistics of two-dimensional lattices with many components". In: *Journal of the Physical Society of Japan* 9.5 (1954), pp. 681–687. DOI: 10.1143/JPSJ.9.681.

[31] F. Y. Wu. "The Potts model". In: *Reviews of Modern Physics* 54 (1 1982), pp. 235–268. DOI: 10.1103/REVMODPHYS.54.235.

[32] F. Corberi, L. F. Cugliandolo, M. Esposito, and M. Picco. "Multinucleation in the first-order phase transition of the 2D Potts model". In: *Journal of Physics: Conference Series* 1226 (2019), p. 012009. DOI: 10.1088/1742-6596/1226/1/012009.

[33] L. F. Cugliandolo. "Critical percolation in bidimensional coarsening". In: *Journal of Statistical Mechanics* 2016.11 (2016), p. 114001. DOI: 10.1088/1742-5468/2016/11/114001.

[34] F. Corberi and P. Politi. "Foreword". In: *Comptes Rendus Physique* 16.3 (2015). Coarsening dynamics / Dynamique de coarsening, pp. 255–256. DOI: HTTPS://DOI.ORG/10.1016/J.CRHY.2015.05.003.

[35] I. M. Lifshitz. "Kinetics of ordering during second-order phase transitions". In: *Journal of Experimental and Theoretical Physics (U.S.S.R.)* 15.5 (1962).

[36] S. M. Allen and J. W. Cahn. "A microscopic theory for antiphase boundary motion and its application to antiphase domain coarsening". In: *Acta Metallurgica* 27.6 (1979), pp. 1085–1095. DOI: 10.1016/0001-6160(79)90196-2.

[37] T. Ohta, D. Jasnow, and K. Kawasaki. "Universal scaling in the motion of random interfaces". In: *Physical Review Letters* 49 (17 1982), pp. 1223–1226. DOI: 10.1103/PHYSREVLETT.49.1223.

[38] P. L. Krapivsky, S. Redner, and E. Ben-Naim. *A Kinetic View of Statistical Physics*. Cambridge University Press, 2010. DOI: 10.1017/CBO9780511780516.

[39] R. J. Glauber. "Time-dependent statistics of the Ising model". In: *Journal of Mathematical Physics* 4.2 (1963), pp. 294–307. DOI: 10.1063/1.1703954.

[40] B. Derrida and R. Zeitak. "Distribution of domain sizes in the zero temperature Glauber dynamics of the one-dimensional Potts model". In: *Physical Review E* 54 (3 1996), pp. 2513–2525. DOI: 10.1103/PHYSREVE.54.2513.

[41] P. L. Krapivsky and E. Ben-Naim. "Domain statistics in coarsening systems". In: *Physical Review E* 56 (4 1997), pp. 3788–3798. DOI: 10.1103/PHYSREVE.56.3788.

[42] S. Redner and P. L. Krapivsky. "Slow coarsening in an Ising chain with competing interactions". In: *Journal of Physics A: Mathematical and General* 31.46 (1998), pp. 9229–9240. DOI: 10.1088/0305-4470/31/46/013.

[43] V. Spirin, P. L. Krapivsky, and S. Redner. "Coarsening in a driven Ising chain with conserved dynamics". In: *Physical Review E* 60 (3 1999), pp. 2670–2676. DOI: 10.1103/PHYSREVE.60.2670.

[44] B. Skorupa, K. Sznajd-Weron, and R. Topolnicki. "Phase diagram for a zero-temperature Glauber dynamics under partially synchronous updates". In: *Physical Review E* 86 (5 2012), p. 051113. DOI: 10.1103/PHYSREVE.86.051113.

[45]   K. Humayun and A. J. Bray. "Non-equilibrium dynamics of the Ising model for T less-than/equal-toTc". In: *Journal of Physics A: Mathematical and General* 24.8 (1991), pp. 1915–1930. DOI: 10.1088/0305-4470/24/8/030.

[46]   A. J. Bray. "Theory of phase ordering kinetics". In: *Physica A: Statistical Mechanics and its Applications* 194.1 (1993), pp. 41–52. DOI: 10.1016/0378-4371(93)90338-5.

[47]   K. Binder and D. Stauffer. "Theory for the slowing down of the relaxation and spinodal decomposition of binary mixtures". In: *Phys. rev. lett.* 33 (17 1974), pp. 1006–1009. DOI: 10.1103/PHYSREVLETT.33.1006.

[48]   K. Binder, D. Stauffer, and H. Müller-Krumbhaar. "Theory for the dynamics of clusters near the critical point. i. relaxation of the glauber kinetic ising model". In: *Phys. rev. b* 12 (11 1975), pp. 5261–5287. DOI: 10.1103/PHYSREVB.12.5261.

[49]   K. Binder. "Theory for the dynamics of "clusters." ii. critical diffusion in binary systems and the kinetics of phase separation". In: *Phys. rev. b* 15 (9 1977), pp. 4425–4447. DOI: 10.1103/PHYSREVB.15.4425.

[50]   H. Furukawa. "Structure functions of quenched off-critical binary mixtures and renormalizations of mobilities". In: *Phys. rev. lett.* 43 (2 1979), pp. 136–139. DOI: 10.1103/PHYSREVLETT.43.136.

[51]   J. L. Lebowitz, J. Marro, and M.H. Kalos. "Dynamical scaling of structure function in quenched binary alloys". In: *Acta metallurgica* 30.1 (1982), pp. 297–310. DOI: 10.1016/0001-6160(82)90069-4.

[52]   P. Fratzl and J. L. Lebowitz. "Universality of scaled structure functions in quenched systems undergoing phase separation". In: *Acta metallurgica* 37.12 (1989), pp. 3245–3248. DOI: HTTPS://DOI.ORG/10.1016/0001-6160(89)90196-X.

[53] V. Spirin, P. L. Krapivsky, and S. Redner. "Fate of Zero-temperature Ising Ferromagnets". In: *Physical Review E* 63 (3 2001), p. 036118. DOI: 10.1103/PHYSREVE.63.036118.

[54] V. Spirin, P.L. Krapivsky, and S. Redner. "Freezing in Ising ferromagnets". In: *Physical Review E* 65 (1 2001), p. 016119. DOI: 10.1103/PHYSREVE.65.016119.

[55] V. Spirin. "Anomalous phase ordering kinetics in Ising spin systems". PhD thesis. Boston University, 2002.

[56] K. Barros, P. L. Krapivsky, and S. Redner. "Freezing into stripe states in two-dimensional ferromagnets and crossing probabilities in critical percolation". In: *Physical Review E* 80 (4 2009), p. 040101. DOI: 10.1103/PHYSREVE.80.040101.

[57] J. Olejarz, P. L. Krapivsky, and S. Redner. "Fate of 2D kinetic ferromagnets and critical percolation crossing probabilities". In: *Physical Review Letters* 109 (19 2012), p. 195702. DOI: 10.1103/PHYSREVLETT.109.195702.

[58] J. J. Arenzon, A. J. Bray, L. F. Cugliandolo, and A. Sicilia. "Exact results for curvature-driven coarsening in two dimensions". In: *Physical Review Letters* 98 (14 2007), p. 145701. DOI: 10.1103/PHYSREVLETT.98.145701.

[59] L. F. Cugliandolo. "Topics in coarsening phenomena". In: *Physica A: Statistical Mechanics and its Applications* 389.20 (2010). Proceedings of the 12th international summer school on fundamental problems in Statistical Physics, pp. 4360–4373. DOI: 10.1016/J.PHYSA.2009.12.036.

[60] J. L. Cardy. "Critical percolation in finite geometries". In: *Journal of Physics A: Mathematical and General* 25.4 (1992), pp. L201–L206. DOI: 10.1088/0305-4470/25/4/009.

[61] H. T. Pinson. "Critical percolation on the torus". In: *Journal of Statistical Physics* 75.5 (1994), pp. 1167–1177. DOI: 10.1007/BF02186762.

[62] G. Pruessner and N. R. Moloney. "Winding clusters in percolation on the torus and the möbius strip". In: *Journal of Statistical Physics* 115.3 (2004), pp. 839–853. DOI: 10.1023/B:JOSS.0000022376.25660.7B.

[63] R. P. Langlands, C. Pichet, Ph. Pouliot, and Y. Saint-Aubin. "On the universality of crossing probabilities in two-dimensional percolation". In: *Journal of Statistical Physics* 67.3 (1992), pp. 553–574. DOI: 10.1007/BF01049720.

[64] M. B. Isichenko. "Percolation, statistical topography, and transport in random media". In: *Reviews of Modern Physics* 64 (4 1992), pp. 961–1043. DOI: 10.1103/REVMODPHYS.64.961.

[65] J. Hoshen and R. Kopelman. "Percolation and cluster distribution. I. Cluster multiple labeling technique and critical concentration algorithm". In: *Physical Review B* 14 (8 1976), pp. 3438–3445. DOI: 10.1103/PHYSREVB.14.3438.

[66] H. J. Herrmann, D. C. Hong, and H. E. Stanley. "Backbone and elastic backbone of percolation clusters obtained by the new method of "burning'". In: *Journal of Physics A: Mathematical and General* 17.5 (1984), pp. L261–L266. DOI: 10.1088/0305-4470/17/5/008.

[67] B. Derrida and D. Stauffer. "Corrections to scaling and phenomenological renormalization for 2-dimensional percolation and lattice animal problems". In: *Journal de Physique Archives* 46.10 (1985), pp. 1623–1630. DOI: 10.1051/JPHYS:0198500460100162300.

[68] R. Zallen and H. Scher. "Percolation on a continuum and the localization-delocalization transition in amorphous semiconductors". In: *Physical Review B* 4 (12 1971), pp. 4471–4479. DOI: 10.1103/PHYSREVB.4.4471.

[69] T. Blanchard, F. Corberi, L. F. Cugliandolo, and M. Picco. "How soon after a zero-temperature quench is the fate of the Ising model sealed?" In: *EPL* 106.6 (2014), p. 66001. DOI: 10.1209/0295-5075/106/66001.

[70] T. Blanchard, L. F. Cugliandolo, M. Picco, and A. Tartaglia. "Critical percolation in the dynamics of the 2D ferromagnetic Ising model". In: *Journal of Statistical Mechanics* 2017.11 (2017), p. 113201. DOI: 10.1088/1742-5468/AA9348.

[71] A. Tartaglia, L. F. Cugliandolo, and M. Picco. "Coarsening and percolation in the kinetic 2D Ising model with spin exchange updates and the Voter model". In: *Journal of statistical mechanics: theory and experiment* 2018.8 (2018), p. 083202. DOI: 10.1088/1742-5468/AAD366.

[72] A. Tartaglia, L. F. Cugliandolo, and M. Picco. "Phase separation and critical percolation in bidimensional spin-exchange models". In: *EPL (Europhysics Letters)* 116.2 (2016), p. 26001. DOI: 10.1209/0295-5075/116/26001.

[73] G. M. T. Watts. "A crossing probability for critical percolation in two dimensions". In: *Journal of Physics A: Mathematical and General* 29.14 (1996), pp. L363–L368. DOI: 10.1088/0305-4470/29/14/002.

[74] J. H. Simmons, P. Kleban, and R. M. Ziff. "Percolation crossing formulae and conformal field theory". In: *Journal of Physics A: Mathematical and Theoretical* 40.31 (2007), F771–F784. DOI: 10.1088/1751-8113/40/31/F03.

[75] L. F. Cugliandolo. "Coarsening phenomena". In: *Comptes Rendus Physique* 16.3 (2015). Coarsening dynamics / Dynamique de coarsening, pp. 257–266. DOI: HTTPS://DOI.ORG/10.1016/J.CRHY.2015.02.005.

[76] L. F. Cugliandolo. "Geometric aspects of ordering phenomena". In: *Comptes Rendus Physique* 18.1 (2017). Prizes of the French academy of sciences 2015 / Prix de l'Académie des sciences 2015, pp. 5–18. DOI: HTTPS://DOI.ORG/10.1016/J.CRHY.2016.10.002.

[77] A. Sicilia, J. J. Arenzon, A. J. Bray, and L. F. Cugliandolo. "Domain growth morphology in curvature-driven two-dimensional coarsening". In: *Physical Review E* 76 (6 2007), p. 061116. DOI: 10.1103/PHYSREVE.76.061116.

[78] A. Sicilia, Y. Sarrazin, J. J. Arenzon, A. J. Bray, and L. F. Cugliandolo. "Geometry of phase separation". In: *Physical Review E* 80 (3 2009), p. 031121. DOI: 10.1103/PHYSREVE.80.031121.

[79] F. Corberi, L. F. Cugliandolo, F. Insalata, and M. Picco. "Coarsening and percolation in a disordered ferromagnet". In: *Physical Review E* 95 (2 2017), p. 022101. DOI: 10.1103/PHYSREVE.95.022101.

[80] C. Godrèche and M. Pleimling. "Freezing in stripe states for kinetic Ising models: a comparative study of three dynamics". In: *Journal of Statistical Mechanics* 2018.4 (2018), p. 043209. DOI: 10.1088/1742-5468/AAB67B.

[81] H. Ricateau, L. F. Cugliandolo, and M. Picco. "Critical percolation in the slow cooling of the bi-dimensional ferromagnetic Ising model". In: *Journal of Statistical Mechanics* 2018.1 (2018), p. 013201. DOI: 10.1088/1742-5468/AA9BB4.

[82] A. Tartaglia, L. F. Cugliandolo, and M. Picco. "Percolation and coarsening in the bidimensional voter model". In: *Physical Review E* 92 (4 2015), p. 042109. DOI: 10.1103/PHYSREVE.92.042109.

[83] P. Mullick and P. Sen. "Zero-temperature coarsening in the Ising model with asymmetric second-neighbor interactions in two dimensions". In: *Physical Review E* 95 (5 2017), p. 052150. DOI: 10.1103/PHYSREVE.95.052150.

[84] A. J. Bray and K. Humayun. "Universality class for domain growth in random magnets". In: *Journal of Physics A: Mathematical and General* 24.19 (1991), pp. L1185–L1191. DOI: 10.1088/0305-4470/24/19/010.

[85] H. Park and M. Pleimling. "Aging in coarsening diluted ferromagnets". In: *Physical Review B* 82 (14 2010), p. 144406. DOI: 10.1103/PHYSREVB.82.144406.

[86]   C. Aron, C. Chamon, L. F. Cugliandolo, and M. Picco. "Scaling and super-universality in the coarsening dynamics of the 3D random field Ising model". In: *Journal of Statistical Mechanics: Theory and Experiment* 2008.05 (2008), P05016. DOI: 10.1088/1742-5468/2008/05/P05016.

[87]   B. Biswal, S. Puri, and D. Chowdhury. "Domain growth in weakly disordered magnets". In: *Physica A: Statistical Mechanics and its Applications* 229.1 (1996), pp. 72–92. DOI: HTTPS://DOI.ORG/10.1016/0378-4371(95)00467-X.

[88]   S. Tojo, Y. Taguchi, Y. Masuyama, T. Hayashi, H. Saito, and T. Hirano. "Controlling phase separation of binary Bose-Einstein condensates via mixed-spin-channel Feshbach resonance". In: *Physical Review A* 82 (3 2010), p. 033609. DOI: 10.1103/PHYSREVA.82.033609.

[89]   Y. Kawaguchi, H. Saito, K. Kudo, and M. Ueda. "Spontaneous magnetic ordering in a ferromagnetic spinor dipolar Bose-Einstein condensate". In: *Physical Review A* 82 (4 2010), p. 043627. DOI: 10.1103/PHYSREVA.82.043627.

[90]   S. De, D. L. Campbell, R. M. Price, A. Putra, B. M. Anderson, and I. B. Spielman. "Quenched binary Bose-Einstein condensates: Spin-domain formation and coarsening". In: *Physical Review A* 89 (3 2014), p. 033631. DOI: 10.1103/PHYSREVA.89.033631.

[91]   J. Hofmann, S. S. Natu, and S. S. Das. "Coarsening dynamics of binary Bose condensates". In: *Physical Review Letters* 113 (9 2014), p. 095702. DOI: 10.1103/PHYSREVLETT.113.095702.

[92]   Hiromitsu Takeuchi. "Domain-area distribution anomaly in segregating multi-component superfluids". In: *Physical Review A* 97 (1 2018), p. 013617. DOI: 10.1103/PHYSREVA.97.013617.

[93]   G. L. Oppo, A. J. Scroggie, and W. J. Firth. "Characterization, dynamics and stabilization of diffractive domain walls and dark ring cavity solitons in

parametric oscillators". In: *Physical Review E* 63 (6 2001), p. 066209. DOI: 10.1103/PHYSREVE.63.066209.

[94] I. M. Lifshitz and V. V. Slyozov. "The kinetics of precipitation from supersaturated solid solutions". In: *Journal of Physics and Chemistry of Solids* 19.1 (1961), pp. 35–50. DOI: 10.1016/0022-3697(61)90054-3.

[95] S. Nanako, B. Shreya, and P. B. Blakie. "Domain percolation in a quenched ferromagnetic spinor condensate". In: *New Journal of Physics* 19.9 (2017), p. 095003. DOI: 10.1088/1367-2630/AA7E70.

[96] L. McNally, E. Bernardy, J. Thomas, A. Kalziqi, J. Pentz, S. P. Brown, B. K. Hammer, P. J. Yunker, and W. C. Ratcliff. "Killing by Type VI secretion drives genetic phase separation and correlates with increased cooperation". In: *Nature Communications* 8 (2017). DOI: 10.1038/NCOMMS14371.

[97] A. Cavagna, D. Conti, C. Creato, L. Del Castello, I. Giardina, T. S. Grigera, S. Melillo, L. Parisi, and M. Viale. "Dynamic scaling in natural swarms". In: *Nature Physics* 13.9 (2017), pp. 914–918. DOI: 10.1038/NPHYS4153.

[98] J. Olejarz, P. L. Krapivsky, and S. Redner. "Zero-temperature freezing in the three-dimensional kinetic Ising model". In: *Physical Review E* 83 (3 2011), p. 030104. DOI: 10.1103/PHYSREVE.83.030104.

[99] J. Olejarz, P. L. Krapivsky, and S. Redner. "Zero-temperature relaxation of three-dimensional Ising ferromagnets". In: *Physical Review E* 83 (5 2011), p. 051104. DOI: 10.1103/PHYSREVE.83.051104.

[100] C. M. Newman and D. L. Stein. "Blocking and persistence in the zero-temperature dynamics of homogeneous and disordered ising models". In: *Phys. rev. lett.* 82 (20 1999), pp. 3944–3947. DOI: 10.1103/PHYSREVLETT.82.3944.

[101] C. M. Newman and D. L. Stein. "Zero-temperature dynamics of Ising spin systems following a deep quench: results and open problems". In: *Physica A:*

Statistical Mechanics and its Applications 279.1 (2000), pp. 159–168. DOI: 10.1016/S0378-4371(99)00511-7.

[102] J. A. Glazier, S. P. Gross, and J. Stavans. "Dynamics of two-dimensional soap froths". In: *Physical Review A* 36 (1 1987), pp. 306–312. DOI: 10.1103/PHYSREVA.36.306.

[103] J. A. Glazier, M. P. Anderson, and G. S. Grest. "Coarsening in the two-dimensional soap froth and the large-Q Potts model: A detailed comparison". In: *Philosophical Magazine B* 62.6 (1990), pp. 615–645. DOI: 10.1080/13642819008215259.

[104] G. L. Thomas, R. M. C. de Almeida, and F. Graner. "Coarsening of three-dimensional grains in crystals, or bubbles in dry foams, tends towards a universal, statistically scale-invariant regime". In: *Physical Review E* 74 (2 2006), p. 021407. DOI: 10.1103/PHYSREVE.74.021407.

[105] D. J. Srolovitz, M. P. Anderson, P. S. Sahni, and G. S. Grest. "Computer simulation of grain growth—II. Grain size distribution, topology, and local dynamics". In: *Acta Metallurgica* 32.5 (1984), pp. 793–802. DOI: 10.1016/0001-6160(84)90152-4.

[106] V. E. Fradkov and D. Udler. "Two-dimensional normal grain growth: topological aspects". In: *Advances in Physics* 43.6 (1994), pp. 739–789. DOI: 10.1080/00018739400101559.

[107] D. Raabe. "Scaling Monte Carlo kinetics of the Potts model using rate theory". In: *Acta Materialia* 48.7 (2000), pp. 1617–1628. DOI: 10.1016/S1359-6454(99)00451-6.

[108] D. Zöllner. "A Potts model for junction limited grain growth". In: *Computational Materials Science* 50.9 (2011), pp. 2712–2719. DOI: 10.1016/J.COMMATSCI.2011.04.024.

[109] K. L. Babcock, R. Seshadri, and R. M. Westervelt. "Coarsening of cellular domain patterns in magnetic garnet films". In: *Physical Review A* 41 (4 1990), pp. 1952–1962. DOI: 10.1103/PHYSREVA.41.1952.

[110] E. A. Jagla. "Numerical simulations of two-dimensional magnetic domain patterns". In: *Physical Review E* 70 (4 2004), p. 046204. DOI: 10.1103/PHYSREVE.70.046204.

[111] J. C. M. Mombach, M. A. Z. Vasconcellos, and R. M. C. de Almeida. "Arrangement of cells in vegetable tissues". In: *Journal of Physics D: Applied Physics* 23.5 (1990), pp. 600–606. DOI: 10.1088/0022-3727/23/5/021.

[112] J. C. M. Mombach, R. M. C. de Almeida, and J. R. Iglesias. "Mitosis and growth in biological tissues". In: *Physical Review E* 48 (1 1993), pp. 598–602. DOI: 10.1103/PHYSREVE.48.598.

[113] D. Weaire and N. Rivier. "Soap, cells and statistics — random patterns in two dimensions". In: *Contemporary Physics* 50.1 (2009), pp. 199–239. DOI: 10.1080/00107510902734680.

[114] G. S. Grest, M. P. Anderson, and D. J. Srolovitz. "Domain-growth kinetics for the Q-state Potts model in two and three dimensions". In: *Physical Review B* 38 (7 1988), pp. 4752–4760. DOI: 10.1103/PHYSREVB.38.4752.

[115] S. A. Safran, P. S. Sahni, and G. S. Grest. "Fluctuations and kinetics of domain growth in two dimensions". In: *Physical Review B* 26 (1 1982), pp. 466–469. DOI: 10.1103/PHYSREVB.26.466.

[116] S. A. Safran, P. S. Sahni, and G. S. Grest. "Kinetics of ordering in two dimensions. I. Model systems". In: *Physical Review B* 28 (5 1983), pp. 2693–2704. DOI: 10.1103/PHYSREVB.28.2693.

[117] M. P. O. Loureiro, J. J. Arenzon, L. F. Cugliandolo, and A. Sicilia. "Curvature-driven coarsening in the two-dimensional Potts model". In: *Physical Review E* 81 (2 2010), p. 021129. DOI: 10.1103/PHYSREVE.81.021129.

[118] M. P.O. Loureiro, J. J. Arenzon, and L. F. Cugliandolo. "Geometrical properties of the Potts model during the coarsening regime". In: *Physical Review E* 85 (2 2012), p. 021135. DOI: 10.1103/PHYSREVE.85.021135.

[119] E. E. Ferrero and S. A. Cannas. "Long-term ordering kinetics of the two-dimensional q-state Potts model". In: *Physical Review E* 76 (3 2007), p. 031108. DOI: 10.1103/PHYSREVE.76.031108.

[120] M. J. de Oliveira, A. Petri, and T. Tomé. "Glassy states in lattice models with many coexisting crystalline phases". In: *Europhysics Letters (EPL)* 65.1 (2004), pp. 20–26. DOI: 10.1209/EPL/I2003-10060-0.

[121] M. J. de Oliveira, A. Petri, and T Tomé. "Crystal vs. glass formation in lattice models with many coexisting ordered phases". In: *Physica A: Statistical Mechanics and its Applications* 342.1 (2004). Proceedings of the VIII Latin American workshop on nonlinear phenomena, pp. 97–103. DOI: 10.1016/J.PHYSA.2004.04.104.

[122] J. Olejarz, P. L. Krapivsky, and S. Redner. "Zero-temperature coarsening in the 2D Potts model". In: *Journal of Statistical Mechanics* 2013.06 (2013), P06018. DOI: 10.1088/1742-5468/2013/06/P06018.

[123] J. Denholm and S. Redner. "Topology-controlled potts coarsening". In: *Physical Review E* 99 (6 2019), p. 062142. DOI: 10.1103/PHYSREVE.99.062142.

[124] W. Krauth. *Statistical Mechanics: Algorithms and computations*. Oxford Master Series in Physics. Oxford University Press, UK, 2006.

[125] N. Metropolis, A. W. Rosenbluth, M. N. Rosenbluth, A. H. Teller, and E. Teller. "Equation of state calculations by fast computing machines". In: *The Journal of Chemical Physics* 21.6 (1953), pp. 1087–1092. DOI: 10.1063/1.1699114.

[126] D. P. Landau and K. Binder. *A guide to Monte Carlo simulation in Statistical Physics*. Cambridge University Press, 2009.

[127] U. Wolff. "Collective Monte Carlo updating for spin systems". In: *Physical Review Letters* 62 (4 1989), pp. 361–364. DOI: 10.1103/PHYSREVLETT.62.361.

[128] P. Tamayo, R. C. Brower, and W. Klein. "Single-cluster Monte Carlo dynamics for the Ising model". In: *Journal of Statistical Physics* 58.5 (1990), pp. 1083–1094. DOI: 10.1007/BF01026564.

[129] J. Kaupužs, J. Rimšāns, and R. V. N. Melnik. "Parallelization of the Wolff single-cluster algorithm". In: *Physical Review E* 81 (2 2010), p. 026701. DOI: 10.1103/PHYSREVE.81.026701.

[130] G. N. Hassold and E. A. Holm. "A fast serial algorithm for the finite temperature quenched Potts model". In: *Computers in Physics* 7.1 (1993), pp. 97–107. DOI: 10.1063/1.168481.

[131] A. B. Bortz, M. H. Kalos, and J. L. Lebowitz. "A new algorithm for Monte Carlo simulation of Ising spin systems". In: *Journal of Computational Physics* 17.1 (1975), pp. 10–18. DOI: 10.1016/0021-9991(75)90060-1.

[132] J. L. Doob. "Topics in the theory of Markoff chains". In: *Transactions of the American Mathematical Society* 58.52 (1942), pp. 37–64. DOI: 10.1090/S0002-9947-1942-0006633-7.

[133] J. L. Doob. "Markoff chains—denumerable case". In: *Transactions of the American Mathematical Society* 58.3 (1945), pp. 455–473. DOI: 10.2307/1990339.

[134] A. F. Voter. "Introduction to the Kinetic Monte Carlo method". In: *Radiation Effects in Solids*. Ed. by K. E. Sickafus, E. A. Kotomin, and B. P. Uberuaga. Dordrecht: Springer Netherlands, 2007, pp. 1–23.

[135] J. R. Beeler. "Displacement spikes in cubic metals. I. α-Iron, Copper, and Tungsten". In: *Physical Review* 150 (2 1966), pp. 470–487. DOI: 10.1103/PHYSREV.150.470.

[136] W. M. Young and E. W. Elcock. "Monte Carlo studies of vacancy migration in binary ordered alloys: I". In: *Proceedings of the Physical Society* 89.3 (1966), pp. 735–746. DOI: 10.1088/0370-1328/89/3/329.

[137] D. R. Cox and H. D. Miller. *The theory of stochastic processes*. Spottiswoode, Ballantyne & Co. Ltd, 1965.

[138] D. T. Gillespie. "A general method for numerically simulating the stochastic time evolution of coupled chemical reactions". In: *Journal of Computational Physics* 22.4 (1976), pp. 403–434. DOI: 10.1016/0021-9991(76)90041-3.

[139] D. T. Gillespie. "Exact stochastic simulation of coupled chemical reactions". In: *The Journal of Physical Chemistry* 81.25 (1977), pp. 2340–2361. DOI: 10.1021/J100540A008.

[140] D. G. Doran. "Computer simulation of displacement spike annealing". In: *Radiation Effects* 2.4 (1970), pp. 249–267. DOI: 10.1080/00337576908243987.

[141] J. M. Lanore. "Simulation de l'evolution des defauts dans un reseau par le methode de monte-carlo". In: *Radiation Effects* 22.3 (1974), pp. 153–162. DOI: 10.1080/10420157408230773.

[142] H. L. Heinisch. "Defect production in simulated cascades: Cascade quenching and short-term annealing". In: *Journal of Nuclear Materials* 117 (1983), pp. 46–54. DOI: 10.1016/0022-3115(83)90008-9.

[143] R. Gordon. "Adsorption isotherms of lattice gases by computer simulation". In: *The Journal of Chemical Physics* 48.3 (1968), pp. 1408–1409. DOI: 10.1063/1.1668820.

[144] F. F. Abraham and G. M. White. "Computer simulation of vapor deposition on two-dimensional lattices". In: *Journal of Applied Physics* 41.4 (1970), pp. 1841–1849. DOI: 10.1063/1.1659113.

[145] C. S. Kohli and M. B. Ives. "Computer simulation of crystal dissolution mor-
       phology". In: *Journal of Crystal Growth* 16.2 (1972), pp. 123–130. DOI: 10.
       1016/0022-0248(72)90103-0.

[146] G. H. Gilmer. "Growth on imperfect crystal faces: I. Monte-Carlo growth rates".
       In: *Journal of Crystal Growth* 36.1 (1976), pp. 15–28. DOI: 10.1016/0022-
       0248(76)90209-8.

[147] M. Bowker and D. A. King. "Adsorbate diffusion on single crystal surfaces: I.
       The influence of lateral interactions". In: *Surface Science* 71.3 (1978), pp. 583–
       598. DOI: 10.1016/0039-6028(78)90449-1.

[148] D. A. Reed and G. Ehrlich. "Surface diffusivity and the time correlation of
       concentration fluctuations". In: *Surface Science* 105.2 (1981), pp. 603–628.
       DOI: 10.1016/0039-6028(81)90021-2.

[149] P. A. Rikvold. "Simulations of a stochastic model for cluster growth on a square
       lattice". In: *Physical Review A* 26 (1 1982), pp. 647–650. DOI: 10.1103/
       PHYSREVA.26.647.

[150] E. S. Hood, B. H. Toby, and W. H. Weinberg. "Precursor-mediated molecular
       chemisorption and thermal desorption: the interrelationships among energetics,
       kinetics, and adsorbate lattice structure". In: *Physical Review Letters* 55 (22
       1985), pp. 2437–2440. DOI: 10.1103/PHYSREVLETT.55.2437.

[151] S. V. Ghaisas and A. Madhukar. "Monte-Carlo simulations of MBE growth
       of III–V semiconductors: The growth kinetics, mechanism, and consequences
       for the dynamics of RHEED intensity". In: *Journal of Vacuum Science &
       Technology B: Microelectronics Processing and Phenomena* 3.2 (1985), pp. 540–
       546. DOI: 10.1116/1.583173.

[152] A. F. Voter. "Classically exact overlayer dynamics: Diffusion of RSahnhodium
       clusters on Rh(100)". In: *Physical Review B* 34 (10 1986), pp. 6819–6829. DOI:
       10.1103/PHYSREVB.34.6819.

[153] P. S. Sahni, D. J. Srolovitz, G. S. Grest, M. P. Anderson, and S. A. Safran. "Kinetics of ordering in two dimensions. II. Quenched systems". In: *Physical Review B* 28 (5 1983), pp. 2705–2716. DOI: 10.1103/PHYSREVB.28.2705.

[154] R. Porkess. *Collins Internet-Linked Dictionary of Statistics*. HarperCollins Publishers, 2005.

[155] M. Plischke, Z. Rácz, and D. Liu. "Time-reversal invariance and universality of two-dimensional growth models". In: *Physical Review E* 35 (7 1987), pp. 3485–3495. DOI: 10.1103/PHYSREVB.35.3485.

[156] S. Redner. *A guide to first-passage processes*. Cambridge University Press, 2001.

[157] A. Gal and O. Raz. "Precooling strategy allows exponentially faster heating". In: *Physical review letters* 124 (6 2020), p. 060602. DOI: 10.1103/PHYSREVLETT. 124.060602.

[158] R. Zallen. "Polychromatic percolation: Coexistence of percolating species in highly connected lattices". In: *Physical Review B* 16 (4 1977), pp. 1426–1435. DOI: 10.1103/PHYSREVB.16.1426.

[159] S. Sheffield and A. Yadin. "Tricolor percolation and random paths in 3D". In: *Electronic Journal of Probability* 19 (2014), 23 pp. DOI: 10.1214/EJP.V19-3073.